Dissertation

submitted to the

Combined Faculties for the Natural Sciences and for Mathematics of the Ruperto-Carola

University of Heidelberg, Germany

for the degree of

Doctor of Natural Sciences

presented by

Rainer Beck, Diplom-Biologe

born in Berchtesgaden

Oral examination:.....

Molecular Mechanisms of COPI Vesicle Biogenesis

Referees: Prof. Dr. Felix Wieland

Prof. Dr. Walter Nickel

Für Katharina

Table of Contents

Abstract

COPI vesicles are defined by a coat consisting of (i) the small GTPase Arf1 and (ii) coatomer. Arf1 in its GTP-loaded form recruits coatomer to the membrane to form a COPI vesicle. GTP hydrolysis leads to uncoating, and is catalyzed by (iii) ArfGAP-activity. In this work we studied the molecular contributions of the named three key players in order to further elucidate the mechanisms underlying COPI vesicle biogenesis and functions:

(i) We show that Arf1-GTP induces positive membrane curvature, and find that the small GTPase can dimerize on the membrane. Investigating a possible link between Arf1 dimerization and curvature formation, we isolated an Arf1-mutant (Arf1-Y35A) that cannot dimerize. Although it was capable to exert the classical role of Arf1 as a coat receptor, it could not mediate the formation of COPI vesicles and is lethal in yeast. Strikingly, this mutant was not able to deform membranes, suggesting that GTP-specific dimerization of Arf1 is a critical step which induces membrane curvature during the formation of coated vesicles. We observed that, while the curvature in the budding zone of a COPI vesicle is mediated by coatomer, Arf1 contributes to membrane tension in such a way that fission can occur.

(ii) The heptameric coat complex coatomer exists in four isoforms, defined by their γ1/γ2 and ζ1/ζ2 subunits, which are distributed differentially over the Golgi. Here we show a biochemical characterization of the four recombinant isoforms of the heptameric complex. We demonstrate that the recombinant protein complexes yield COPI-vesicles in vitro with an efficiency comparable to coatomer isolated from tissue.

(iii) To investigate roles of ArfGAP activity during in vitro budding, we find that catalytic amounts of full length ArfGAP1 reduce the yield of COPI-coated vesicles significantly, in line with the proposed function of the enzyme to mediate the

uncoating reaction. We also experimentally addressed discrepancies in the literature about the role of ArfGAP1 during COPI-vesicle formation.

Abstract (German version)

COPI Vesikel sind definiert durch eine Proteinhülle bestehend aus der kleinen GTPase Arf1 und Coatomer. Während der COPI Vesikel Biogenese rekrutiert Arf1-GTP Coatomer an die Membran. Von einer ArfGAP Aktivität katalysierten GTP Hydrolyse revertiert diese Membran Verankerung. In dieser Arbeit wurden die drei oben genannten Schlüsselproteine, Arf1, Coatomer und ArfGAP1 näher charakterisiert, um Aufschlüsse über die molekularen Mechanismen zu erhalten, welche COPI Vesikel Biogenese und Funktion zu Grunde liegen:

(i) Wir zeigen in dieser Arbeit, dass Arf1-GTP positive Membran Kurvatur induziert und beobachten, dass die kleine GTPase an Membranen dimerisiert. Um einen möglichen Zusammenhang zwischen Arf1-Dimerisierung und Membran Kurvatur zu untersuchen, wurde eine Arf1 Mutante isoliert (Arf1-Y35A), welche nicht mehr dimerisieren kann. Obwohl dieses monomere Arf1 noch in der Lage ist der klassischen Rolle von Arf1 als Coatomer Rezeptor nachzukommen, hat es seine Kompetenz zur Vesikelbiogenese verloren, und ist letal in Hefe. Erstaunlicherweise ist diese Mutante auch nicht mehr in der Lage Membranen zu deformieren, was nahe legt, dass GTP-spezifische Dimerisierung von Arf1 ein kritischer Schritt für die Bildung von COPI Vesikeln ist. Unseren Beobachtungen nach trägt Arf1, obwohl die Kurvatur eines knospenden COPI Vesikels von Coatomer hervorgerufen wird, zur Membrandeformation bei, die notwendig für die Abschnürung eines Vesikels ist.

(ii) Der heptamere Proteinkomplex Coatomer existiert in vier möglichen Isoformen, welche durch ihre γ1/γ2, ζ1/ζ2 Untereinheiten definiert und differenziell über den Golgi verteilt sind. Im Rahmen diese Arbeit wurde eine biochemische Charakterisierung der vier rekombinant hergestellten Isoformen durchgeführt. Unsere Ergebnisse zeigen, dass alle vier rekombinanten Komplexe, verglichen mit

aus Gewebe gewonnenem Coatomer, eine vergleichbare Effizienz zur Vesikelgenerierung aufweisen. Im Rahmen vorläufiger Ergebnisse, die noch einer genaueren Prüfung Stand halten müssen, finden wir jedoch Unterschiede bezüglich der Frachtspezifität der Vesikel, was für eine differenzielle Rollenverteilung für COPI im sekretorischen Transport spricht. Zuletzt wurden mit Hilfe von reinstem rekombinanten Coatomer elektronenmikroskopische Strukturanalysen gestartet.

(iii) Um Funktionen der ArfGAP-Aktivität während der COPI Vesikelbiogenese näher zu beleuchten, zeigen wir mit rekombinantem ArfGAP1, dass bereits katalytische Mengen des Enzyms die Ausbeute an umhüllten Vesikeln drastisch reduzieren. Dies ist in Übereinstimmung mit der bisher angenommenen Funktion dieses Enzyms als Mediator der ‚Uncoating' Reaktion. Darüber hinaus wurden Diskrepanzen in der Literatur bezüglich der genauen Funktion von ArfGAP1 untersucht, und im Lichte von neueren Erkenntnissen erklärt.

Abbreviations

endoplasmic reticulum (ER)

signal recognition particle (SRP)

ER-Golgi intermediate compartment (ERGIC)

coat protein complex I (COPI)

coat protein complex II (COPII)

trans-Golgi network (TGN)

clathrin coated vesicles (CCV)

clathrin adaptor proteins (AP)

Guanosin diphosphate (GDP)

Guanosin triphosphate (GTP)

Guanine nucleotide exchange factor (GEF)

Adenine diphosphate (ADP)

Adenine triphosphate (ATP)

ADP *ribosylation* factor1 (*Arf1*)

Brefeldin A (BFA)

ARF *nucleotide*-binding-site opener (ARNO)

Golgi-specific brefeldin-A-resistant factor 1 (*GBF1)*

Introduction

The secretory pathway

Intracellular pathways of newly synthesized proteins involve the endoplasmic reticulum (ER) and the Golgi-apparatus (Jamieson and Palade, 1966). Transported are membrane proteins, soluble lysosomal/vacuolar and secreted proteins, which have common signal sequences. Besides allowing post-translational modifications such as protein-folding, disulfide bond formation, glycosylation, tyrosine sulphation, or proline-hydroxylation, the main task of the secretory machinery is the distribution of proteins and lipids to their final destinations, a prerequisite for lipid and organelle homeostasis.

If properly folded, secretory proteins are taken up from the Endoplasmic Reticulum (ER) by COPII vesicles, which are one class of protein coated vesicular carriers (Barlowe, *et al.*, 1994). The COPII vesicle coat consists of the small GTPase Sar1, the heterodimeric Sec23/24 complex and the heterotetrameric Sec13/31 complex. En route towards the Golgi-apparatus lies the ER-Golgi intermediate compartment (ERGIC), an area defined by the presence of the lectin ERGIC-53 (Hauri, *et al.*, 2000). Since ER/Golgi recycling membrane proteins are concentrated in COPI-positive structures at the ERGIC, whereas secretory cargo is predominantly found in COPI-negative regions of it, the ERGIC is thought to represent the first entity discriminating between anterograde and retrograde transport destination (Martinez-Menarguez, *et al.*, 1999).

Protein and lipid cargo is then transported along the Golgi-apparatus, consisting of distinct cisternae with different protein compositions, until it exiting at the *trans*-Golgi network (TGN).

Secretory cargo has to be sorted at the TGN, depending on the final destination, and is directed towards lysosomes, endosomes or the plasma membrane. On the post-Golgi level, trafficking is

mediated by clathrin coated vesicles (CCV) (reviewed in (Rodriguez-Boulan and Musch, 2005). Similar to the COPII system, CCV biogenesis mainly involves sequential binding of the small GTPase Arf1 for (the clathrin adaptor proteins AP-1, 3, 4), and Arf6 (for AP-2) (Paleotti, *et al.*, 2005), the clathrin adaptor protein complexes (reviewed in (Owen, *et al.*, 2004), and the heterohexameric coat protein clathrin.

COPI- mediated Transport

For intra-Golgi transport, two views exist: cisternal progression/maturation and vesicular transport. The cisternal progression/maturation model postulates the transport of anterograde cargo *en bloc* (Glick and Malhotra, 1998). This would be achieved by assembly of new cisternae at the *cis*-Golgi (potentially from fusion of pre-Golgi carriers), which then would mature and along the Golgi, and finally disassemble at the *trans*-Golgi. Therefore, anterograde cargo would not leave the lumen of cisternae. Protein homeostasis and the integrity of cisternae with distinct compositions (such as *cis*- or *trans*-specific Golgi-resident proteins and lipids), would be mediated by exclusively retrograde directed COPI vesicles.

In contrast to this view, the vesicular transport model postulates the transport of anterograde cargo between static cisternae via coordinated budding and fusion reactions of anterograde-directed COPI vesicles (Rothman and Wieland, 1996). This debated role of COPI vesicles in anterograde transport, besides their established role as retrograde carriers, would demand at least two distinct populations of COPI vesicles. Up to now, it is still under debate how intra-Golgi transport is achieved.

Formation of COPI-coated vesicles

Activation of cytosolic Arf1 initially loaded with GDP is the first step in COPI vesicle biogenesis. Guanine nucleotide exchange factors (GEFs), containing a central Sec7 domain (Chardin, *et al.*, 1996), stimulate the binding of GTP to Arf1. This nucleotide exchange causes a conformational change of the GTPase, leading to the exposure of an N-terminal myristoyl-anchor covalently bound to an amphiphatic helix, which allows stable membrane association of the protein (Franco, *et al.*, 1996; Antonny, *et al.*, 1997). This energetically unfavorable exposure of the amphipatic helix/myristoyl moiety of Arf1-GTP in the absence of membranes ensures that no misactivation occurs in the cytosol.

The lower molecular weight GEFs, like ARNO and cytohesins, are bound to the membrane via a phosphoinositides-specific PH domain (Klarlund, *et al.*, 2000; De Matteis, *et al.*, 2005). In contrast to the small GEFs, Gbf1, a large Sec7 domain GEF, is probably the relevant exchange factor involved in COPI biogenesis, as it localizes to the *cis*-Golgi and its activity can be inhibited by Brefeldin-A (BFA) (Zhao, *et al.*, 2002; Niu, *et al.*, 2005).

In contrast to COPII- or CCV-coat proteins, coatomer is recruited *en bloc* (Hara-Kuge, *et al.*, 1994) through the binding to Arf1-GTP through the β- und γ-COP subunits (Zhao, *et al.*, 1997; Zhao, *et al.*, 1999). The Golgi-localized membrane protein p23, by binding the γ-COP subunit (Harter, *et al.*, 1996), facilitates this recruitment. In addition, the complex also binds cytoplasmic tails of transmembrane proteins bearing a KKXX sequence at their C-termini (Cosson and Letourneur, 1994). After recruitment and interaction with certain members of the p23 family (containing KKXX motives), coatomer undergoes a conformational change (Reinhard, *et al.*, 1999; Langer, *et al.*, 2008), and a coated bud is formed, followed by vesicle fission from the donor membrane.

ArfGAP1 activity and COPI vesicle formation

Uncoating of COPI vesicles is mediated by an ArfGTPase activating activity, for which three Golgi-specific enzymes are described, ArfGAPs1-3 (Frigerio, *et al.*, 2007). This activity stimulates the hydrolysis of GTP in Arf1, yielding Arf-GDP that no longer binds to membranes and thus dissociates from the vesicle, initiating coat disassembly (Cukierman, *et al.*, 1995; Reinhard, *et al.*, 2003; Tanigawa, *et al.*, 1993). Interestingly, an ArfGAP activity is needed also in the formation of COPI-coated vesicles, to allow uptake of cargo proteins (Nickel, *et al.*, 1998; Malsam, *et al.*, 1999; Pepperkok, *et al.*, 2000; Lanoix, *et al.*, 2001). Various reports have appeared in the past on the molecular mechanism that underlie vesicle formation, mainly based on *in vitro* reconstitution experiments (Reinhard, *et al.*, 2003; Serafini, *et al.*, 1991; Ostermann, *et al.*, 1993; Serafini, *et al.*, 1991). Varying functions have been reported for roles that ArfGAP proteins play in COPI vesicle biogenesis. Specifically, ArfGAP1 on the one hand was described as an enzyme to catalyze uncoating of COPI coated vesicles (Cukierman, *et al.*, 1995; Reinhard, *et al.*, 2003; Tanigawa, *et al.*, 1993), and on the other hand as a stoichiometric structural coat component (Yang, *et al.*, 2002). In order to investigate COPI vesicle formation in a reconstituted system, in the frame of this thesis, an assay was developed that allows vesicle formation and purification in the presence of GTP, rather than its poorly hydrolyzable analogs, in the numbers needed for quantitative analyses. This and other experiments performed in the frame of the present thesis allow a close examination of the roles that ArfGAP1 plays in COPI vesicle biogenesis and significantly addresses some of the discrepancies in the field.

A novel Role for Arf1 during COPI vesicle Biogenesis

Small GTPases of the Ras superfamily are key regulators of many important cellular functions (Vetter and Wittinghofer, 2001). They work as molecular switches that cycle between an

inactive GDP-bound state, and an active GTP-bound state. Activation occurs by the exchange of GDP to GTP, while inactivation is mediated by GTP hydrolysis. Effectors of GTP-binding proteins are defined as molecules that bind more tightly to the GTP-bound state, resulting in a biological function.

The small GTPase Arf1 is involved in the recruitment of coat protein complexes that polymerize on endomembranes to form transport vesicles (Serafini, *et al.*, 1991; D'Souza-Schorey and Chavrier, 2006). Activated Arf1 is always membrane associated since in this conformation its myristoylated N-terminal amphipatic α-helix is exposed, ensuring membrane anchorage (Antonny, *et al.*, 1997). As coat proteins can only bind to the active GTPase (Zhao, *et al.*, 1997; Boehm, *et al.*, 2001; Austin, *et al.*, 2002), Arf1 is a key regulator of vesicle coating and uncoating. Indeed, activation of Arf1 is a prerequisite for coat recruitment (Donaldson, *et al.*, 1992; Ooi, *et al.*, 1998; Stamnes and Rothman, 1993), and Arf1-mediated GTP hydrolysis is necessary for coat release (Tanigawa, *et al.*, 1993; Zhu, *et al.*, 1998). Arf1-GTP is directly involved in the recruitment of coatomer (Zhao, *et al.*, 1997; Donaldson, *et al.*, 1992), the coat of COPI vesicles (Waters, *et al.*, 1991), and of the clathrin adaptor complexes AP-1 (Stamnes and Rothman, 1993), AP-3 (Ooi, *et al.*, 1998) and AP-4 (Boehm, *et al.*, 2001). Coatomer directly interacts with Arf1 through binding of several of its subunits in a GTP-dependent manner. There is evidence that more than one Arf1-GTP molecule may bind to one coatomer complex (Sun, *et al.*, 2007). This finding is in agreement with estimations of an Arf1 to coatomer stoichiometry on COPI-coated vesicles of at least 3:1 (Serafini, *et al.*, 1991; Sohn, *et al.*, 1996; Helms, *et al.*, 1993). These observations suggest that Arf1, which like most other Ras-like GTPases is a monomer in its cytosolic form, may oligomerize upon activation on membranes. Zhe Sun showed in her doctoral thesis that that Arf1, when bound to GTP, in fact forms a dimer on the membrane, and provided evidence that this dimerization is required to generate COPI vesicles.

Interestingly, during the course of this thesis, we found that Arf1-GTP induces positive membrane curvature, as shown by tubulation of membrane sheets, whereas a non-dimerizing Arf1-mutant lacks this activity. Moreover, we observed that the tubulation-deficient Arf1 mutant Arf1-Y35A still promotes the formation of coated buds, however the fission step seems to be impaired in case of this Arf1-construct, suggesting that Arf1-mediated membrane curvature is a requirement for the fission step of COPI vesicles.

Functions of coatomer isotypes

In the late Golgi/endocytic pathways, a variety of coat proteins are known, including four different tetrameric adaptor complexes, some of which use the clathrin system as an outer shell of their coat (Robinson, 2004). Thus, for particular pathways, the selection of cargo as well as the direction might be determined by individual coats. In line with this, the COPI coat consists of coatomer, which is a stable cytoplasmic complex of seven subunits, α-, β-, β′-, γ-, δ-, ε-, and ζ-COP, and the small GTPase Arf1. The observation that COPI vesicles participate in several transport directions is difficult to rationalize with just a single isoform of the complex (reviewed in (Bonfanti, *et al.*, 1998). The question if transport in both directions are performed by COPI vesicles or if they are exclusively retrograde carriers within the Golgi and from the Golgi to the ER is still under debate. Genome analyses identified a second isoform for each of the two coatomer subunits, γ- and ζ-COP (Blagitko, *et al.*, 1999), the paralogs γ2- and ζ2-COP. Previously, the corresponding cDNAs were expressed as tagged constructs (Futatsumori, *et al.*, 2000), and the endogenous gene products were shown to be incorporated into coatomer complexes in a stoichiometric manner, which resulted in three major isoforms of the complex with the compositions γ1ζ1-, γ1ζ2-, and γ2ζ1-COP (Wegmann, *et al.*, 2004). By using polyclonal antibodies specific against γ1-, γ2-, and ζ2-COP, the localization of coatomer isoforms in NRK cells had been investigated by immunoelectron microscopy, and a striking

heterogeneity within the Golgi apparatus was found: whereas γ1- and ζ2-COP seemed to be restricted to the early Golgi and a pre-Golgi compartment, the majority of γ2-COP-containing isoforms of the complex was localized to the trans side of the organelle (Moelleken, *et al.*, 2007). With this hint of homogeneously coated COPI vesicles, defined by their γ/ζ subunit composition, an approach was started to express and purify recombinant coatomer isoforms that could be used in COPI-reconstitution assays in order to correlate coat complexes to putative cargo proteins or lipids. In this work, we showed the purification of such recombinant coatomer isoforms and the an initial biochemical and structural characterization.

Results Part I
Roles of ArfGAP-activity in COPI vesicle biogenesis and function

In the first part of this thesis, the molecular roles of ArfGAP1 were investigated more closely. As a first step, peptide antibodies were raised and characterized in various applications. Furthermore, the cDNA encoding full length ArfGAP1 was cloned into a Pichia pastoris expression vector, and the protein was expressed and purified. Functional analysis on the enzyme was performed by investigating the activity of ArfGAP1 on GTP hydrolysis in Arf1. Furthermore, the function of this GTP hydrolysis, and thereby roles of ArfGAP1 in COPI vesicle biogenesis, was investigated in COPI-vesicle reconstitution assays. To this end, the resulting data was compared to opposing reports in the literature and the differences were explored experimentally.

Generation and characterization of an ArfGAP1 antibody

Peptide antibodies directed against the sequence EPPKAKSPSSDSWTC (amino acids 335-349 of 415 total) were raised in rabbits (Pineda Antibodies, Berlin). The immune sera were analyzed by Western blotting with rabbit liver cytosol, and final bleeds (90 days after immunization) were taken after signal intensity reached a maximum. The final sera of rabbit 3 turned out to be most sensitive and were therefore chosen for affinity purification by binding to the antigenic peptide, coupled to thiopropyl-sepharose, and elution at acidic pH. SDS-PAGE and Western blot analysis of 20 µg rat liver cytosol was performed before and after affinity purification, as shown (Waters, *et al.*, 1991)(Figure 1).

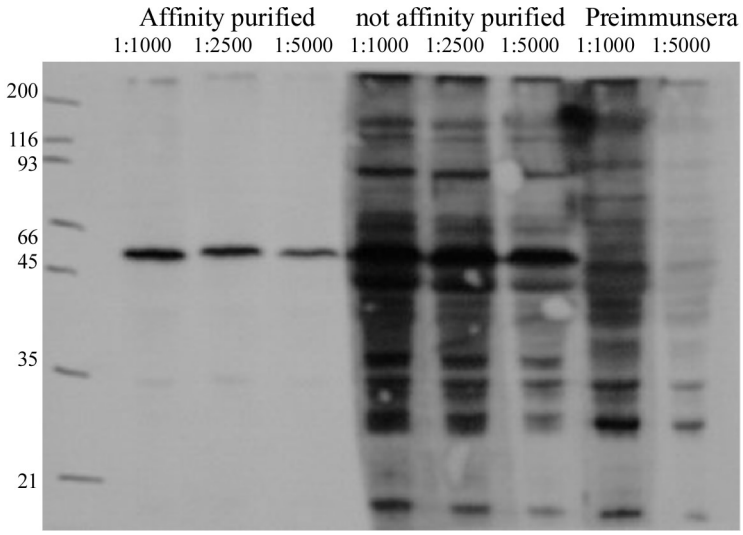

Figure 1. Characterization of an ArfGAP1 antibody. 20 mg of rat liver cytosol was applied to 12% SDS-PAGE and Western blot analysis was performed using preimmune and immune sera of ArfGAP1in the dilutions indicated.

To further characterize the antibody, Vero cells were fixed and endogenous ArfGAP1 was stained by immunofluorescence microscopy (Figure 2). This yielded a perinuclear staining similar as described in (Liu, *et al.*, 2005), that was absent in cells treated with secondary antibody only (not shown). Please note that immunofluorescence applications were not planned in the frame of this particular project, therefore the (known) subcellular localization of ArfGAP1 was only briefly investigated to test the antibody's capability in immunocytostaining (Figure 2).

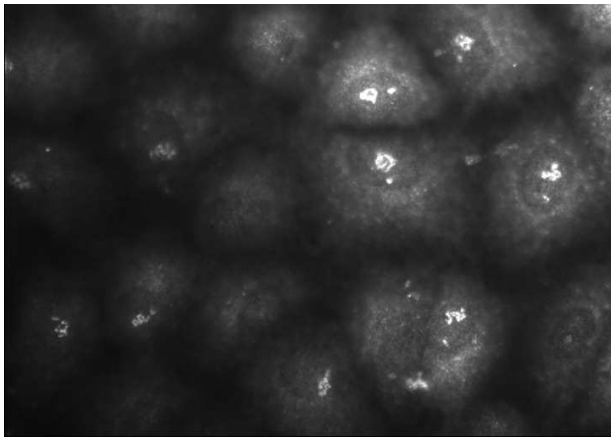

Figure 2. ArfGAP1 localization in vivo. The affinity purified antibody was used at a 1:1000 dilution and shows a perinuclear staining, presumably Golgi.

To test the antibody's capability to immunoprecipitate native ArfGAP1, the protein was overexpressed in *Pichia pastoris* and, after cell lysis and ultracentrifugation, the soluble protein extract was incubated with ArfGAP1 antibody that has been covalently crosslinked to protein-A sepharose. After removal of unbound material, samples were eluted at acidic pH and analyzed by SDS-PAGE followed by Western blotting using the antisera against ArfGAP1 (Figure 3)

Figure 3. ArfGAP1 IP from cytosol. 1 mg rat liver cytosol was used for immunoprecipitation, using 10µl affinity purified ArfGAP1 antibody covalently crosslinked to 20µl protein-A beads (IP). On the right hand lane (cytosol), 50µg rat liver cytosol was used for Western blotting

To estimate the efficiency of the immunoprecipitation, three successive rounds of IPs were performed with rabbit liver cytosol, and the supernatants were analyzed by SDS-PAGE and Western blotting for the presence of any remaining ArfGAP1 after the immunodepletion reaction (Figure 4). Obviously, one round of IP was sufficient to remove any detectable ArfGAP1 signal from the cytosol. Cytosol treated with preimmune serum still contains the protein, so does untreated cytosol.

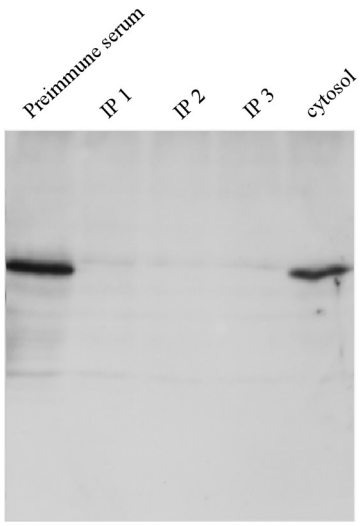

Figure 4. ArfGAP1 immunodepletion. Up to 5 mg rat liver cytosol were treated by three successive rounds of IP with the ArfGAP1 antibody and the supernatant of each round is loaded on the gel (IP1-3). As a control, the supernatant of the same amount cytosol immunoprecipitated with preimmune serum is loaded, which did not lead to a reduction of ArfGAP1, as expected (preimmune serum). The last lane shows the Western blot signal of untreated cytosol.

Cloning of full length ArfGAP1-wt and mutants into a *Pichia pastoris* expression vector

ArfGAP1 is not soluble when expressed in a prokaryotic environment, therefore a yeast expression system was chosen. To this end, the ArfGAP1 cDNA was cloned into a pPicZ-A (Invitrogen) Pichia expression vector by Iris Leibknecht.

Expression of full length ArfGAP1 in *Pichia pastoris*

ArfGAP1-HIS6 was expressed in Pichia pastoris according to the manufacturer's recommendations at 30° for 24 hours in small scale (15 ml culture), and the overexpressed protein was analyzed for solubility after centrifugation at 100,000g by SDS-PAGE and Western blotting with the anti-ArfGAP1 antisera. Full-length ArfGAP1 was not soluble under these conditions (data not shown). Therefore, to improve solubility, various expression conditions

were checked. Soluble ArfGAP1 was obtained by expression at 20°C for 36 hours, and this defined the standard for all successive expressions of ArfGAP1-constructs in *Pichia pastoris*.

Purification of full-length ArfGAP1-HIS$_6$ from *Pichia pastoris*

Protein expression was scaled up to 2 liters and after cell lysis and centrifugation, Ni^{++}-NTA purification was performed. After dialysis against a zinc-containing buffer, 1.2 mg ArfGAP1 was obtained at a concentration of 0.2 mg/ml (Figure 5).

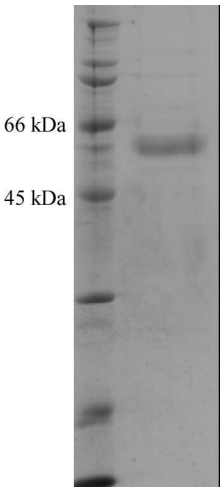

Figure 5. ArfGAP1 Ni++-NTA purification. The final fraction of the full-length ArfGAP1-purification from Pichia was checked by SDS-PAGE and Coomassie staining.

Purification of full length myristoylated Arf1

In this work, the original purification protocol for the expression and isolation of full length, untagged and myristoylated Arf1 (Franco, *et al.*, 1995) was modified, which allowed a faster and more reliable purification procedure. In short, cDNAs for humanArf1-wt and yeast N-myristoyltransferase (NMT) were co-transformed into a *E.coli* BL21 expression strain (Invitrogen) from a bicistronic plasmid. Before induction with IPTG, the medium of the main culture was supplied with myristate coupled to fatty acid-free bovine serum albumin (BSA).

Expression was carried out at 27°C to facilitate myristoylation. After cell lysis and ultracentrifugation, the protein extract was subjected to a 35% ammonium sulphate precipitation. The precipitated material, enriched for myrArf1, was desalted by gelfiltration (PD10, GE Healthcare), subjected to DEAE anion exchange chromatography, and eluted with a linear gradient from 0 to 1M potassium chloride in 10 column volumes. Typically, Arf1 eluted in the first peak and yielded a 90% enrichment for the myristoylated form (Figure 6).

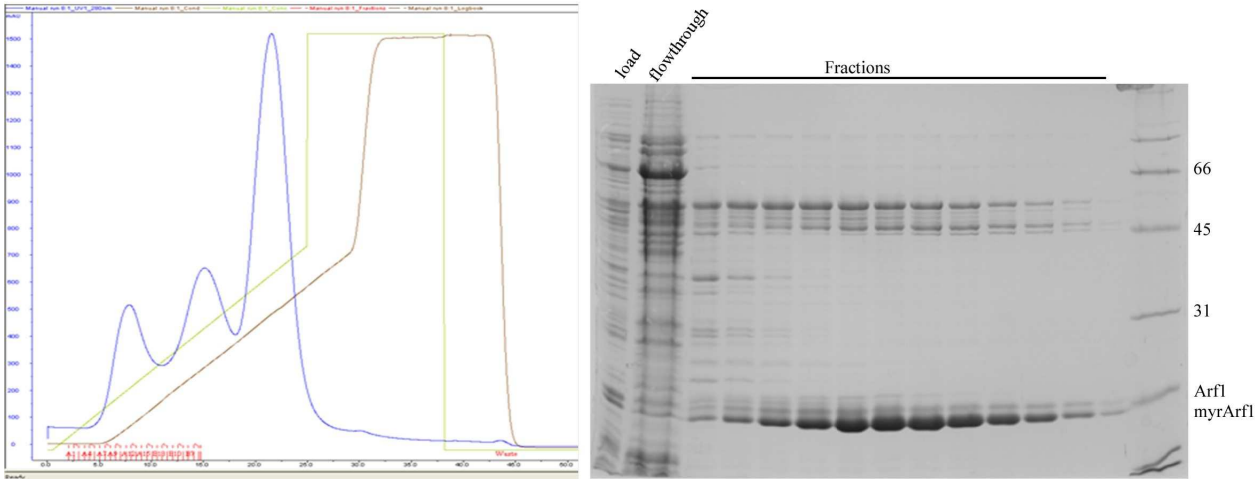

Figure 6. Purification of full length myristoylated Arf1. Left: DEAD anion-exchange chromatography profile. Absorbance in blue, KCl gradient in green, conductivity in brown. Right: Fractions of the first peak were analyzed by SDS-PAGE and Coomassie staining.

For further purification and quantitative separation of myristoylated from non-myristoylated Arf1, a reversed phase hydrophobic interaction chromatography was performed. In short, the Arf1 sample was adjusted to 3M potassium chloride and bound to a phenyl-sepharose column. Fractionated elution was performed by applying a descending gradient from 3 to 0 M KCl. Fractions were collected and analyzed by SDS-PAGE. Figure 7 shows an efficient removal of contaminating proteins (compare (Figure 6), right), as well as separation of myristoylated Arf1 (lanes 6 and 7) from non-myristoylated Arf1 (lane5).

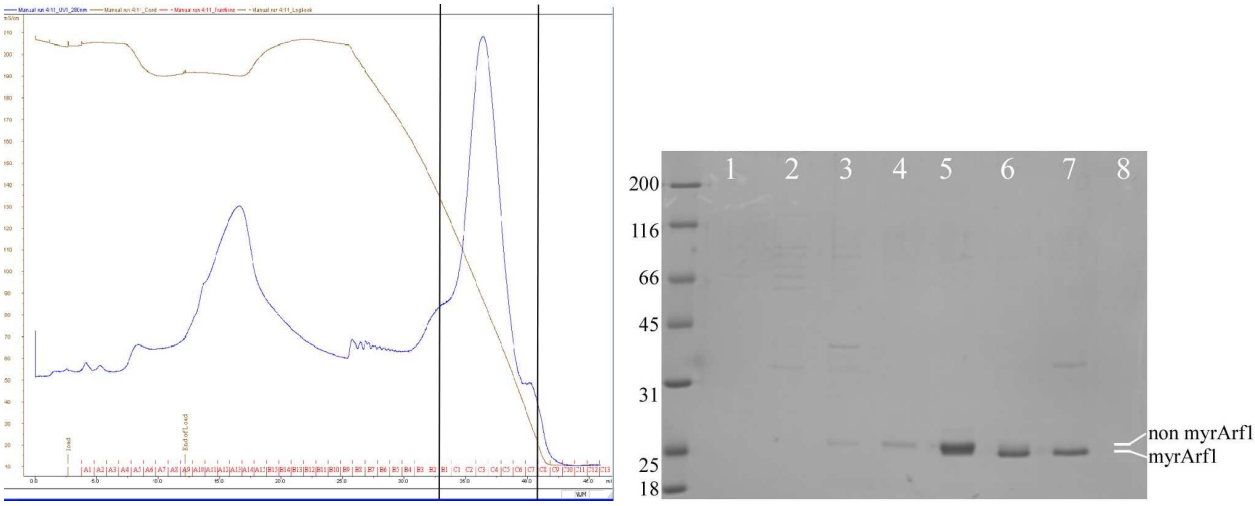

Figure 7. Reversed phase hydrophobic interaction chromatography. Left: Elution profile, OD280 in blue, conductivity in brown. Black bars indicate the fractions that were analyzed by SDS-PAGE. Right: SDS-PAGE and Coomassie staining of the Arf1-containing fraction that eluted from the column with descending salt concentration from left to right. The bands in lanes 6 and 7 correspond to purified myristoylated Arf1, the double band in lane 5 in addition contains some remaining non-myristoylated protein.

Measuring ArfGAP1 activity

In order to further characterize the recombinant ArfGAP1 from Pichia p., its activity was investigated (Antonny, *et al.*, 1997). This is performed in a fluorimeter assay, where a conformational change in Arf1, mediated by a ArfGAP1-mediated GTP hydrolysis, is followed over time by measuring tryptophane fluorescence. Golgi-like liposomes were prepared and extruded through polycarbonate filter membranes (Avestin) to select for size (Mayer, *et al.*, 1986). The homogeneity of this liposomal pool was assessed by dynamic light scattering, as shown in (Figure 8). A homogeneous pool of liposomes was obtained, with an estimated hydrodynamic radius of 30-40 nm. It was shown that under such conditions, membrane curvature is high enough to result in a strong activation of ArfGAP1 (Bigay, *et al.*, 2003).

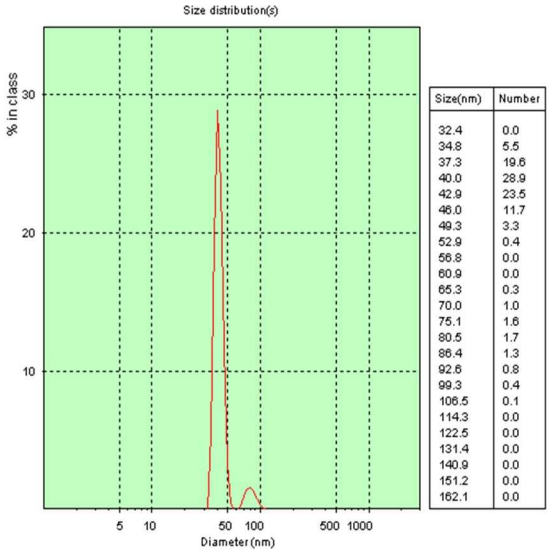

Size(nm)	Number
32.4	0.0
34.8	5.5
37.3	19.6
40.0	28.9
42.9	23.5
46.0	11.7
49.3	3.3
52.9	0.4
56.8	0.0
60.9	0.0
65.3	0.3
70.0	1.0
75.1	1.6
80.5	1.7
86.4	1.3
92.6	0.8
99.3	0.4
106.5	0.1
114.3	0.0
122.5	0.0
131.4	0.0
140.9	0.0
151.2	0.0
162.1	0.0

Figure 8. Dynamic light scattering of liposomes. The liposome preparation was subjected to extrusion through 30n, polycarbonate filter membranes . The homogeneity of the resulting population was checked by dynamic light scattering. A predominant peak corresponding to an average hydrodynamic radius of 40nm was obtained, together with a contaminating 80-90 nm population that only reflected about 2-5 percent of the total liposomes.

Full length myristoylated Arf1-GDP was incubated with 30 nm liposomes in the presence of excess GTP (200x). After addition of EDTA, nucleotide exchange occurs and triggers a conformational change in Arf1 which can be observed as an increase in fluorescence. After 10 min, the reaction was stopped by addition of $MgCl_2$, and a plateau was reached. Addition of ArfGAP1 triggers GTP hydrolysis, which resulted in a decrease of fluorescence (Figure 9). The non-hydrolyzable GTP-analog, GTPγS, did not lead to a decrease of the signal (not shown), as expected. This data showed that ArfGAP1-mediated GTP hydrolysis takes place and confirms the activity of both recombinant myrArf1 and ArfGAP1.

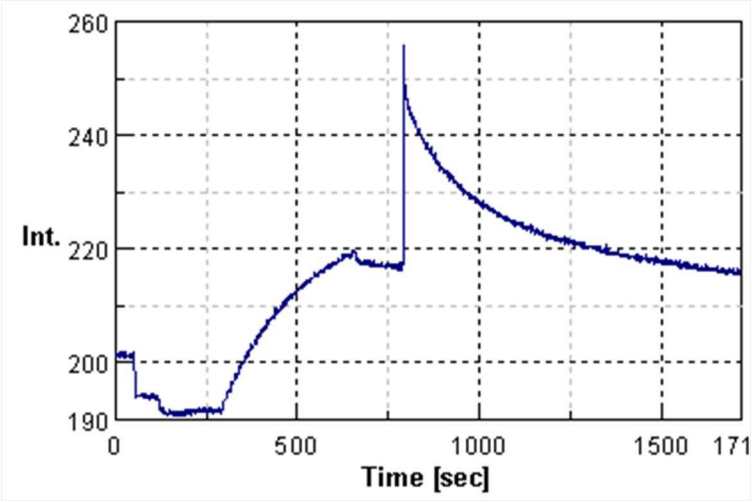

Figure 9. ArfGAP1 activity on liposomes. Full length myristoylated Arf1-GDP is incubated with liposomes and excess GTP in 1mM Mg++. After addition of the chelator EDTA, spontaneous diffusion takes place, allowing the loading of Arf1 with the excess nucleotide, resulting in a measurable increase of tryptophan fluorescence. The reaction was stopped by readdition of Mg++. Substoichiometric addition of ArfGAP1 initiated the reverse reaction and (after subtraction of the backbone fluorescence spike after addition of the protein), resulting in decrease of fluorescence to the previous level of Arf-GDP.

A truncation mutant of ArfGAP1, which lacks the motif for curvature sensitivity and hence increased activity, ArfGAP1$_{\Delta 197\text{-}415}$, exerted a strongly reduced activity on 30 nm liposomes, comparable to that described for curvature insensitive mutants (Bigay, *et al.*, 2005), data not shown.

GTP-hydrolysis prevents the accumulation of COPI coated vesicles *in vitro*

With the required minimal COPI-budding machinery at hand (Reinhard, *et al.*, 2003; Bremser, *et al.*, 1999), the role of ArfGAP1 in COPI-vesicle formation could be investigated on Golgi-membranes. To this end, a robust budding assay had to be established, that allowed vesicle formation under conditions where GTP-hydrolysis was permitted (to allow investigations both on GTP hydrolysis and uncoating, as well as cargo uptake), and could be controlled by addition of exogenous recombinant ArfGAP1. The first step was to remove residual GAP-activity from both the donor Golgi membranes and cytosol, (as the source for soluble COPI-machinery

proteins), in order to allow sufficient accumulation of COPI-coated vesicles by blocking the uncoating reaction mediated by ArfGAP1.

By IP, ArfGAP1 could be efficiently depleted from the cytosol, (see Figure 4), and treatment of Golgi membranes with 250mM salt (Ostermann, *et al.*, 1993) yielded a reduction of membrane-associated ArfGAP1 of about 90% as shown (Figure 10). Further increase of the salt concentration did not lead to any improvement on ArfGAP1 removal. As a control, the integral membrane protein p115 was not affected by salt treatment.

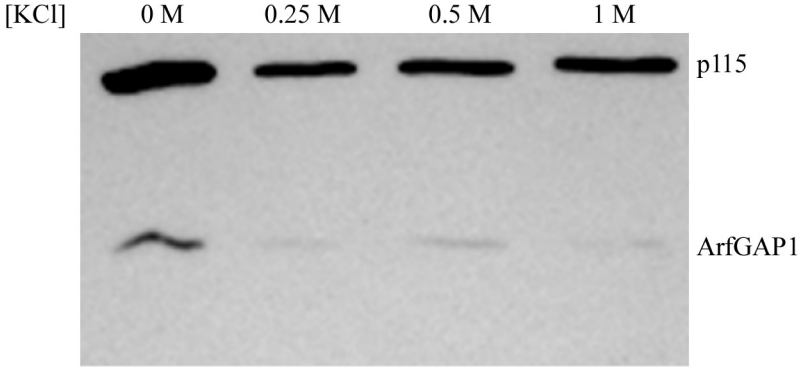

Figure 10. Removal of ArfGAP1 from Golgi membranes by salt treatment. 200 µg of Golgi-enriched membranes from rat liver were incubated with varying concentrations of potassium chloride on ice for 10 minutes, in order to break ionic interactions of integral membrane proteins or phospholipid headgroups with loosely associated soluble proteins (like ArfGAP1), followed by recovery of the membranes by centrifugation and SDS-PAGE analysis and Western blotting.

Despite an efficient reduction of ArfGAP1 activities on both cytosol and Golgi membranes, we never obtained detectable amounts of COPI vesicles under GTP conditions (not shown) by using the established COPI budding assay (Serafini, *et al.*, 1991) when using cytosol as the source for soluble proteins. Since there are two more ArfGAPs known as effectors of Arf1 on the Golgi, ArfGAP2 and ArfGAP3, antibodies against these proteins were raised and characterized by Carolin Weimer. With these tools at hand, cytosol was immunodepleted as described for ArfGAP1 (Figure 4). This resulted in a clear reduction of ArfGAP1-3 signals (Figure 11, left). As a control, treatment with ArfGAP-antibodies did not affect the level of Arf1. In addition, Golgi membranes were treated with 250 mM KCl to remove residual ArfGAPs1-3 (Figure 11,

right). In contrast to ArfGAP1, which could be removed by salt treatment (compare Figure 10), no detectable ArfGAP2 and ArfGAP3 signals were obtained under these conditions. As a control, the integral membrane protein p23 was not affected by salt treatment.

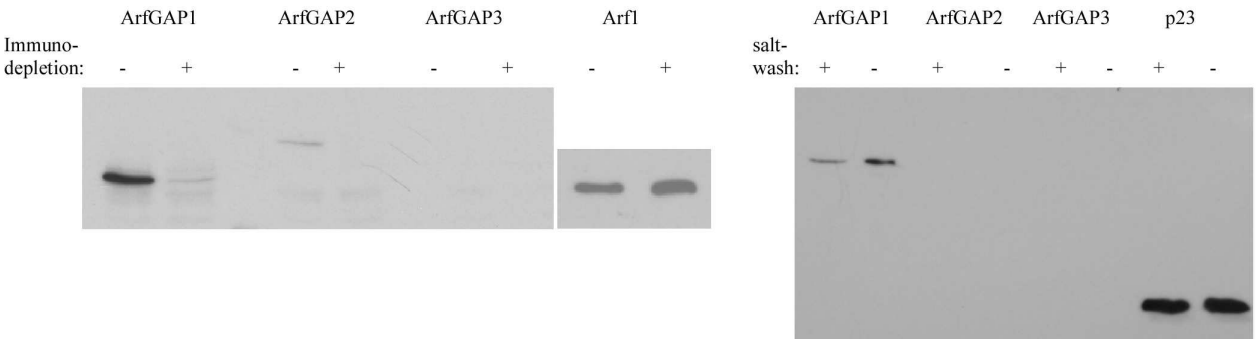

Figure 11. Removal of ArfGAPs1-3 from Golgi and cytosol. Left: ArfGAPs1-3 depletion. As in the previous experiment, immunodepletion was performed by using antibodies against ArfGAPs1-3. A significantly higher amount of ArfGAP1 was detected in 1mg of total cytosol, compared to GAPs2 and3, which was significantly reduced after immunodepletion. Right: 200µg rat liver Golgi membranes were treated with 250 mM potassium chloride to remove ArfGAPs 1-3. Salt treatment significantly reduced the levels for ArfGAP1, compared to the untreated sample, whereas ArfGAPs2-3 could not be detected on the Golgi under those conditions. As a control, the integral membrane protein p23 was unaffected by salt treatment.

Even under these conditions, when Golgi-ArfGAPs were reduced by at least two orders of magnitude, no detectable amounts of COPI-coated vesicles were obtained under GTP-hydrolysis permissive conditions, in contrast to budding assays in the presence of GTPγS (not shown). Since it could not be excluded that other factors than ArfGAPs1-3 drive GTP hydrolysis in Arf1, such as unknown GAPs or unspecific hydrolases, and therefore either prevent the formation of an Arf1-GTP dependent priming-complex, and/or promote the uncoating reaction too fast to isolate a detectable amount of coated vesicles (Tanigawa, *et al.*, 1993), a reconstitution assay with defined recombinant machinery proteins w**as** employed, that allowed for purification of COPI-vesicles in a faster scale.

The COPI-budding assay

Established budding protocols in the presence of GTP using isopycnic sucrose density gradient centrifugations (Serafini, *et al.*, 1991) are not suitable to prepare sufficient amounts of coated

vesicles, as the centrifugation times of 16 to 18 hours are too long to prevent uncoating. Another drawback of this procedure was that the results were hard to reproduce in terms of vesicle yield, and large quantities of the required materials (Golgi membranes and soluble budding machinery proteins) were needed (Malsam, *et al.*, 1999). This was partially solved by increasing the centrifugal force of the gradient from 100,000g to 400,000g (Malsam, *et al.*, 2005). This allowed a faster isolation of the vesicles, but controls showed that due to the high centrifugal force, soluble coatomer had sedimented into the fractions of 40-42% sucrose, even in the absence of membranes (data not shown). Therefore, although detectable amounts of GTP vesicles could be generated using this method, Western blot analysis proved to be difficult as the protocol did not allow to distinguish between coated membranes and soluble coat (data not shown).

In order to isolate the vesicles in a rapid way via a gentle centrifugation step and separating donor membranes, contaminating remnants and soluble coatomer from the COPI-vesicle fractions, a new approach was established during the course of this work. To reconstitute COPI vesicles in vitro, recombinant myristoylated wild type Arf1 and rabbit liver coatomer (Pavel, *et al.*, 1998) was incubated with rat liver Golgi membranes (Tabas and Kornfeld, 1979) in the presence of guanine nucleotides and an ATP regenerating system. The components were incubated at 37°C for 10 min to allow for COPI vesicle biogenesis. Reactions were stopped on ice and the salt concentration was raised to 250 mM KCl to release vesicles from their Golgi tethers. Donor membranes were pelleted by centrifugation at 12,000 g, the supernatant contained a mixture of COPI vesicles, soluble proteins and remnant Golgi fragments. This supernatant was loaded on top of two sucrose cushions and centrifuged at 100,000 g for 50 min. Aggregated material was then found at the bottom of the tube, COPI coated vesicles were concentrated in the 37-45 % sucrose interphase, whereas non-coated membranes, COPI-coated remnants, as

well as soluble proteins, stayed above this interphase (Figure 12). The purified vesicles were then further characterized by Western blot and electron microscopy. Under theses centrifugation conditions coatomer does not sediment into the vesicle fraction.

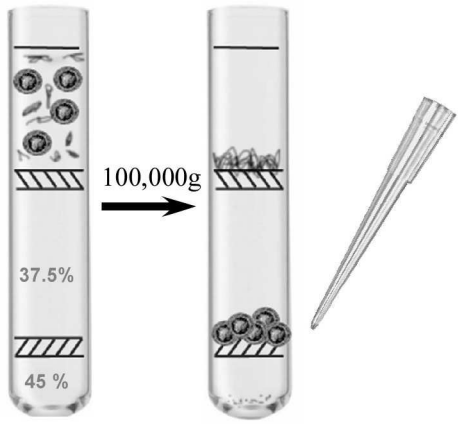

Figure 12. The COPI vesicle reconstitution assay. After incubation of Arf1, coatomer and salt washed rat liver Golgi, the donor membranes are pelleted and the supernatant, containing a mixture of COPI-vesicles, membrane fragments, coated remnants and soluble protein was laid on top of two sucrose cushions and purified by centrifugation. COPI vesicles are found in the 45%-37.5% interphase.

As a source for soluble budding machinery components, either purified proteins (Figure 13, left), or cytosol (Figure 13, right), were incubated with Golgi membranes. An input sample (0.5 % of the total reaction volume) was taken after the incubation step (lanes I). After isolation of the generated COPI-coated vesicles from the 45 % and 37.5 % sucrose interphase, 50 % of the isolated vesicle fractions were separated by SDS-PAGE and analyzed by Western blotting with antibodies against coatomer subunits, Arf1 and p24 (lanes V).

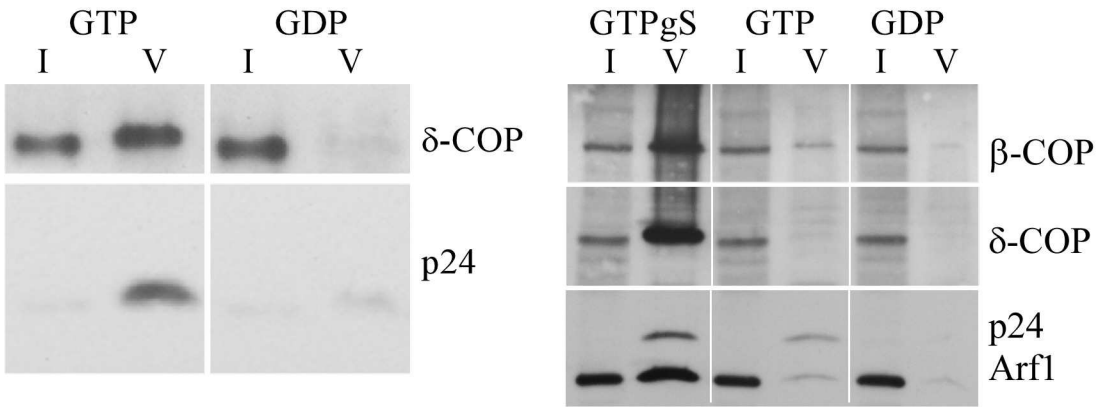

Figure 13. COPI-budding is nucleotide dependent. Left: The budding assay using salt-washed Golgi membranes and recombinant Arf1 and coatomer to reconstitute COPI-budding. In this case the amount of ArfGAPs in this system is small enough to allow for efficient purification of COPI-coated vesicles in a GTP-dependent manner. Right: the budding assay with cytosol as source for soluble budding machinery. Under these conditions, only with the non-hydrolyzable guanine-nucleotide GTPγS was a significant amount of vesicles generated, as estimated by SDS-PAGE and Western blot analysis against COP-subunits and the membrane protein p24.

When cytosol was used, very weak signals were obtained under GTP-conditions, comparable to background signals in the GDP control. Only a non-hydrolyzable GTP-analog like GTPγS yielded significant amounts of coated vesicles.

To further assess if the nucleotide dependent signals in the vesicle fractions indeed reflected COPI vesicles, electron microscopy of the samples was performed on carbon grids stained with uranyl acetate. As illustrated in (Figure 14), a homogeneous pool of protein coated structures with an average diameter of about 70-80 nm was isolated. These structures were absent from samples generated under GDP conditions, where also no Western blot signals were obtained.

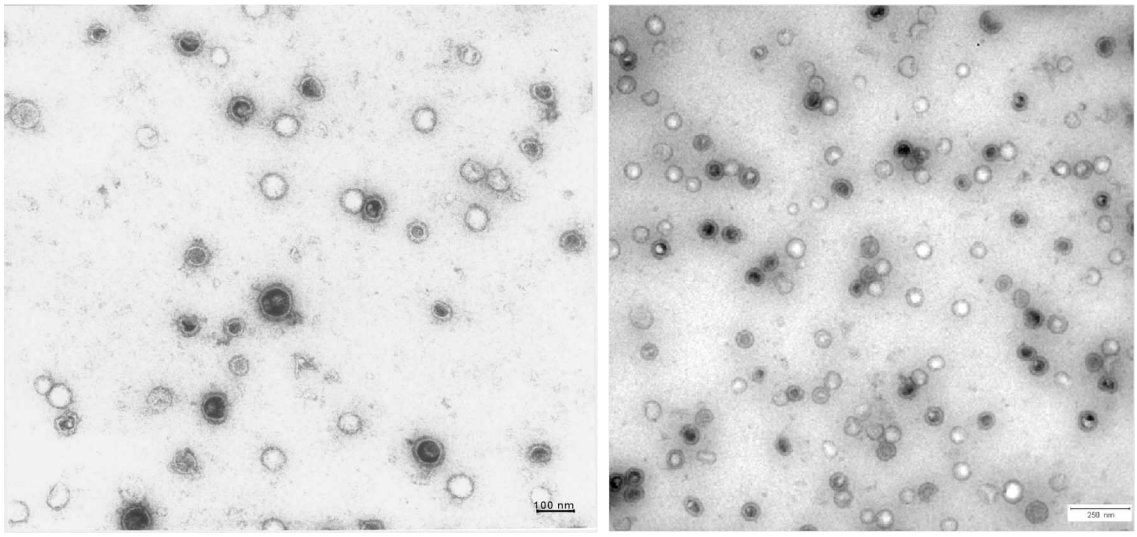

Figure 14. Electron microscopy of COPI-coated vesicles. Typical populations of COPI-vesicles yielding homogeneous pools of structures 70-80nm in diameter. In some cases the uranyl acetate entered the sample, which resulted in dark staining, compared to the white surface staining of intact vesicles. Left: scale bar 100nm, right: scale bar 250 nm.

ArfGAP1 activity and vesicle formation

It was shown before that the ArfGAP1-catalytical domain alone is sufficient to release coatomer from COPI-coated liposomes (Reinhard, *et al.*, 2003). In order to verify these results with full length ArfGAP1, which became available during this work, and in a more physiological context by using Golgi membranes instead of synthetic liposomes, the budding assays described above were used to study the role of ArfGAP1 in COPI vesicle formation. To this end, vesicles were generated in the presence of GTP and varying amounts of ArfGAP1 (Figure 15).

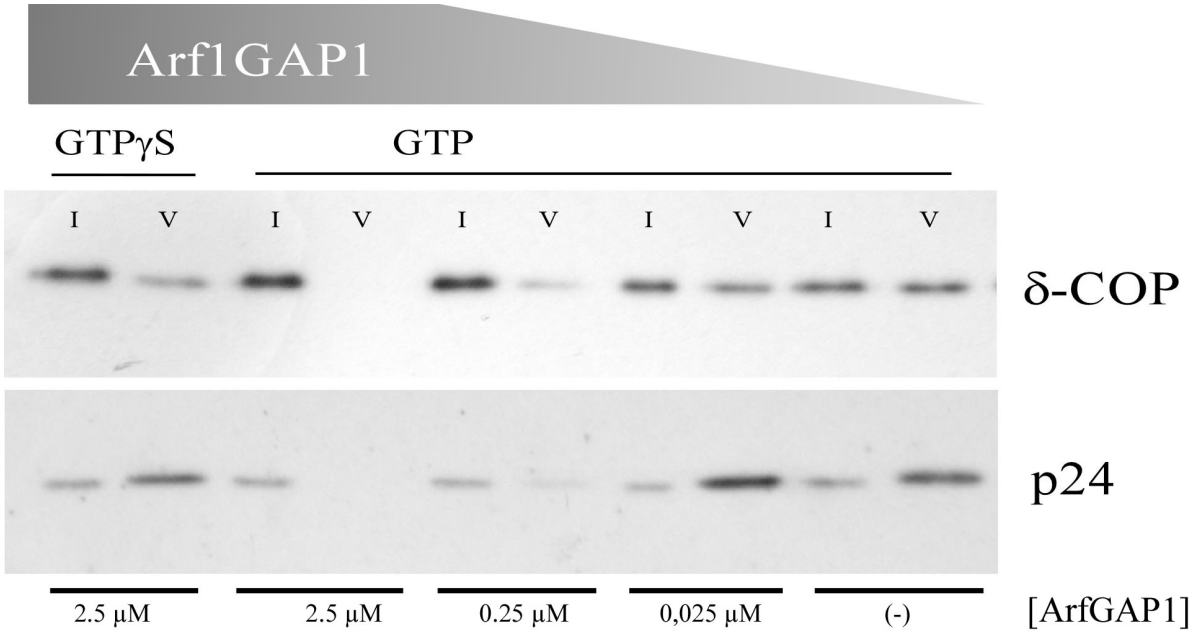

Figure 15. ArfGAP1 antagonizes the accumulation of COPI-coated vesicles. Budding assays were performed in the presence of GTPγS or GTP with varying amounts of ArfGAP1 present during the incubation. Vesicles were purified as described above and analyzed by SDS-PAGE and Western blotting against δ-COP and p24. For each sample, 0.5% of total input (I) and 50% of the purified vesicle fraction (V) was loaded.

In the presence of 2.5 µM ArfGAP1, no signals were detected under GTP conditions, whereas the non hydrolyzable GTP analog, GTPγS, was not affected by ArfGAP1 activity. Reducing the amount of ArfGAP1 in the system stepwise by a factor of ten gave rise to Western blot signals for coat proteins (δ-COP) and membranes (p24). At a concentration of 250 nM ArfGAP1, partial uncoating took place, as the signals were reduced as compared to GTPγS conditions, or to conditions where no ARFGAP1 was added. Quantitative analysis of three independent experiments are summarized in (Figure 16).

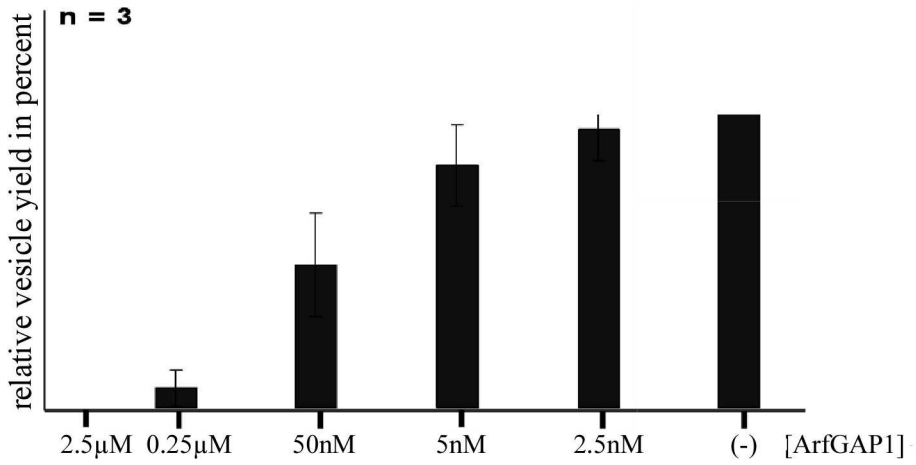

Figure 16. ArfGAP1 antagonizes the accumulation of COPI-coated vesicles. Coatomer signals from three independent budding experiments with varying amounts of ArfGAP1 were quantified. Vesicle yield is concentration-dependent with regard to the amount of ArfGAP1 in the system.

In order to verify that the detected coatomer signals in the Western blot analysis could be correlated to the presence of membranes the lipid content of the samples was assessed by electrospray ionization tandem mass spectrometry (Figure 17).

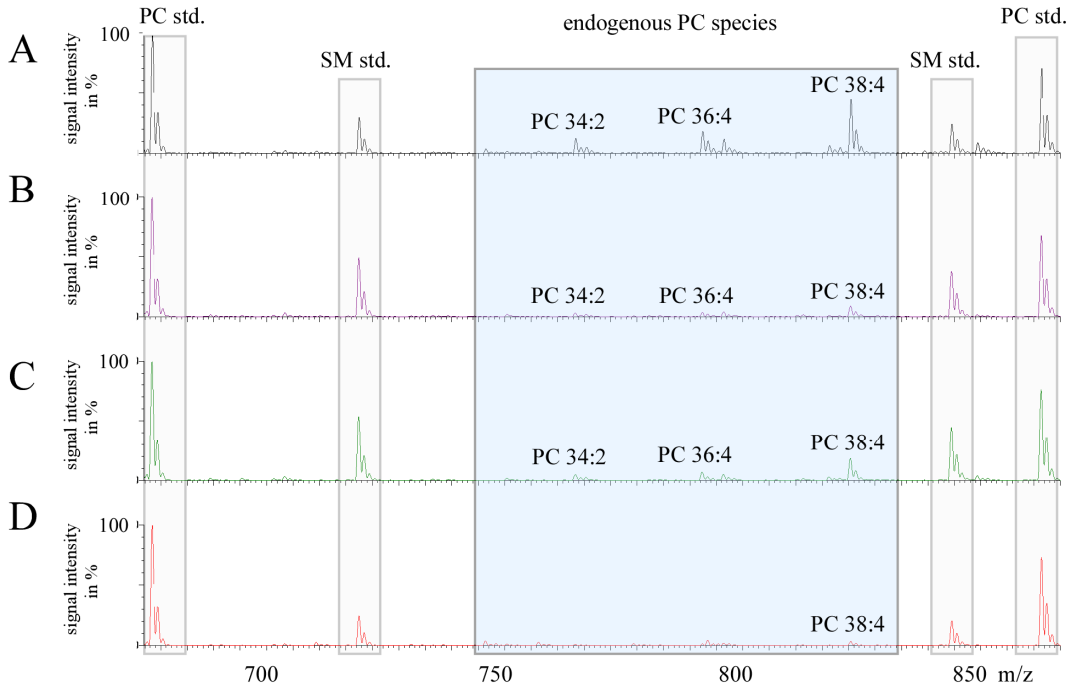

Figure 17. ESI-MS to assess lipid content in vesicle fractions. Budding assays were performed with varying amounts of ArfGAP1, and after lipid extraction, subjected to electrospray ionization tandem mass spectrometry to assess the lipid content of the samples. Profiles of the most prominent phosphatidyl choline molecular species (PC 34:2, PC 36:4, PC 38:4) are depicted,

indicated by the box. Positive control (GTPγS, profile A), profiles B (GTP, 250 nM ArfGAP1) and C (GTP, 25 nM ArfGAP1). No detectable lipid was present in profile D (negative control, lacking both GTP and Arf1GAP1).

ArfGAP1-activity allows uptake of anterograde cargo into COPI vesicles

It has been shown before that by blocking GTP-hydrolysis during their formation, COPI-coated vesicles are depleted of cargo (Nickel, *et al.*, 1998; Malsam, *et al.*, 1999; Pepperkok, *et al.*, 2000). To investigate the influence of ArfGAP1-activity on cargo uptake into COPI-vesicles, budding assays with varying amounts of ArfGAP1 were performed. We sought to find ArfGAP1 concentrations that would allow to isolate and analyze COPI coated vesicles, but at the same time would provide enough ArfGAP1 activity to allow to analyze an influence on cargo uptake by GTP-hydrolysis. A typical ArfGAP1 titration in the budding assay is shown in (Figure 18), left hand side.

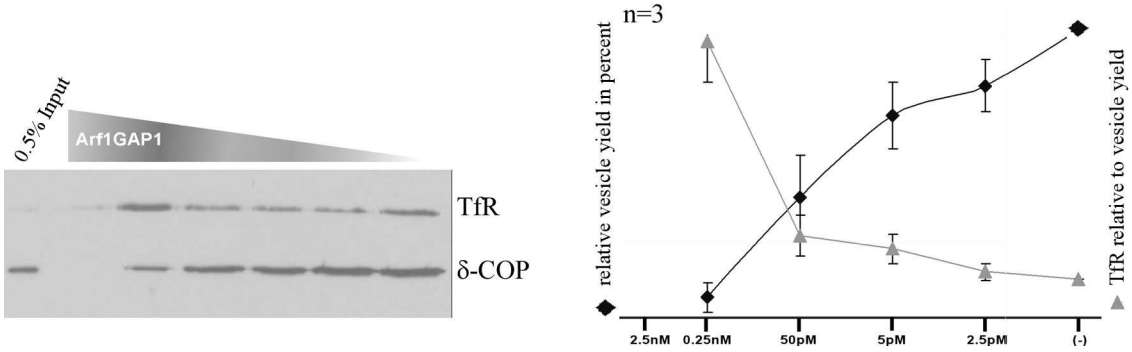

Figure 18. ArfGAP1 promotes uptake of anterograde cargo into COPI vesicles. Left: Budding assays in the presence of decreasing amounts of ArfGAP1. Coatomer and a model marker for anterograde cargo, transferrin receptor (TfR), were analyzed in the presence of varying ArfGAP1 concentrations. Right: coatomer signals were plotted as a function of ArfGAP1 decreasing concentration (squares). Cargo per vesicle (TfR / coatomer) was plotted as a function of decreasing ArfGAP1 concentration (triangles).

As we have shown that coatomer signals can be correlated to membranes, and therefore COPI vesicles, we correlated the transferrin receptor signals (as model protein for anterograde cargo)

in each lane to the corresponding δ-COP signals on the Western blot, in order to obtain a signal for the ratio of cargo per vesicle. As can be seen in Figure 18 right panel, cargo per vesicle increases with the amount of ArfGAP1 given (light grey curve), whereas the overall vesicle yield goes down (dark grey curve) at the same time. Taken together, these results confirm that ArfGAP1-mediated GTP-hydrolysis is required for cargo uptake, as described previously in the literature, but this time under more physiologically relevant conditions by using Golgi enriched membranes and full-length proteins. This bivalent function of ArfGAP1, to drive uncoating and cargo uptake by GTP hydrolysis, is debated however in the literature and will be subject of the next chapters:

A two-step incubation system for COPI-budding challenges the prevalent model of ArfGAP1 in COPI-vesicle biogenesis

Previous studies had defined the minimal machinery for COPI vesicle biogenesis and had demonstrated that ArfGAP-mediated GTP hydrolysis leads to uncoating (Reinhard, *et al.*, 2003). This view was expanded by the current work where full-length ArfGAP1 and Golgi membranes were used. However, another research group reported an essential role for ArfGAP1 in vesicle biogenesis, rather than uncoating, and described the enzyme to represent a stoichiometric component of the COPI-coat (Yang, *et al.*, 2002), and that by abolishing ArfGAP1 catalytic activity, vesicle formation was impaired (Lee, *et al.*, 2005). These findings are in contrast to what we and others (Cukierman, *et al.*, 1995; Reinhard, *et al.*, 2003; Tanigawa, *et al.*, 1993; Bigay, *et al.*, 2003) had observed and therefore the two-step incubation system described by these authors was used to investigate this discrepancy. Briefly, Arf1 and coatomer were incubated with Golgi membranes and bound material was recovered by centrifugation and resuspended. The samples were then incubated a second time, now with ArfGAP1. After

removal of the donor Golgi membranes by centrifugation, the supernatant (now containing a mixture of soluble coat proteins and vesicles) was analyzed by Western blotting and electron microscopy, using gold-conjugated antibodies against COP-subunits (Figure 19).

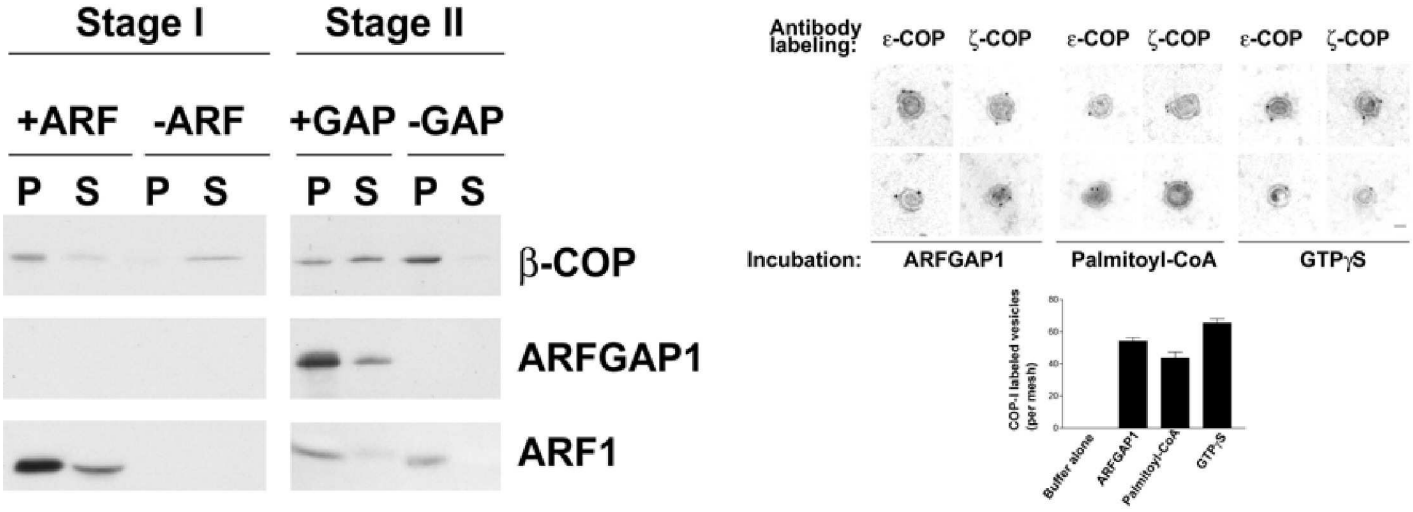

Figure 19. The two step incubation system. Taken from Yang *et al*. J Cell Biol 159, 69-78 (2002). Left: Arf1 and coatomer were recruited to the Golgi membrane, coatomer binding was dependent on the presence of Arf1-GTP. The pellets from stage I were resuspended and incubated in the presence of ArfGAP1 (stageII). After removal of the donor membranes by centrifugation, the supernatants of stage II were subjected to SDS-PAGE and analyzed by Western blotting against β-COP, ArfGAP1 and Arf1 antibodies. Right: COPI-vesicles purified from the stage II supernatant and labeled with gold-conjugated antibodies against COP-subunits.

These data suggest a function for ArfGAP1 different to that observed by others and us and therefore the experiments were performed under the very same conditions, in order to investigate the cause of these discrepancies. An additional control was included, where the salt concentration was raised to 250 mM KCl in the second stage incubation, to ensure that tethered vesicles were released from the donor membranes prior to centrifugation Figure 20 (Serafini, *et al.*, 1991; Serafini and Rothman, 1992).

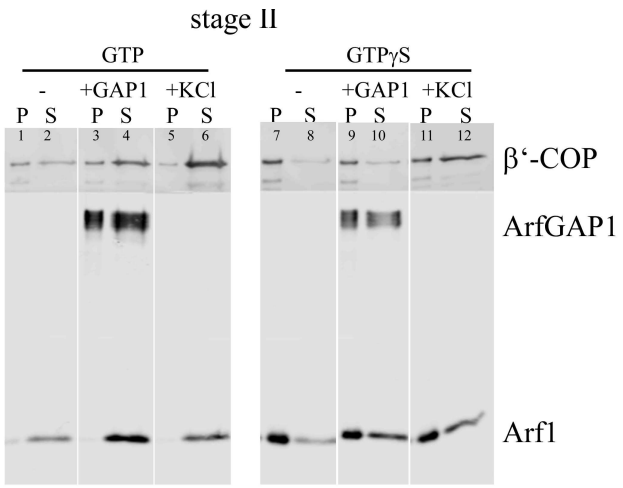

Figure 20. The two stage incubation system. Stage I stands for Arf1 and coatomer recruitment to Golgi membranes and is not shown in the figure. Soluble material is removed by centrifugation, the pellet is resuspended and incubated in stage II, either with buffer as a control, or with ArfGAP1, or 250mM KCl (stage II). These conditions were analyzed in the presence of either GTP or GTPγS.

Coatomer recruitment took place in the presence of GTP, whereas no coat was bound to the salt-washed Golgi membranes when Arf1 was omitted (not shown). The second step incubation of the resuspended pellet from stage I was carried out with buffer alone, ArfGAP1, or high salt, in the presence of either GTP or GTPγS. Addition of either ArfGAP1 or salt was required to obtain significant signals in the supernatant of stage II after centrifugation under GTP conditions, whereas only high salt yielded signals for coatomer when GTP hydrolysis was blocked by GTPγS. This control also demonstrates that no material was released non-specifically, for example by mechanical manipulation of the samples, as had been suggested in the literature (Yang, *et al.*, 2002).

On Golgi membranes, targeting of COPI vesicles is a multilayered process involving SNAREs, Rabs and tethers (Pfeffer, 1999). Tether pairs of the Golgin family (Barr, 2000), coiled-coil proteins that are regulated by small GTPases (Whyte and Munro, 2002; Gillingham and Munro, 2003; Shorter and Warren, 2002), may have roles in both grasping vesicles before release from the donor membranes (Orci, *et al.*, 2000; Orci, *et al.*, 1998) and capturing them at the target membrane. Experimentally, such interactions often can be abrogated by salt treatment, and this

is a step required in established *in vitro* assays to release formed vesicles from the donor Golgi (Serafini, *et al.*, 1991; Serafini and Rothman, 1992).

The experiment showed that ArfGAP1 is not required for COPI-vesicle biogenesis. The protein might help, however, to release coated vesicles form the Golgi membranes if the interactions with tethers are not dissociated by high salt. These findings were underlined by using the GTP-locked version Arf1-Q71L with GTP: again, COP signals in the stage II supernatant were only obtained by adding salt (Figure 21, compare lanes 10 and 12). Strikingly, ArfGAP1 signals were found in the supernatants independent of GTP hydrolysis, even when no coatomer (be it soluble or membrane-bound) was detected in the stage II supernatant, Figure 20, lane 10 and Figure 21, lane 10).

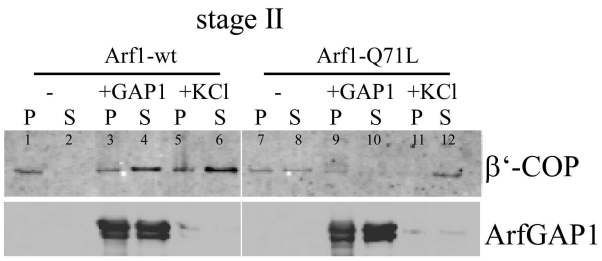

Figure 21. The two step reconstitution system with an GTP-locked Arf1-mutant. After Arf1 and coatomer binding to the membrane (stage I, not shown), samples were incubated in the presence or absence of ArfGAP1 or KCl (stage II). Lanes 1-6 Arf1-wt, lanes 7-12 Arf1-Q71L.

This shows that the assay is not suitable to discriminate between ArfGAP1 associated with remnant membranes or with COPI vesicles. To further assess if the released proteins of the stage II supernatant are membrane-bound, (Yang, *et al.*, 2005) subjected stage II supernatants to ultracentrifugation at 200,000g for 1h. We repeated this experiment, including an additional high-salt control. In accordance to the results published in (Yang, *et al.*, 2005), ArfGAP1 and coatomer signals were detected in the pellet (Figure 22, lane 3). However, when the GTP-locked

mutant Arf1-Q71L was used, only by prior addition of salt were coatomer signals detected in the pellet (Figure 22, compare lanes 9 and 11), in agreement with the above mentioned experiments. Interestingly, ArfGAP1 was detected in the pellet in the absence of COP signals, under conditions when GTP hydrolysis was prevented (Figure 22, lane 9). This again demonstrates that ArfGAP1 signals in this assay do not allow to discriminate between ArfGAP1 bound to remnant membranes or to COPI vesicles.

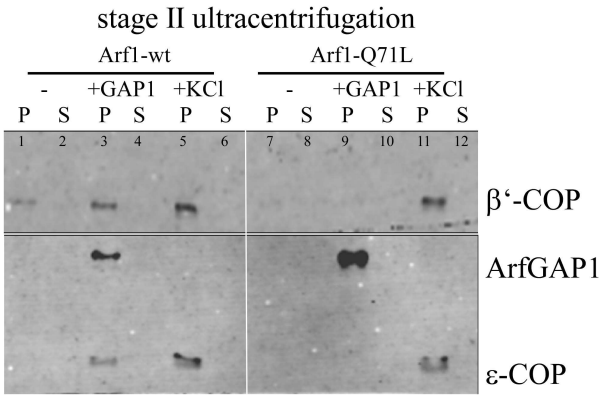

Figure 22. Solubility of proteins from the stage II incubation. Released material from the stage II incubation was subjected to 200,000g 1h.

To further challenge the conclusions in (Yang, *et al.*, 2005) based on such experiments, we analyzed the solubility of both coatomer and ArfGAP1 during ultracentrifugation for 1h, under varying centrifugal forces. To this end, the recombinant proteins were cleared of aggregates by a low spin centrifugation for 10 min and subjected to various centrifugation forces as indicated in Figure 23. Supernatants and pellets were analyzed by SDS-PAGE and Western Blot, and solubility was defined as the ratio of signal intensity of supernatant / pellet. While ArfGAP1, in the absence of membranes, remained soluble in all cases, coatomer sedimented quantitatively under these conditions.

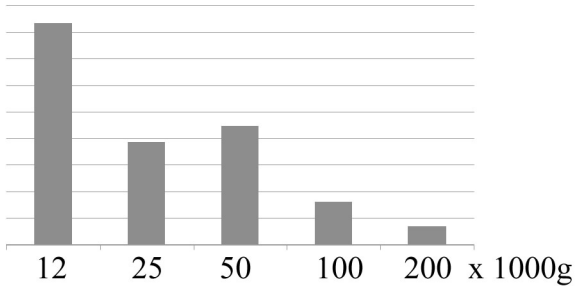

Figure 23. Solubility of coatomer in dependence of centrifugal force for 1h.

In order to estimate how much of the coat signals in the supernatant actually reflect membrane associated COP, the samples were loaded on isopycnic sucrose density gradients to separate membrane-bound from soluble material (Figure 24).

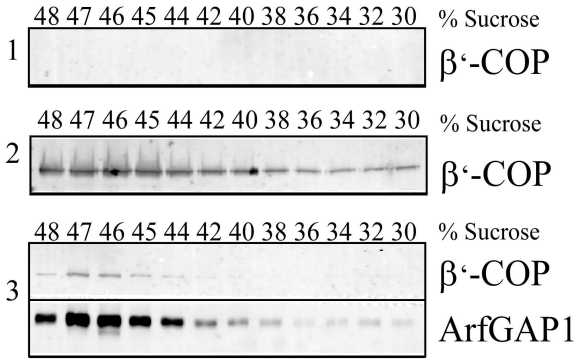

Figure 24. Floatation of the stage II supernatants. Samples were scaled up 5-fold and subjected to an isopycnic sucrose density gradient floatation. Fractions between 48% and 30% sucrose were analyzed by SDS-PAGE and Western blotting and assessed for the presence of b'-COP, ArfGAP1 and Arf1.

On gradient 1, as a control, a sample was loaded that contained neither ArfGAP1 nor high salt during the stage II incubation. As expected, no material was detected at the density of COPI-coated vesicles (between 44% and 38% sucrose). In gradient 3, the stage II supernatant generated in the presence of ArfGAP1 and GTP was analyzed. Under these conditions only minute quantities of coatomer could be detected at 44% to 38% sucrose. In the stage II supernatant containing 250 mM salt however, larger amounts of membrane-bound coatomer were found (gradient 2), suggesting that the addition of salt without any additional mechanical

manipulations is an efficient way to release vesicles from their Golgi tethers in the absence of ArfGAP1.

The stoichiometry of Arf1 to coatomer on COPI vesicles

(Yang, *et al.*, 2002) reported ArfGAP1 is essential for COPI-vesicle biogenesis and is a stoichiometric component of the COPI-coat. In contrast, we found that the enzyme antagonizes the accumulation of coated COPI-vesicles *in vitro* in a catalytic manner by catalyzing GTP-hydrolysis and thereby driving the uncoating reaction. This apparent discrepancy could at least partially be solved by the experiments shown above. (Yang, *et al.*, 2002) also reported that Arf1 does represent a coat component, as they never saw signals for the small GTPase on the 'vesicles' that were purified from the supernatant of their two step incubation (Figure 19, left). We could not confirm this by using the same experimental conditions, but rather obtained reasonably strong signals for Arf1 in the Western blots. Therefore, the Arf1 to coatomer ratio on COPI vesicles was investigated. There was evidence that more than one Arf1 binds to coatomer (Serafini, *et al.*, 1991; Sun, *et al.*, 2007; Sohn, *et al.*, 1996; Helms, *et al.*, 1993; Beck, *et al.*, 2008) and recent findings (see Part II of this thesis) showed that Arf1 needs to be a dimer in order to induce vesicle formation. In order to investigate the stoichiometry of coatomer and Arf1 on COPI vesicles, budding assays were performed in the presence of various guanine nucleotides, and vesicular components were quantified by SDS-PAGE and Western blotting in comparison with marker proteins that were loaded at defined amounts. Recombinant Arf1 and ε-COP were used as standards to quantify the amounts of Arf1 and coatomer in the vesicle fractions (Figure 25).

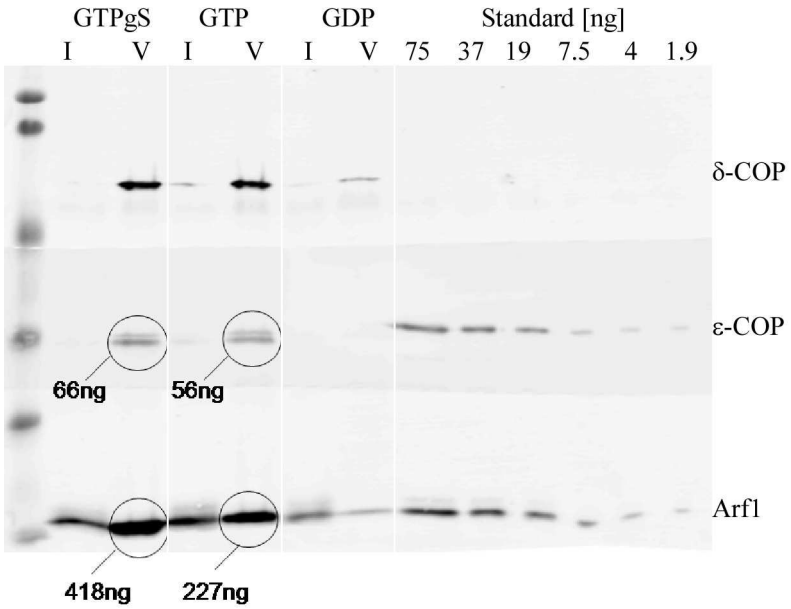

Figure 25. Stoichiometry of Arf1 and coatomer. COPI-vesicles were purified and analyzed by Western blotting using antibodies against COP-subunits and Arf1. Recombinant ε-COP and Arf1 are loaded at the indicated amounts in order to quantify the signals in the vesicle fractions (V).

These quantifications yielded a molar ratio of Arf1 to coatomer of about 10/1 under GTPγS conditions, and is in agreement with data published before (Sohn, *et al.*, 1996). In the presence of GTP, the ratio was decreased to six Arf1 per one coatomer. From Arf1 binding assays to Golgi, it is known that the membranes cannot be saturated by Arf1 (Helms, *et al.*, 1993). The authors proposed the existence of two Arf1-pools, one specifically bound e.g. via protein-protein interactions, the other one by unspecific affinity of Arf1-GTP to the membrane. Since the latter pool might bias the result, COPI-vesicles were purified and extracted with an excess of liposomes, in order to allow unspecific membrane-associated Arf1 to diffuse and bind to the excess liposomal membranes. After incubation, COPI-coated vesicles were separated from the liposomes by centrifugation through a 25% sucrose layer and analyzed by SDS-page and Western blotting to quantify the amount of Arf1 per coatomer. As a result, an about twofold reduction of Arf1 per coatomer after back loading was observed (Figure 26).

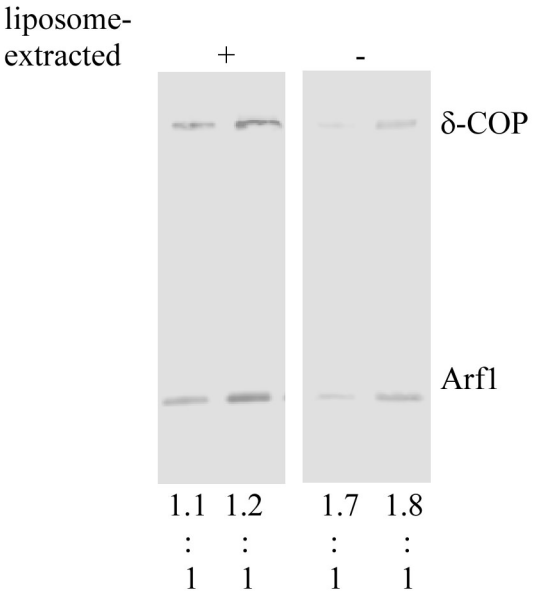

Figure 26. Liposome extraction of COPI-vesicles to remove unspecifically bound Arf1. The signals were quantified and the ratio of signal intensity of Arf per coatomer was determined before or after back loading.

From this we assumed that about half of Arf1 quantified on the vesicles before backloading was bound specifically. This reduces the Arf/coatomer ratio to about 4-5 / 1 for GTPγS conditions, and to about 3-4 / 1 in the presence of GTP, in agreement with (Serafini, *et al.*, 1991). These results are summarized in Figure 27.

	GTPγS	GTP	GTPγS	GTP
Lipid extracted	-	-	+	+
Arf1 / coatomer on COPI-vesicle	10	6	4-5	3-4

Figure 27. Arf1 to coatomer stoichiometry on COPI-vesicles.

In order to further analyze if Arf1 in fact is part of the COPI coat, we performed COPI vesicle assays in the presence of excess Arf1, but with coatomer as the limiting factor for the budding reaction, as shown in Figure 28.

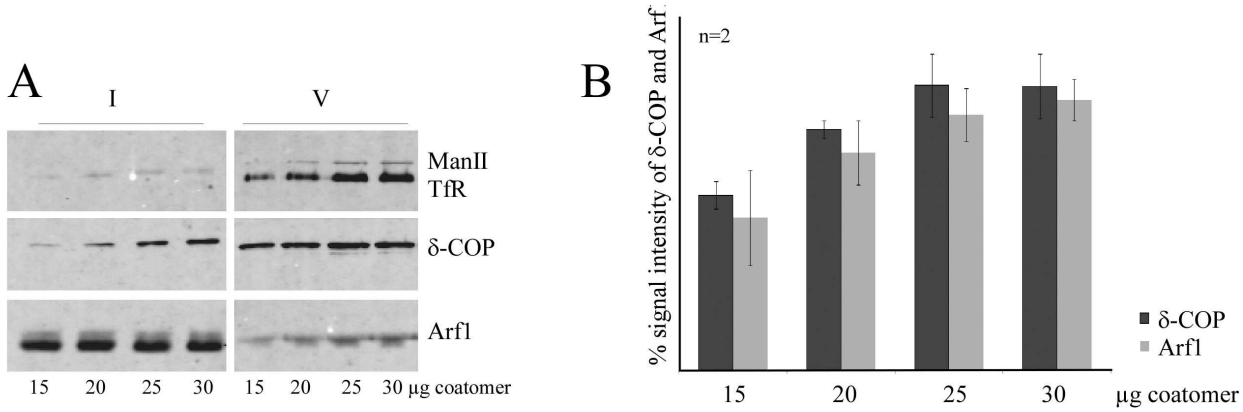

Figure 28. Arf1 stoichiometry on COPI vesicles with coatomer as limiting factor. A: COPI vesicles were purified in the presence of GTP under conditions where coatomer is the limiting factor for vesicle yield. 0.5% input (I) and 50 % of the vesicle fractions (V) with varying amounts of coatomer (and constant amounts of Arf1 and Golgi) as indicated, were subjected to SDS PAGE and Western blot analysis. B: Quantification of COP and Arf1 signals as a function of coatomer concentration.

Under such conditions, both COPI and Arf1 signals increased with the amount of coatomer given, demonstrating that Arf1 is included into COPI vesicles before they undergo uncoating. Likewise, an anterograde cargo marker (transferrin receptor (TfR)) and a retrograde cargo, (mannosidase-II (ManII) show coatomer dependence. Thus, Arf1 is an integral part of the coat.

Results Part II
A novel role for Arf1-GTP in COPI vesicle biogenesis

In the second part of this thesis we focused on Arf1, which is, like other small GTPases of the Ras superfamily, a key regulator of various cellular functions (Vetter and Wittinghofer, 2001). Arf1 is involved in the recruitment of coat protein complexes that polymerize on endomembranes to form transport vesicles (Serafini, *et al.*, 1991; D'Souza-Schorey and Chavrier, 2006). Activated Arf1 is always membrane associated since in this conformation its myristoylated N-terminal amphipatic α-helix is exposed, ensuring membrane anchorage (Antonny, *et al.*, 1997). As coat proteins can only bind to the active GTPase (Zhao, *et al.*, 1997; Boehm, *et al.*, 2001; Austin, *et al.*, 2002), Arf1 is a key regulator of vesicle coating and uncoating. Indeed, activation of Arf1 is a prerequisite for coat recruitment (Donaldson, *et al.*, 1992; Ooi, *et al.*, 1998; Stamnes and Rothman, 1993), and Arf1-mediated GTP hydrolysis is necessary for coat release (Tanigawa, *et al.*, 1993; Zhu, *et al.*, 1998). Arf1-GTP is directly involved in the recruitment of coatomer (Zhao, *et al.*, 1997; Donaldson, *et al.*, 1992), the coat of COPI vesicles (Waters, *et al.*, 1991), and of the clathrin adaptor complexes AP-1 (Stamnes and Rothman, 1993), AP-3 (Ooi, *et al.*, 1998) and AP-4 (Boehm, *et al.*, 2001).

Arf1-GTP generates membrane curvature

In our attempt to understand the mechanism of vesicle budding at a molecular level, and in the light of Arf1's homolog in the COPII pathway, Sar1p, inducing membrane deformation (Lee, *et al.*, 2005), we investigated whether Arf1-GTP also has such a membrane activity. To this end, we made use of a light microscopic liposome tubulation assay, similar to (Roux, *et al.*, 2006). A mix of Golgi-like lipids, containing p23 lipopeptide (Bremser, *et al.*, 1999; Bigay and Antonny,

2005), was spotted on a glass surface and dried. After rehydration, lipid sheets were formed that could be observed by light microscopy. To this end, it was helpful to establish the method with model proteins that (i) did not bring with them the complication of nucleotide exchange and (ii) were known effectors of membrane curvature. To this end, we chose epsin1, which is implicated in clathrin-mediated endocytosis by binding to certain coat components (Chen, *et al.*, 1998). It was shown that the epsin N-terminal homology domain (ENTH) of epsin1 forms an amphipathic α-helix upon Phosphatidylinsositol (4,5)-bis-phosphate (PIP2) binding, and that this leads to the formation of tubules (Ford, *et al.*, 2002). The plasmid encoding ENTH-GST (kindly provided Prof. Dr. by Volker Haucke, FU Berlin) was transformed into BL21 cells and expression of a 2l culture was induced by IPTG, according to standard protocols. The protein extract was incubated with glutathione beads and eluted by thrombin cleavage, which resulted in an enrichment of GST-free ENTH (Figure 29).

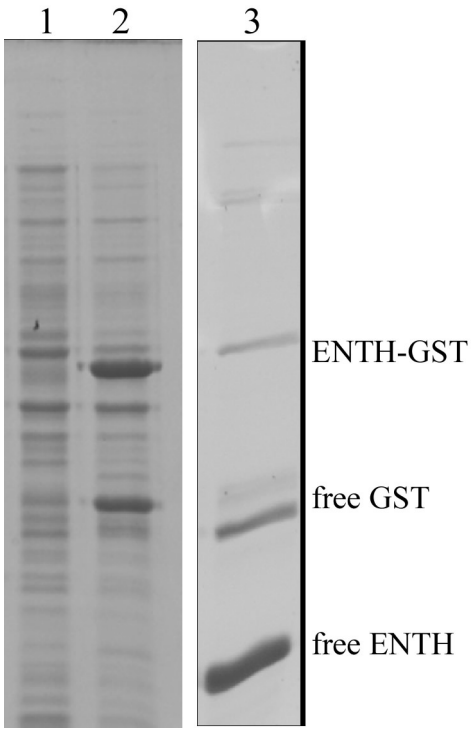

Figure 29. Expression and purification of ENTH. BL21 cells non-induced (lane1) and after IPTG induction (lane2), expressing ENTH-GST. The cleared lysate was incubated with glutathione beads and elution was performed by thrombin cleavage (lane 3).

Tubulation experiments were performed with ENTH in micromolar concentrations, as shown in Figure 30, panel A. As a control, thioredoxin constructs (Trx-cys-p23) were added instead of ENTH and had no effect on lipid morphology (Figure 30, panel B). As a further control, epsin1 had no effect on the lipid surface in the absence of PIP2 (data not shown).

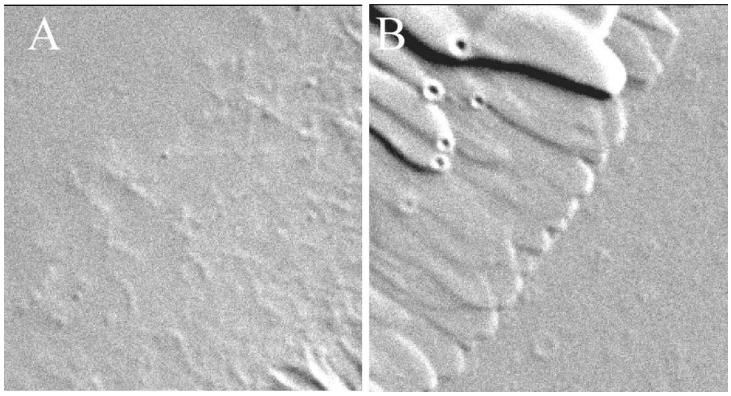

Figure 30. Tubulation of synthetic membrane sheets by epsin1. The protein was added (1µM) to membrane sheets and surface activity was monitored by DIC microscopy (A). Equal or ten-fold increased of free GST (not shown) and thioreoxin constructs had no effect on the lipid surface (B).

With this specific assay at hand, the nucleotide exchange factor ARNO (Chardin, *et al.*, 1996) and GTP were added into the tubulation chambers, and the reaction was started by addition of myristoylated Arf1-GDP. For easier performance of the assays, the DIC setup was replaced by an inverted bright phase microscope which facilitated the injection of the components. As shown in, Arf1 indeed catalyzes the GTP-dependent formation of tubules from lipid bilayers (Figure 31, panel A).

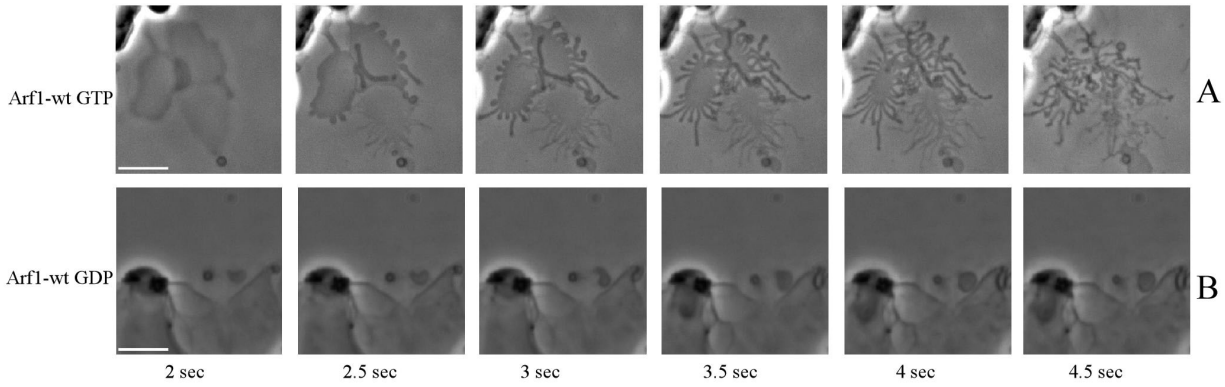

Figure 31. Arf1-mediated tubulation of synthetic lipid sheets. Lipids containing p23 lipopeptide were spotted on a glass surface and hydrated with buffer containing either GTP or GTP and the exchange factor ARNO (50 nM). After addition of myristoylated Arf1-GDP (1 µM), the lipid surface was observed by light microscopy (scale bars 5 µm). Reaction in the presence of Arf1-wt with GTP (panel A), and Arf1-wt with GDP (panel B).

This effect was observed at Arf1 amounts of 0.6 µg protein per µg lipids, similar to the concentration of F-BAR proteins that have been found to form tubules in (Frost, *et al.*, 2008). In the absence of GTP, no tubules were formed (Figure 31, panel B). Membrane activity and curvature induction was strictly dose dependent as shown in (Figure 32).

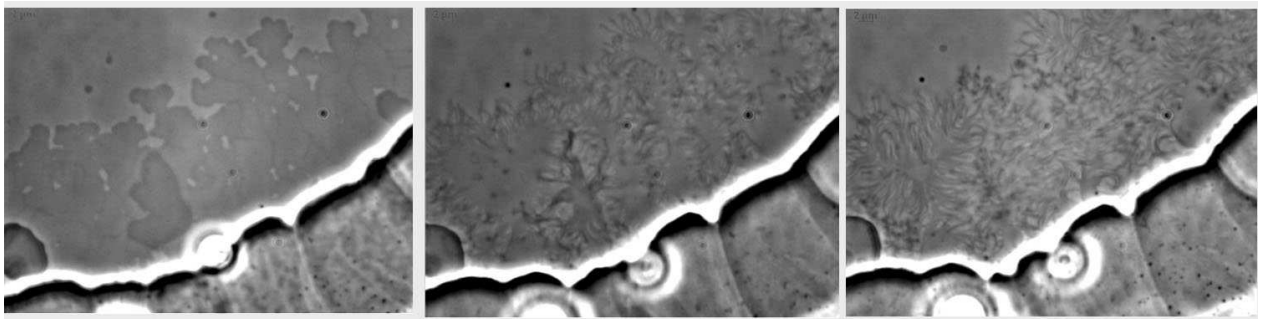

Figure 32. Arf1-mediated tubulation of membranes sheets is dose dependent. Arf1-wt was successively added to the tubulation assay and tubulation was observed with increasing protein concentrations.

Arf1 concentrations of 5 µM and above resulted in rapid tubulation reactions, whereas the efficiency was decreased at concentrations of 2.5 µM. Lowering the amount of Arf1 by a factor of two gave no longer rise to any observable reactions of the membrane surface. The order of addition of reaction partners was interchangeable and each sequence yielded the same result. Real time recordings of these assays allow an easier observation of the tubulation by Arf1GTP, and are found in supporting information (S1, S2 of (Beck, *et al.*, 2008)). Since the tubules were hard to visualize on static images due to the limitation of focus in the Z-axis, their small diameter, resolution plus contrast limitations of a light microscope, stacking and overlay effects due their high abundance, as well as their high motility, we tested if the addition of an Arf1-antibody had any effect on tubulation efficiency, morphology or dynamics. The observed effect of the antisera was dose dependent: in the presence of 1:10 diluted sera, no tubulation occurred (not shown). If tubules were generated in the absence of sera and the antibody was added

afterwards, the tubules immediately ‘froze’ and lost mobility (not shown), most likely due to cross-linking by the epitopes. By stepwise lowering the concentration of Arf1-antisera in the assays, we were able to ‘adjust’ tubulation effects in order to improve visualization. This resulted in much slower reaction times during tubule formation, impaired motility and fewer tubes in general, which facilitated imaging. As a control for specificity of these effects, epsin1 was used in the presence of Arf1 antibody, and as a result, no effect of the sera was observed, even at high concentrations of the antibodies (1:10 dilution of the sera). In the presence of Arf1 and GDP, the antibody also did not lead to tubulation, ruling out the possibility of factors in the sera having surface activity (not shown).

Next, we asked if the presence of coatomer had an effect on tubule formation. As a result, the morphology of the tubules was significantly different, as can be seen in Figure 33.

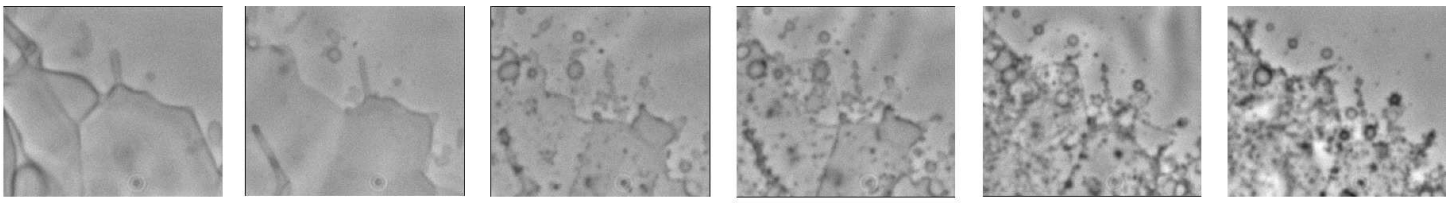

Figure 33. Arf1-mediated tubulation of lipid sheets in the presence of coatomer. ARNO and GTP were added to membrane sheets, then coatomer was added. The reaction was started by addition of Arf1 and formation of tubules was monitored over time as indicated.

Efficient tubulation was observed, however, the average diameter and length of the highly motile tubules seemed to be reduced by a factor of at least 5-10. These observations imply that attributions to curvature, mediated by both Arf1 and coatomer, might have a cumulative effect. Due to limitations of resolutions and contrast in phase contrast light microscopy, such highly dynamic structures were harder to visualize, especially for static images. Next, we asked if the addition of soluble coatomer to tubules generated in the presence of Arf1-GTP had an effect on

lipid topology. As drawback of the experimental setup, it turned out that addition of any solution to the generated tubes resulted in an instant loss of the majority of the tubular structures, most likely by exerting shear forces when adding a flow of additional components or buffer. However, some tubular structures remained and were rapidly degraded by coatomer, as one would expect from a system with the complete budding machinery present (Figure 34).

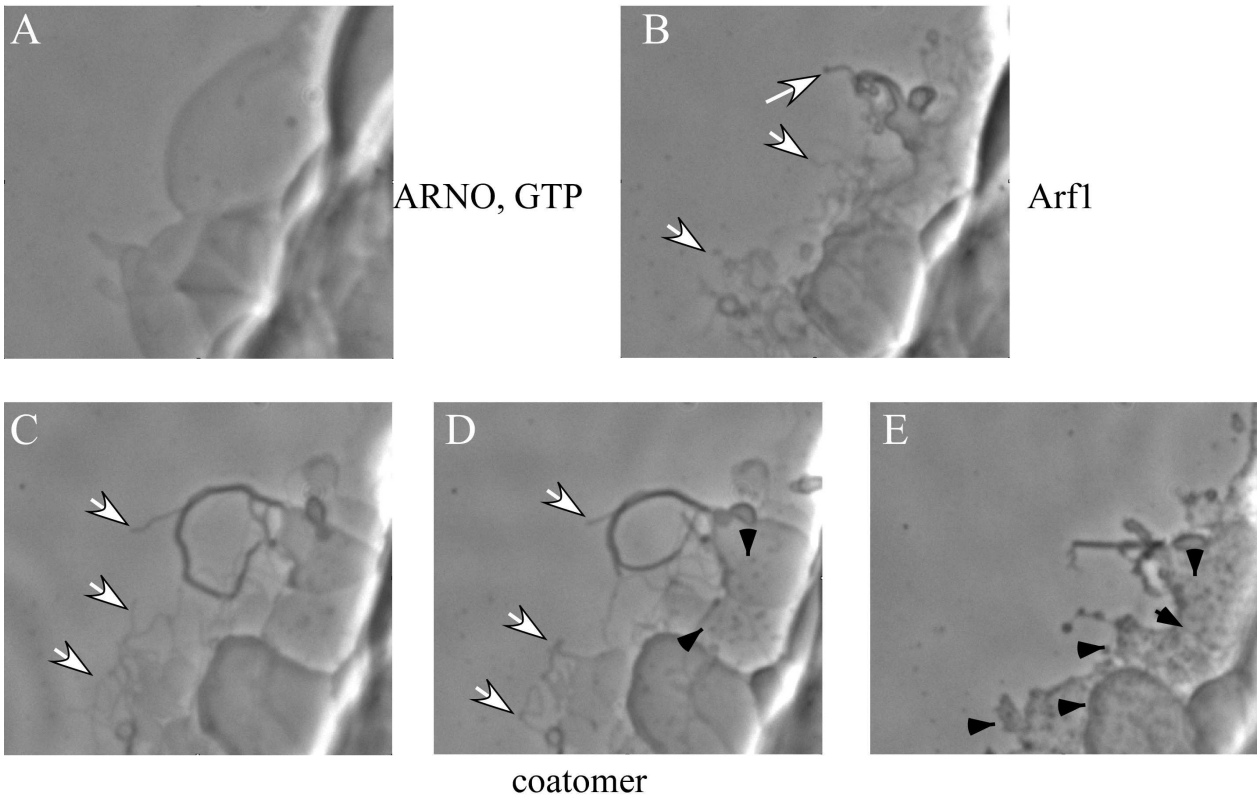

Figure 34. Sequential addition of Arf1 and coatomer on membrane sheets. (A) membrane sheets in the presence of ARNO and GTP. (B) Addition of Arf1 leads to the rapid formation of motile tubular structures of 5-10µm length (white arrows). (C-E) After coatomer addition, Arf1-induced tubes get rapidly shortened (white arrows), while highly motile new tubular structures appear which are significantly smaller (black arrows).

Arf1-GTP dimerizes on membranes

Many of the proteins that directly affect membrane curvature are dimeric or have multiple domains (Martens, *et al.*, 2007; Peter, *et al.*, 2004). As we had indications that Arf1 may

dimerize (Sun, *et al.*, 2007), this possibility was analyzed. To this end, recombinant myristoylated Arf1 was incubated with protein-free liposomes, GTPγS, and chemical crosslinkers. After isolation of the liposome-bound material and analysis by Western blotting, a crosslinker-dependent ~40 kDa band was observed with the homobifunctional thiol reagent Bis-maleimido-hexane (BMH, 0.5 mM, Figure 35, lane 4), as well as with a heterobifunctional reagent (active with thiol and amino groups) N-(ε-maleimido-caproyloxy)-N-hydroxy-succinimide ester (EMCS, 0.5 mM, Figure 35, lane 2). These experiments were performed by Dr. Zhe Sun and demonstrate that Arf1 efficiently dimerizes on membranes dependent on GTP, and in the absence of any additional factors (Beck, *et al.*, 2008).

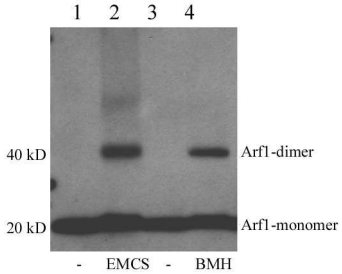

Figure 35. Arf1 dimerizes on membranes. Protein-free liposomes were incubated with full length myristoylated Arf1, GTP, and the crosslinkers EMCS (lane 2) or BMH (lane 4) as indicated. After centrifugation, the liposome-bound material was analyzed by Western blotting with an anti-Arf1 antibody.

To test if Arf1 also dimerizes on Golgi membranes (Beck, *et al.*, 2008), Arf1-wt was incubated with Golgi in the presence of nucleotide (GDPβS or GTPγS) and loaded onto a cushion of 15 % sucrose (wt/vol), followed by a 30 min centrifugation at 14,000 rpm (4°C). Pellets were incubated with varying concentrations of BMH and resuspended in SDS sample buffer. Membrane bound material was analyzed by SDS-PAGE and Western blotting with antibodies against Arf1 (Figure 36). Varying ratios of Arf1 and crosslinker were used as indicated in the figure, which established a saturation effect of the crosslinking agent at less than 20 molecules of BMH per Arf1.

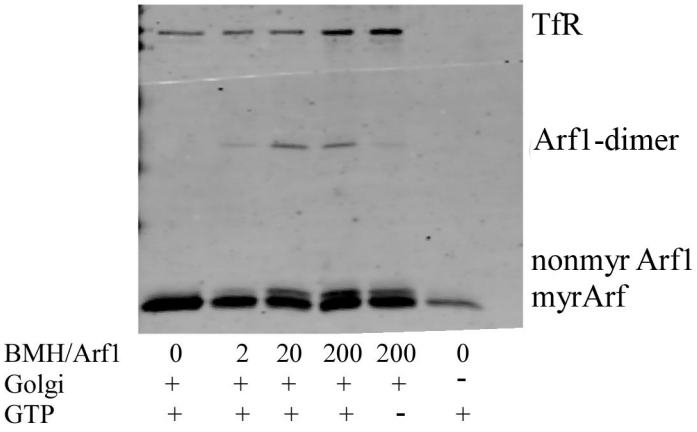

Figure 36. Titration of crosslinker. Varying amounts of the cystein-specific crosslinker BMH as indicated were incubated with Arf1-wt and Golgi membranes and membrane-bound material was analyzed by SDS-PAGE and Western blot with Arf1 antibody.

The Arf1-dimer interface

In order to elucidate a possible Arf1-dimer interface, the following constraints were applied in order to establish a structural model based on the crystal structure available with the highest resolution of a truncated soluble form of Arf1-GTP (PDB code 1O3Y) $N_{\Delta 17}$Arf1 (Shiba, *et al.*, 2003).:

-The N-termini must face the membrane

-Known binding sites for coatomer or ArfGAP1 must be accessible

-The distance of the two cysteins in one Arf1-dimer must be about 16 Å (Dr. Zhe Sun (Beck, *et al.*, 2008))

-Proteomic analysis of an Arf1-dimer did not pick up two peptides, which were, due to covalent crosslink, out of range of masses that were analyzed and therefore could be good candidates of a putative dimer interface (Dr. Zhe Sun, (Beck, *et al.*, 2008))

In collaboration with Dr. Clemens Wild and Prof. Dr. Irmi Sinning, a predicted dimer interface was computed. This yielded a homodimeric model of full length membrane-associated Arf1-GTP, which is symmetric and includes an intermolecular β-sheet completion formed by the interswitch regions. (Figure 37)

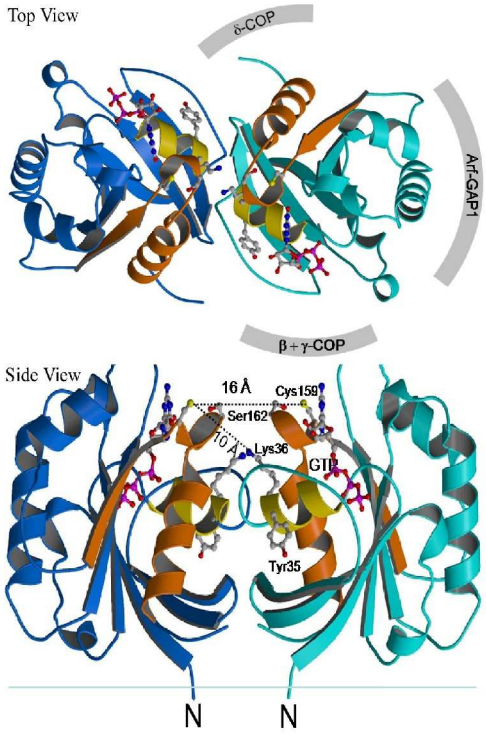

Figure 37. Model of the Arf1-GTP dimer in a view towards the membrane (top view) and from the membrane plane (side view). The model is based on the crystal structure of monomeric Arf1-GTP (PDB code 1O3Y) and the constraints as described in the text. The binding site of the Arf-GAP1 catalytic domain and mapped coatomer interactions are shown schematically for one monomer. The two missing cross-linked peptides from the mass spectrometry experiment are colored in yellow (31-36) and orange (152-178). The crosslinked residues are connected by dashed lines and their distances are indicated (the distance between Cys159 and Lys36 in the model is 10 Å, in accordance with the distance of the functional groups within the crosslinker EMCS). The interface coincides with the binding site of the N-terminal helix in Arf1-GDP and includes an intermolecular β-sheet completion formed by the exposed interswitch regions of Arf1-GTP.

The crystal structures of $N_{\Delta 17}$Arf1-GTP and full length non-myristoylated Arf1-GDP also show a dimer (Shiba, *et al.*, 2003; Amor, *et al.*, 1994), although these proteins were mainly found as monomers in solution, by gel filtration (data not shown). In these crystals, the dimerization interfaces are different from our model of a full length Arf1-GTP dimer, and would not allow the crosslinks we observed with regards to the experimentally determined distance between the two cysteine residues in an Arf1 dimer (Beck, *et al.*, 2008). Often, proteins crystallize in

oligomeric forms, which are not physiologically relevant (crystallographic oligomers). A structure of full length Arf1-GTP is not available because the protein is insoluble in the absence of membranes. This is of importance because the membrane accommodates the hydrophobic regions of Arf1 that are exposed in its GTP state, and may participate in the dimerization by orienting and stabilizing a biologically relevant dimeric structure (Antonny, *et al.*, 1997).

Characterization of an Arf1 variant that cannot dimerize

According to this model, single amino acids within and around the putative interface were exchanged for alanine by Dr. Zhe Sun, and the resulting Arf1 variants were probed for their ability to dimerize. A mutant Arf1-Y35A has lost the ability to dimerize, as analyzed by a crosslink assay of Golgi-bound Arf1 proteins (Figure 38).

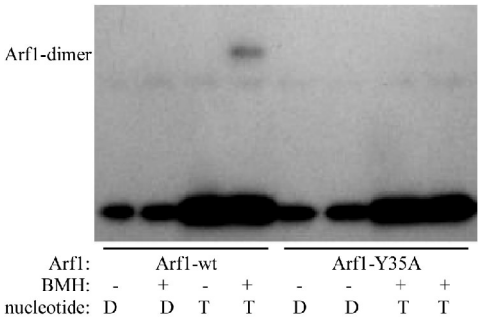

Figure 38. Arf1 chemical crosslinking on Golgi. Golgi-enriched membranes from rat liver were incubated with full length myristoylated Arf1-wt (WT), Arf1-Y35A, GTPγS, and, after recovery of membranes by centrifugation, the crosslinker BMH was added. Membrane-bound material was analyzed by Western blotting with an anti-Arf1 antibody.

As the figure suggests, this monomeric Arf1 variant still responded to the nucleotide present, as the signal intensity for Arf1-Y35A under GTP conditions, compared to GDP, was increased. In order to reveal any functions specific for Arf1 dimerization, we had to make sure that, apart from dimerization, other properties of Arf1-Y35A compare to the wildtype. To this end, a series of experiments were performed to characterize the mutant protein in terms of activity, binding partners and localization.

To assess the functionality of Arf1-proteins in terms of nucleotide exchange, they were incubated with Golgi-enriched membranes, radiolabeled GTP and the Arf-GEF ARNO. Protein-bound and free nucleotide was separated by gel filtration, and the fractions collected were analyzed in a scintillation counter. In detail, 20 µg Golgi-enriched membranes from rat liver were extruded through 200 nm pore size polycarbonate filter membranes (Avestin) and incubated in the presence of Arf1, GTP, [8-3H]-GTP (0.1µCi) and 1 nM ARNO in a final volume of 50 µl. After incubation for 5 minutes at 25°C, the reactions were subjected to gel filtration on Sephadex G-50. Radioactivity of each fraction was plotted against the fraction number (Figure 39).

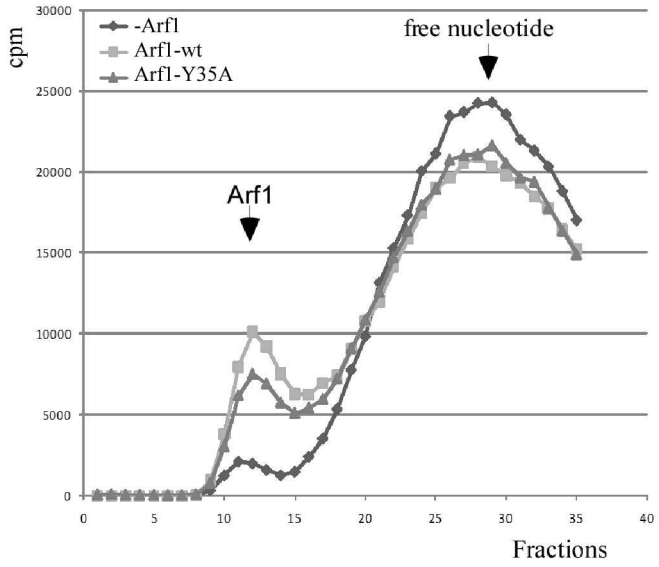

Figure 39. Nucleotide exchange activity on Golgi membranes of Arf1-wt and Arf1-Y35A. Arf1 proteins were incubated with Golgi-enriched membranes, radiolabeled GTP and the Arf-GEF ARNO. Protein-bound and free nucleotide was separated by gel filtration. The fractions collected were analyzed in a scintillation counter and radioactivity was plotted against fraction number

As can be seen, in the absence of recombinant Arf1, the peak corresponding to bound nucleotide (fractions 10-15) was significantly lower than the peaks obtained for Arf1-wt or Arf1-Y35A. From this data, we assessed the nucleotide exchange activity of monomeric Arf1 to about 70% of the wild type. This demonstrated an efficient Arf1-activation on Golgi membranes. Next, we checked Arf1-Y35A activity in a chemically defined system, with Golgi-like synthetic

liposomes instead of Golgi membranes (Figure 40). Relative counts per minute was plotted against the fraction number.

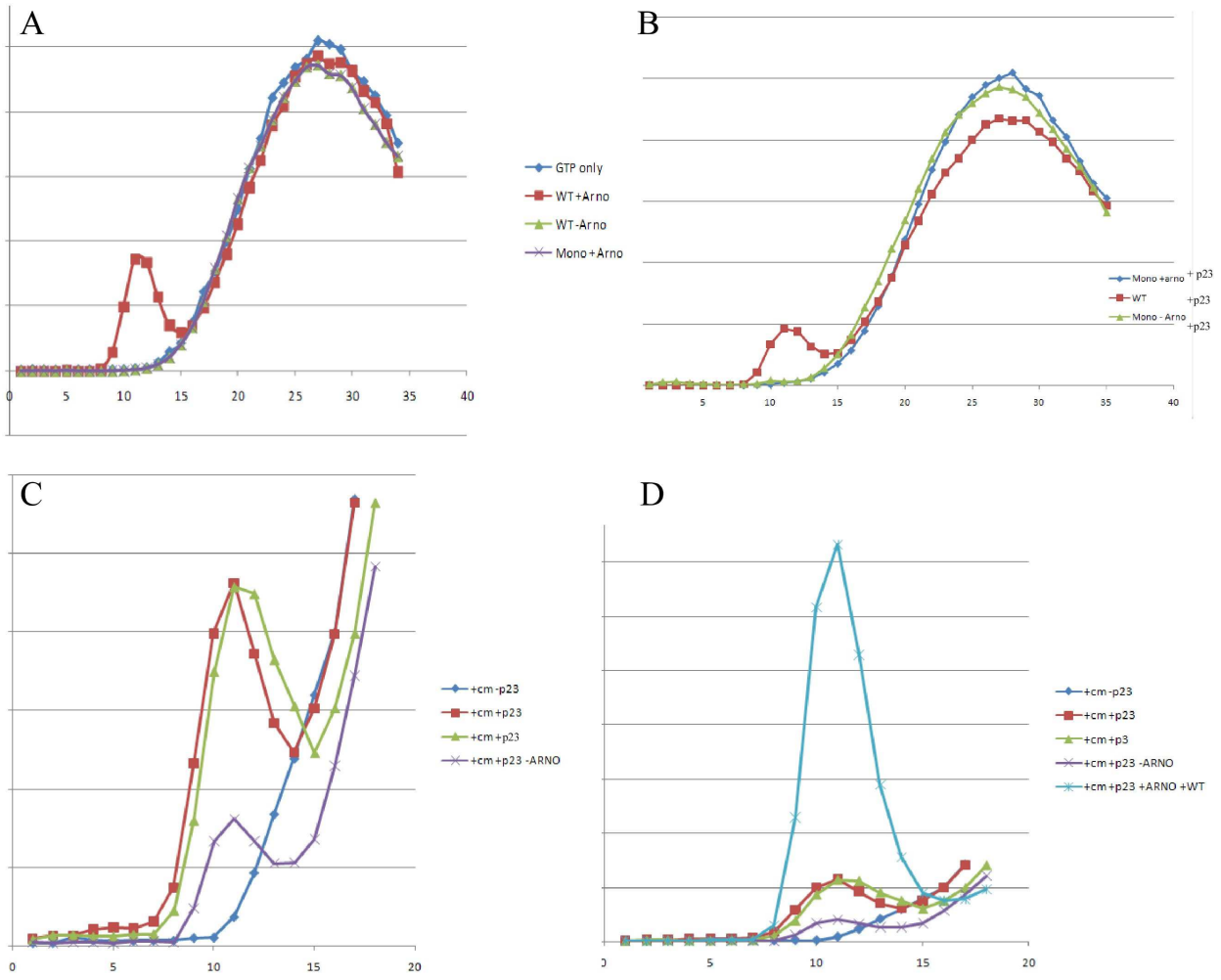

Figure 40. Arf1-Y35A activity on liposomes depends on coatomer and p23. Arf1 proteins were incubated in the presence of radiolabeled GTP and Golgi-like liposomes, and subjected to gel filtration in the absence of presence of p23 lipopeptide and coatomer as indicated. Radioactivity of the fractions is plotted against fraction number. A: in the absence of p23 and coatomer; B: in the presence of p23 as indicated; C: in the presence of both p23 and coatomer as indicated; D: same as C, in the presence of Arf1-wt.

On liposomes, in the absence of any additional factors besides GTP, Arf1 and ARNO, only Arf1-wt, but not the mutant Arf1-Y35A displayed activity as can be seen in Figure 40 A, where only in the presence of Arf1-wt and ARNO radioactivity was detected in the protein containing fractions 10-15. Also, we extracted phospholipids from isolated Golgi-enriched membranes to form liposomes and tested nucleotide exchange activity in the assay. As a result, only Arf1-wt

but not the mutant was active (data not shown). From this we concluded that it is not the lipid content, but rather the absence of accessory proteins that makes mutant Arf1-Y35A bind to Golgi membranes, but not to synthetic liposomes.

We therefore added two components to the system that are known Arf1-interactors in the context of a Golgi environment: first, we prepared liposomes that contained p23 lipopeptide, which is known to interact with Arf1-GDP (Gommel, *et al.*, 2001). As shown in Figure 40 B, the presence of p23 lipopeptide did not lead to any significant GTP loading of Arf1-Y35A, in contrast Arf1-wt displayed activity as expected. Next, we tested the monomeric mutant in the presence or absence of coatomer and p23, as shown in Figure 40 C. As a result, in the absence of either coatomer or p23 alone, Arf1-Y35A did not display any activity in contrast to the wildtype. However, if both p23 and coatomer were present in the system, Arf1-Y35A displayed an ARNO-specific signal that indicated GTP-loading (duplicate measurements red and green curves Figure 40 C) above the background in the absence of ARNO (Figure 40 C).

Thus, on liposomes in the presence of p23 and coatomer, Arf1-Y35A was able to bind, albeit at an extent significantly lower than Arf1-wt, as depicted in Figure 40 D, which contains the same dataset as Figure 40 C, however with Arf1-wt added. Taken together, from this data we concluded that monomeric Arf1-Y35A exhibits a comparable nucleotide exchange activity as Arf1-wt on Golgi membranes, however with chemically defined liposomes, this activity is significantly lower, and has to be classified as inactive in the absence of additional factors such as the cytoplasmic tail of p23 and coatomer.

With this evidence that monomeric Arf1-Y35A can still exhibit the classical nucleotide switch reaction, we asked if the mutant was still able to recruit coat proteins in a GTP dependent manner. To this end, Golgi-enriched membranes were incubated with Arf1-wt, Arf1-Y35A,

GDPβS (D) or GTPγS (T), and Arf1-depleted cytosol (by gel filtration, not shown) as source for coat proteins such as coatomer or adaptin-I. After incubation, the membranes were pelleted by loading the sample onto a cushion of 15 % sucrose, followed by centrifugation. Pellets were resuspended in SDS sample buffer, and after separation by SDS-PAGE, analyzed by Western blotting with antibodies against Arf1, adaptin-1 and the coatomer subunit δ-COP (Figure 41).

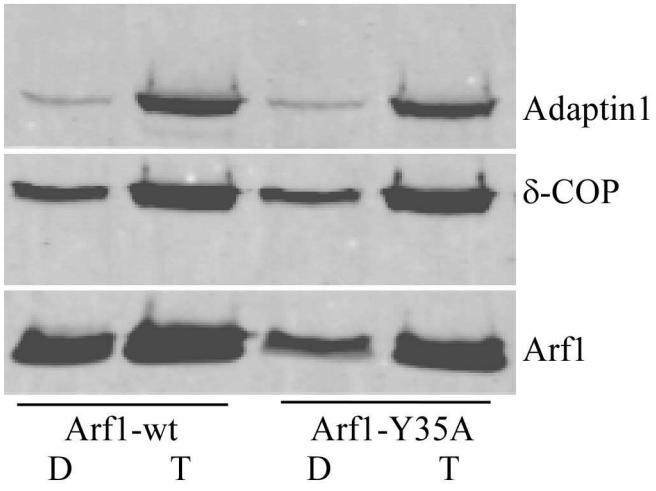

Figure 41. Recruitment of coat complexes to the Golgi membrane by Arf1-wt and Arf-Y35A. Golgi-enriched membranes were incubated with Arf1 constructs and nucleotide (GDPβS (D), GTPγS (T), as indicated. Membrane-bound material was isolated by centrifugation through a 30% sucrose cushion and analyzed by SDS-PAGE and Western blot with antibodies as indicated.

As a result, both Arf1-wt Arf1-Y35A recruited adaptin-I (AP-I) and coatomer to the membrane in a GTP-dependent manner, indicating that monomeric Arf1 can, like the wildtype, exert the classical switch function of Arf1.

In addition to ArfGEF-catalyzed GTP loading and coat recruitment, ArfGAP-mediated GTP hydrolysis is an important criteria of Arf1 activity. Therefore, Arf1-activation by EDTA (compare part 1, measuring ArfGAP1 activity), followed by ArfGAP1-mediated GTP hydrolysis was monitored in a fluorimetric assay. While Arf1-wt was perfectly able to undergo GTP loading and hydrolysis (compare Fig. 9), the monomeric Arf1-Y35A did not display any activity in this assay. As a control, Arf1-wt was added to the same reaction and immediately

responded to the exchange factor, as can be seen by the increased signal indicating GTP-loading of Arf1-wt Figure 42).

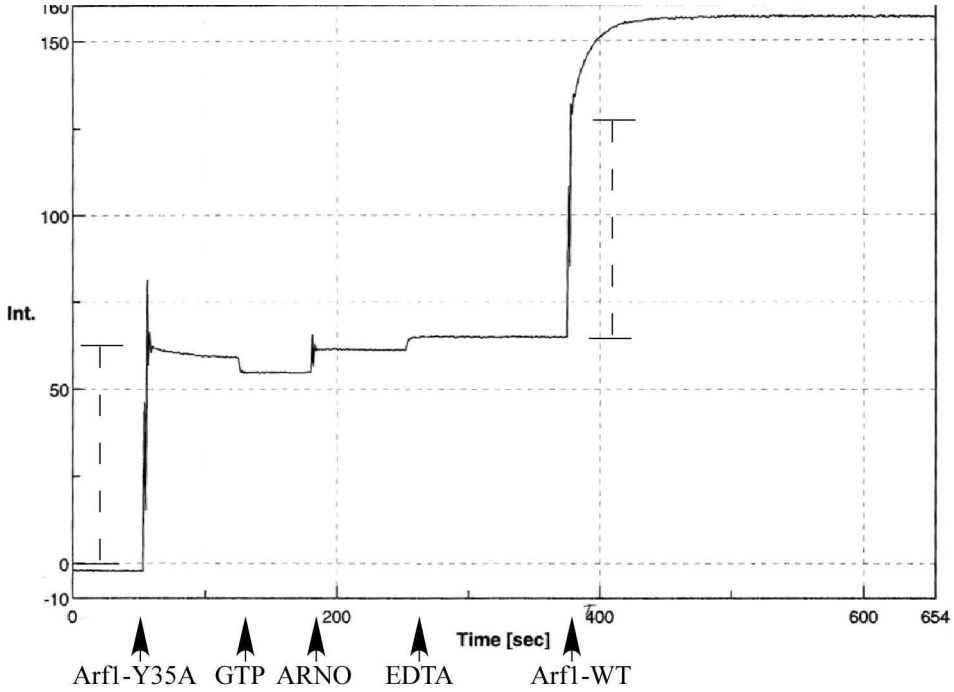

Figure 42. Arf1-Y35 activity in the fluorimetric assay. Liposomes were added to the assay and the Trp-fluorescence was set to zero. Arf1-Y35A was added, as can be seen by the increase of signal indicated by the dashed line. GTP was added as indicated, followed by EDTA to trigger nucleotide exchange. As an additional control, the exchange factor ARNO was added. To test the system, Arf1-wt was added in the same amount as Arf1-Y35A, background fluorescence is again indicated by the dashed line.

The dashed line indicates the spontaneous spike obtained for background fluorescence after addition of Arf1 proteins. In the case of Arf1-Y 35A, after addition of GTP, as indicated in the figure, addition of ARNO did not result in any signal response. To exclude that the ARNO added was inactive, EDTA was added, which again did not result in GTP loading. As a control, to the same reaction Arf1-wt was added (subtract the dashed line for protein backbone fluorescence), which yielded a rapid response and increase of signal, indicating that Arf1-wt, but not the mutant Arf1-Y35A is active in this assay. This result supports the observations from the radio labeling experiments on liposomes (compare Figure 40). In order to measure the mutant's activity in an independent assay, a liposome binding experiment was performed. To this end, Arf1 proteins were incubated with liposomes, and nucleotide exchange was triggered by either

EDTA or ARNO. The membranes were re-isolated by floatation density gradient centrifugation to purify membrane-bound material and analyzed by SDS-PAGE and Western blot using an Arf1-antibody (Figure 43).

Figure 43. Arf1-wt and Arf1-Y35A binding to liposomes in the absence of any additional factors. Arf1 proteins were incubated with rhodamine-phasphatidylethanolamine stained liposomes in the presence of GTP and either EDTA or ARNO, to trigger nucleotide exchange and membrane binding. The suspension was then adjusted to 30% sucrose and the samples were first overlaid with 25% sucrose, followed by buffer containing no sucrose. After centrifugation at 100,000g for 1h, the liposome fraction was collected and analyzed by SDS-PAGE and Western blot with anti-Arf1 antibody.

Whereas Arf1-wt exhibited a GTP dependent binding to the membrane as expected after activation of either EDTA or ARNO (not shown), monomeric Arf1-Y35A did not bind to liposomes with or without p23, which confirmed the results of the fluorimetric assay (Figure 42). Therefore, as a conclusion from three different assays, Arf1-Y35A is not active in terms of nucleotide exchange and membrane binding on liposomes in the absence of additional factors such as p23 and coatomer, but is active on Golgi membranes.

Processes such as Arf1-GTP loading, GTP-hydrolysis, Arf1 binding to the membrane and coat recruitment are highly dynamic and might contain additional layers of complexity that are not yet fully understood. Therefore, to study these reactions together, we exploited a light scattering approach to monitor in real time Arf1-activation, binding, coat recruitment and ArfGAP-mediated release. The scattering of light by a suspension of liposomes mainly depends on the size of the liposomes, their shape, and the refractive index of the lipid membrane. When a protein coat assembles at the liposome surface, the refractive index of the membrane increases,

which results in an increase in light scattering. This can be measured in real time by setting the excitation and emission monochromators to the same wavelength. The assembly of the COPI coat on liposomes results in measurable light-scattering changes, which at first approximation are roughly proportional to the protein mass that is gained or lost by the liposome membrane (Bigay and Antonny, 2005). To this end, Arf1-proteins were added as indicated (after 100 sec), followed by GTP (after 200 sec). Nucleotide exchange was started by the addition of catalytic amounts of ARNO (after 300 sec), and after a further 200 seconds, coatomer was added (Figure 44).

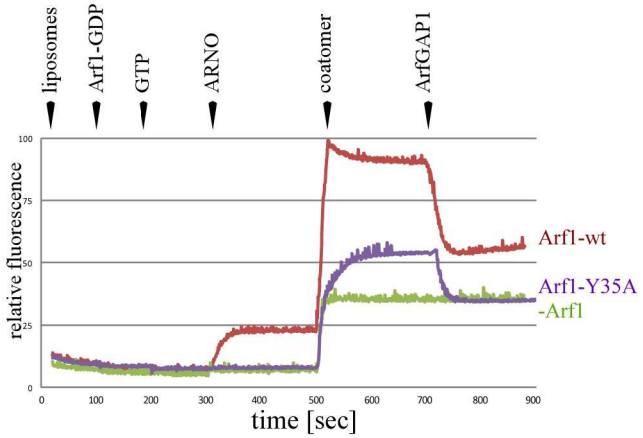

Figure 44. Following coat -recruitment and -release in real time. Golgi like liposomes were incubated with Arf1 proteins in the presence of GTP, and nucleotide exchange was triggered by ARNO as indicated. After Arf1-binding to the membrane, coatomer recruitment and ArfGAP-mediated coat release was monitored as a function of light scattering over time.

The signal observed after addition of coatomer was composed of light scattering of soluble coatomer, plus light scattering of recruited coatomer, as shown by the response in the absence of Arf1. Interestingly, whereas a signal was seen for Arf1-wt after addition of ARNO, nucleotide exchange of Arf1-Y35A seemed to be stimulated by coatomer, in line with the experiments shown above. The signal response of Arf1-Y35A was approximately 50 % of Arf1-wt, but twice as much mutant as wildtype was added to obtain theses curves. From these results, we concluded that on liposomes, the activity of Arf1-Y35A to recruit coatomer was about 20-25% of Arf1-wt. In order to further challenge the nucleotide specificity of the binding observed,

catalytic amounts of recombinant ArfGAP1 were added (after 750 sec). Both, the signals obtained for Arf1-wt and Arf1-Y35A were reversed with similar kinetics and efficiency, indicating that in both cases the proteins were bound via Arf1-GTP and released by GTP hydrolysis.

Next, we asked if Arf1-Y35A localized to the Golgi, as is the wildtype. To this end, Vero cells were transfected with Arf1-wt YFP (Figure 45 upper panel) and Arf1-Y35A YFP (Figure 45, lower panel). The localization was analyzed by immunofluorescence and compared to the staining patterns obtained with an antibody directed against Giantin. This experiment was performed by Dr. Christoph Rutz (Sohn, *et al.*, 1996; Beck, *et al.*, 2008) .

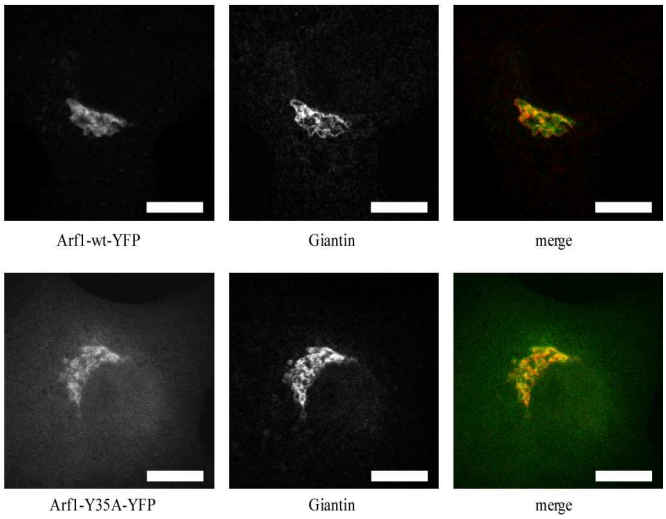

Figure 45. Localization of Arf1 variants in vivo. Vero cells were transfected with Arf1-YFP constructs as indicated and Golgi staining was assessed with the Golgi marker giantin.

Although a higher cytosolic background staining was observed for Arf1-Y35A, both the wildtype and mutant Arf1 localized to the Golgi, which again indicated functionality in the case of mutant Arf1, comparable to the wildtype.

Lack of function of monomeric Arf1 analyzed *in vivo* and *in vitro*

To sum up the results above, Arf1-Y35A fails to dimerize but still is able to exert the classical nucleotide switch reaction and recruitment of coat complexes to the Golgi. In order to elucidate the role of dimerization, we asked if viability was impaired when cells only had monomeric Arf1 available. To this end, in collaboration with the Ed Hurt group, we asked if the loss of Arf1-wt, which is lethal in yeast (Hosobuchi, *et al.*, 1992), could be complemented by Arf1-Y35A expression. Yeast and mammalian Arf1 are 77% identical, functionally redundant (Kahn, *et al.*, 1991), and the amino acid residue Y35 is conserved. Thus, to test the physiological significance of this mutation *in vivo,* Dr. Jochen Bassler expressed the point mutant in *S. cerevisiae*. Since in yeast yArf1 and yArf2 are 96% identical and functionally redundant (Stearns, *et al.*, 1990), plasmids expressing y*Arf1 and yArf1-Y35A* were transformed into an *arf1Δ arf2Δ* deletion strain complemented by a pURA3 yArf1 plasmid (Takeuchi, *et al.*, 2002). To test the growth behavior of the mutant, transformants were forced to lose the URA-plasmid by spotting on SDC+FOA. Whereas wild type Arf1 was able to complement the yeast deletion strain, the *arf1-Y35A* mutation led to lethality at all tested temperatures 23°C, 30°C and 37°C (Figure 46, (Beck, *et al.*, 2008), and data not shown).

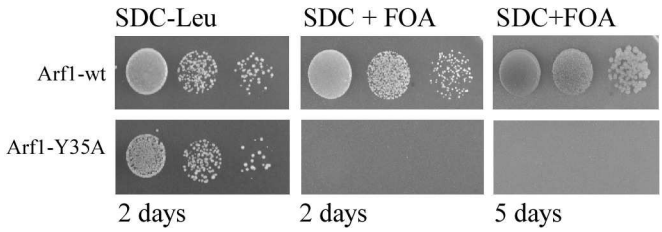

Figure 46. In vivo analysis of Arf1 mutants in yeast. Strain NYY539 (arf1Δ, arf2Δ, pURA3-Arf1) was transformed with pRS315-Arf1, pRS315-arf1-S162A, and pRS315-arf1-Y35A. Transformants were spotted in 10-1 dilution series on synthetic dextrose complete plates (SDC) plus 5-fluorooratic acid monohydrate (FOA). Pictures were taken after 2 days or 5 days incubation at 30°C.

Overexpression of *arf1-Y35A* by the Gal1 promoter had no dominant negative phenotype in a yeast wild type strain (Figure 47).

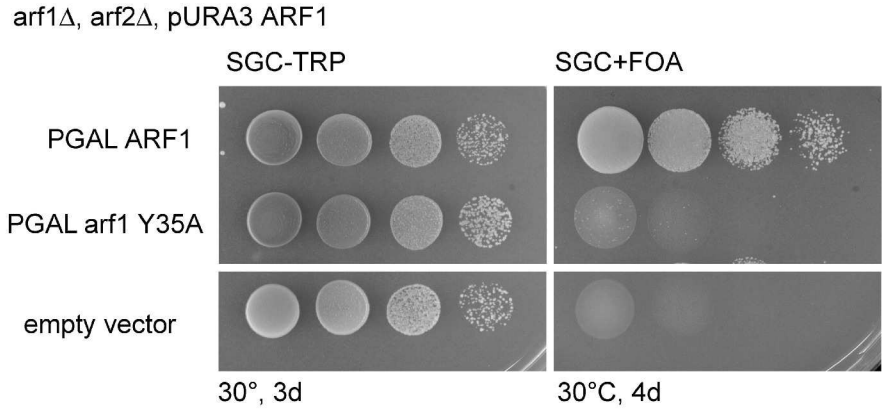

Figure 47. GAL1-over expression of Arf1-Y35A does not rescue the loss of Arf1-wt. The arf1Δarf2Δ (pURA3 ARF1) strain with plasmids encoding the ARF1-wt and Y35A allele under control of the GAL1 promotor. The transformants were then plated on SGC+FOA to remove pURA3 ARF1 plasmid.

Likewise, GAL1 over expression of Arf1-Y35A did not rescue the effect of *arf1-wt* deletion, as shown. Taken together, these experiments strongly indicate that dimerization is essential for the function of Arf1.

In order to put this finding into a functional context, we asked if COPI-coated transport was affected by the monomeric Arf1 mutant. To this end, we tested the point mutant in an *in vitro* budding assay where Arf1 and coatomer were incubated with GTP and Golgi membranes, to induce COPI vesicle formation (Serafini, *et al.*, 1991) (also see Materials and Methods and Part I of this thesis). The vesicles were then purified from the donor membranes by sucrose density gradient centrifugation. A typical result is shown in Figure 48.

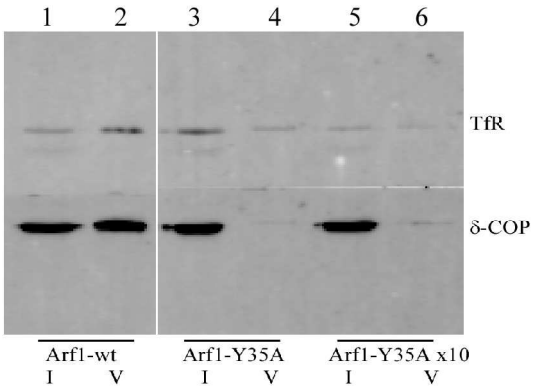

Figure 48. In vitro formation of COPI vesicles in the presence of monomeric or dimeric Arf1. Golgi-enriched membranes were pretreated with 250 mM KCl and incubated with purified constituents of the COPI machinery, such as Arf1-wt or the monomeric mutant Y35A, as well as rabbit liver coatomer and GTP. COPI-coated vesicles were purified by sucrose density gradient centrifugation. For each sample, 5% of total input (labeled as I), as well as 50% of the purified vesicles (labeled as V) were analyzed by SDS-PAGE and Western blotting using antibodies against the coatomer subunit δ-COP and the transmembrane protein transferrin receptor (TfR).

While Arf1-wt yielded strong signals in the vesicle-containing interface between 45% and 37.5% sucrose, indicated by the presence of Western Blot signals for coatomer subunit δ-COP and the membrane protein transferrin receptor (TfR) in lane 2, whereas an identical amount of Arf1-Y35A did not give raise to significant signals (lane4). As the mutated protein has shown reduced coating activity in the SLS experiments (Figure 44), we increased the amount of input Arf1-Y35A by a factor of ten. Again, no significant signals were observed in the respective interface (lane 6). Vesicle formation was further analyzed by negative stain electron microscopy of fractions isolated by isopycnic sucrose density gradient centrifugation according to (Serafini, *et al.*, 1991). This was done by Dr. Zhe Sun and Andrea Hellwig (Beck, *et al.*, 2008; Waters, *et al.*, 1991). As a result, a homogeneous population of vesicles was found in samples with Arf1-wt, whereas only sporadic vesicles were observed with Arf1-Y35A (Figure 49).

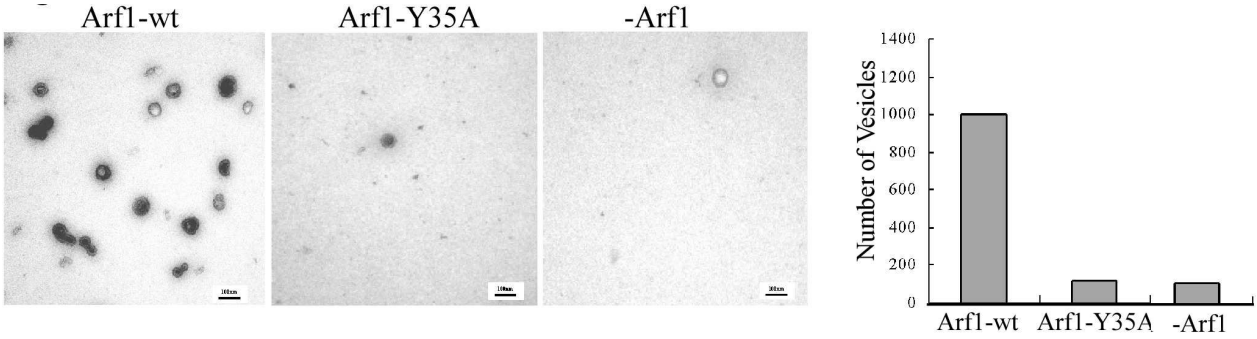

Figure 49. Quantification of vesicle formation in the presence of monomeric or dimeric Arf1. Vesicles were generated either as described, or after isopycnic density gradient centrifugation (Serafini, et al., 1991), followed by negative staining electron microscopy. 20 meshes each of the samples were randomly chosen and the number of vesicles counted.

Quantification of these experiments revealed an amount of vesicles obtained with Arf1-Y35A that did not exceed the numbers obtained by residual endogenous Arf1. Altogether, these experiments indicated that dimerization of Arf1-GTP is necessary for the formation of COPI vesicles, and is critical at a step distinct from coatomer recruitment.

Our finding that dimerization is not critical for coatomer recruitment but is required for vesicle formation indicated that dimeric Arf1 plays a yet unknown role in vesicle formation, possibly related to the membrane deformation activity reported in this work. To challenge this hypothesis, the ability of Arf1-Y35A to induce membrane deformation was assessed. Strikingly, the Arf1 mutant Y35A did not catalyze tubule formation **(**Figure 50**).**

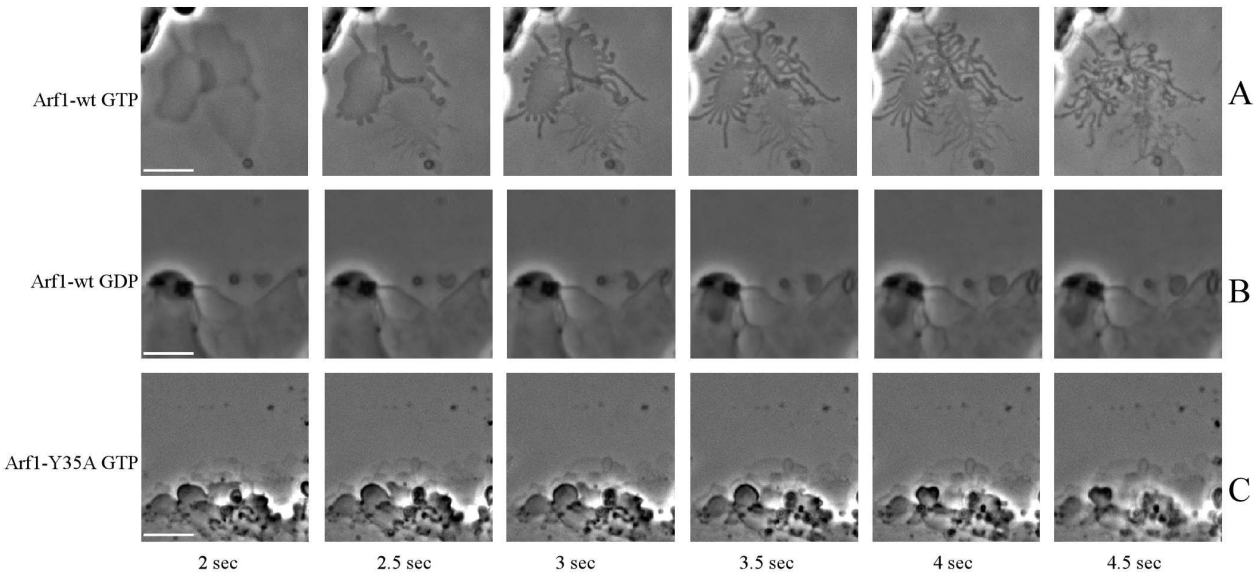

Figure 50. Tubulation of membrane sheets by monomeric and dimeric Arf1. Lipids containing p23 lipopeptide were spotted on a glass surface and hydrated with buffer containing either GTP or GTP and the exchange factor ARNO (50 nM). After addition of myristoylated Arf1-GDP (1 µM), the lipid surface was observed by light microscopy (scale bars 5 µm). Reaction in the presence of Arf1-wt with GTP (A), Arf1-wt with GDP (B), and Arf1-Y35A with GTP (C).

Together, the results in this chapter suggest a mechanism of vesicle biogenesis that critically depends on bending of membranes induced by dimeric Arf1. This revisits the current paradigm for the role of Arf1 in the formation of transport vesicles since the small GTPase was solely seen as a molecular switch that regulates the recruitment of coat proteins to membranes.

Dissecting contributions to membrane deformation by Arf1 and coatomer

So far, we showed that only dimeric Arf1 mediates membrane curvature, and that abolishing this surface activity in case of a monomeric Arf1 mutant, is lethal (Figure 46) since COPI-vesicle biogenesis is impaired (Figure 49). However, coat recruitment can still take place (Figure 41)). At which step is Arf1-mediated membrane curvature coming into play, and is this a step distinct from curvature generated by the coat polymers? To provide answers to this question, electron microscopy was performed with reconstituted liposomal COPI budding assays. To this end, in collaboration with the Briggs lab at EMBL Heidelberg, Golgi-like liposomes containing 1 mol% p23 lipopeptide, and 2 mol% PIP2 were incubated with GTPγS, coatomer, ARNO and Arf1 for 5 min at 37°C (Figure 51) and processed similar to (Bremser, *et al.*, 1999).

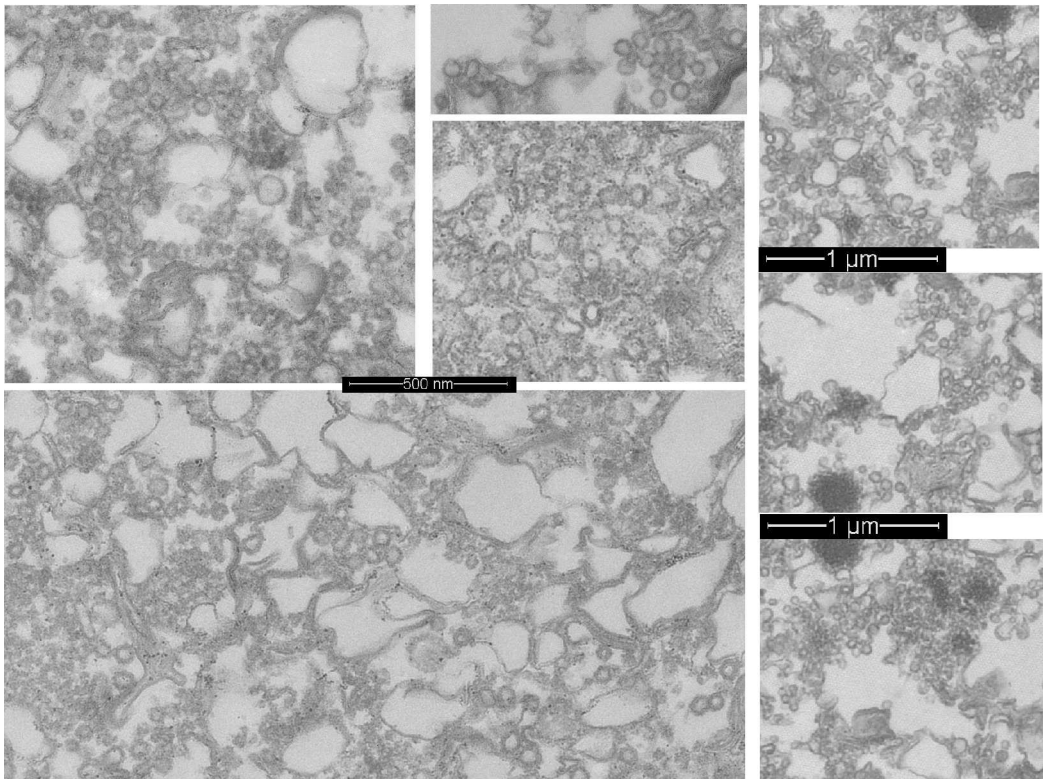

Figure 51. COPI reconstitution assays in the presence of p23 lipopeptide. Incubations of liposomes, GTP, Arf1-wt and coatomer where embedded and sections were analyzed by EM.

Under these conditions, COPI coated liposomes were formed, with an average diameter of 70-80nm. In the absence of p23 lipopeptide, vesiculation was also observed, but with decreased efficiency, as could be estimated from the decreased numbers of ‘vesicles’ and the larger amounts of 400 nm liposomes that have not been converted (Figure 52) As a control, embedded liposomes in the absence of machinery proteins such as Arf1 and coatomer did not yield any protein coated vesicular structures (Figure 53)

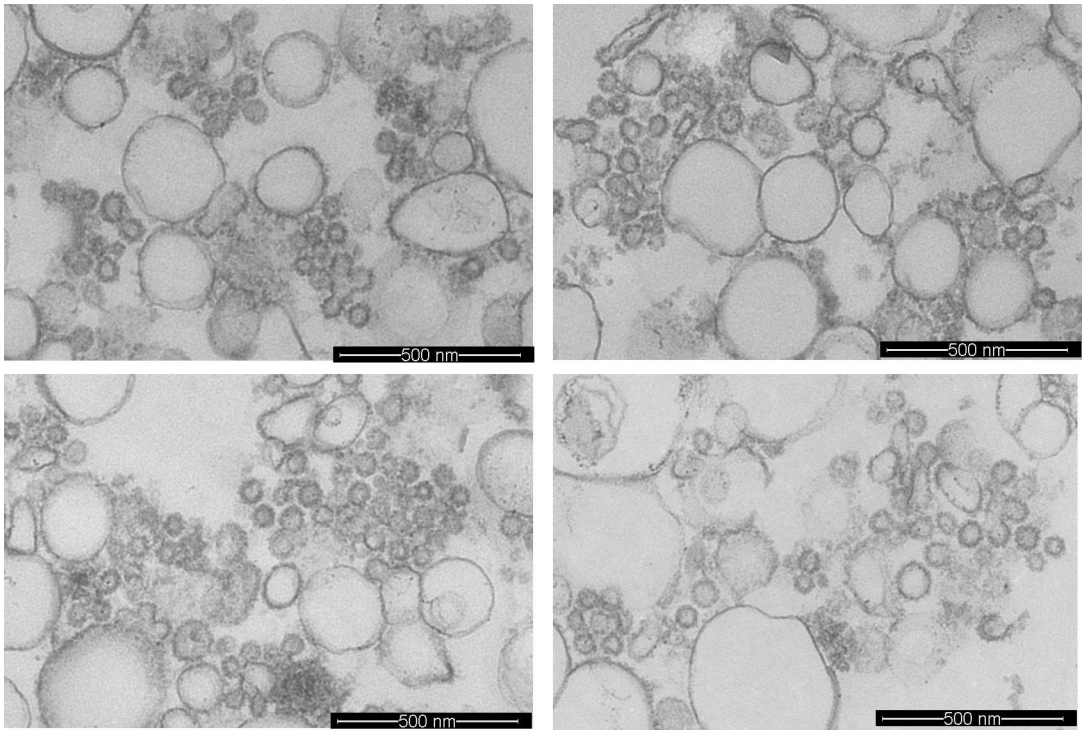

Figure 52. COPI reconstitution assays in the absence of p23 lipopeptide. Incubations of liposomes, GTP, Arf1-wt and coatomer where embedded and sections were analyzed by EM.

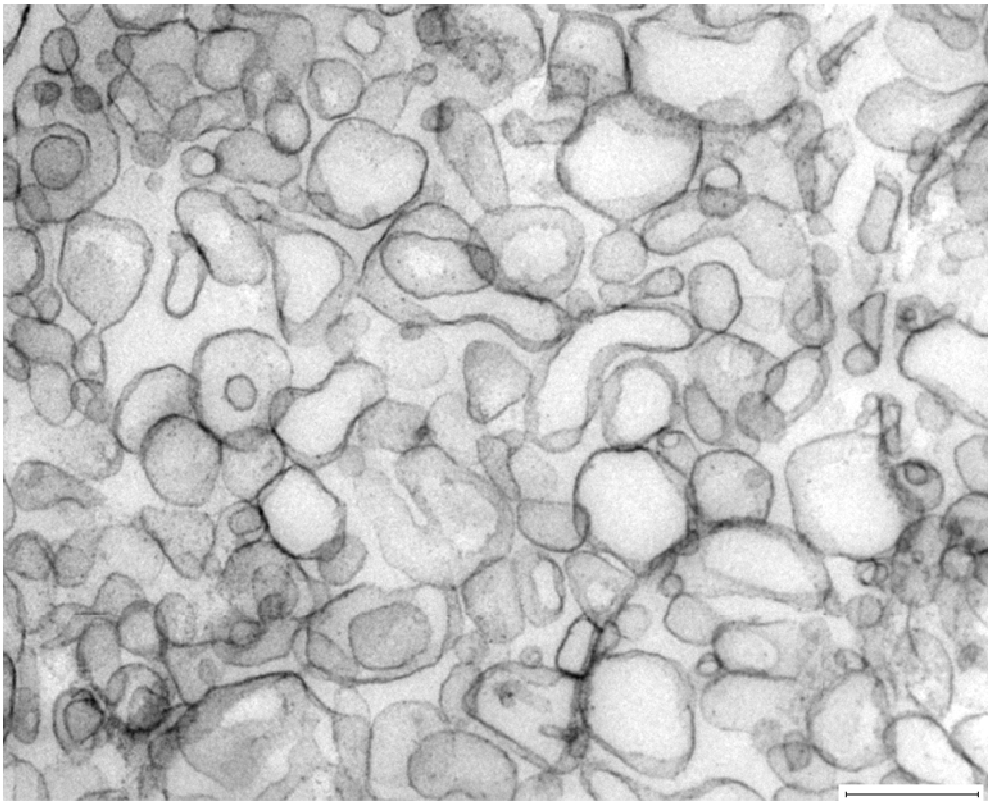

Figure 53. Epon embedding and sections of Golgi-like liposomes.

Taken together, these experiments show that formation of COPI coated liposomes is increased in the presence of the Arf receptor p23 (Bremser, *et al.*, 1999; Gommel, *et al.*, 2001), but the lipopeptide apparently is not essential to drive vesiculation under these conditions. (Bremser, *et al.*, 1999) reported an approximately threefold increase of vesiculation as a result of the quantifications of EM sections, and this may well be in line with the data presented here.

In order to dissect effects of Arf1-wt and mutant Arf1-Y35A that can, as a result of impaired dimerization, no longer affect membrane curvature, cryo EM studies were performed in collaboration with John Briggs (EMBL), with liposomes containing p23 lipopeptide and Arf1-wt or Arf1-Y35A. As a first control, Golgi-like liposomes containing 1mol% p23 and 2mol% PIP2 were incubated in the presence of ARNO, Arf1-wt and coatomer, but in the absence of nucleotide (Figure 54)

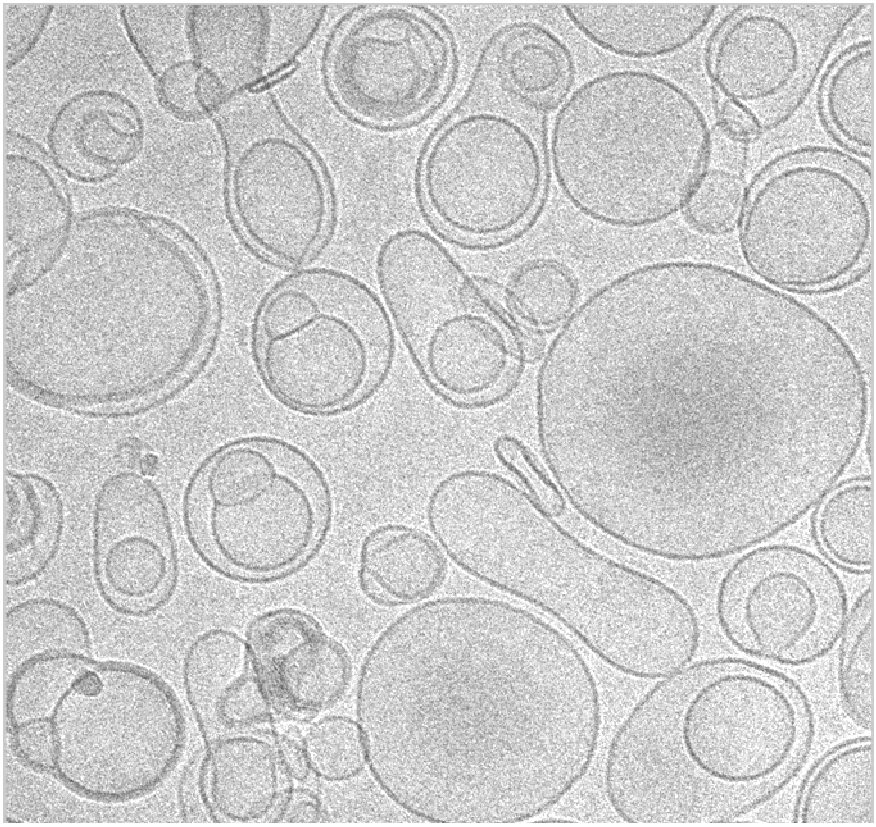

Figure 54. Cryo EM of liposomes. All machinery components for COPI vesicle reconstitution were present, with the exception of nucleotide.

Next, COPI reconstitution assays were performed in the presence of GTPγS, Arf1-wt and coatomer and analyzed by cryo EM (Figure 55)

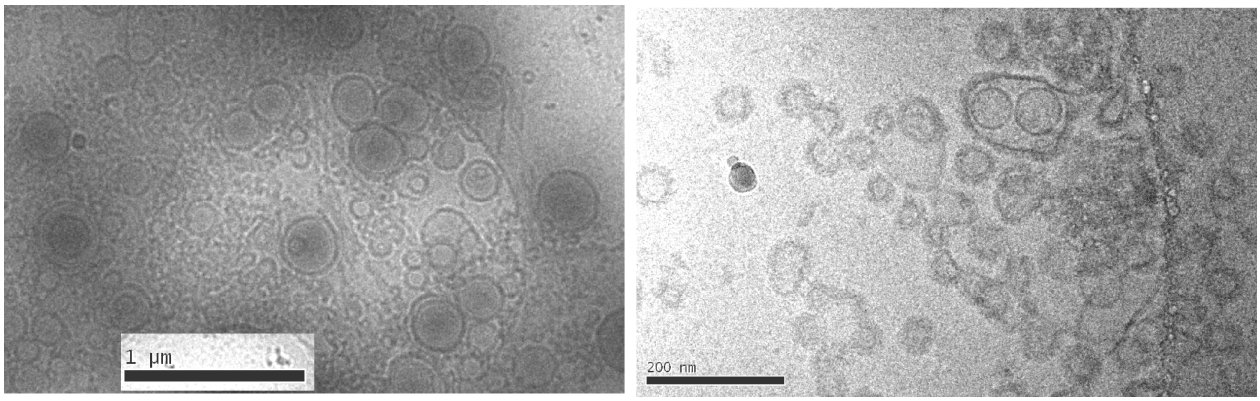

Figure 55. Cryo EM of liposomes. COPI vesicle reconstitution from liposomes with GTP, ARNO, coatomer and Arf-wt.

As can be seen from the pictures, the morphology of the liposomes is strikingly different after incubation with the COPI coat components in the presence of GTPγS. When the monomeric Arf1-Y35A was used instead or Arf1-wt, the reaction seemed to be arrested at the bud, implying that Arf1-mediated curvature is a prerequisite for the fission step (Figure 56).

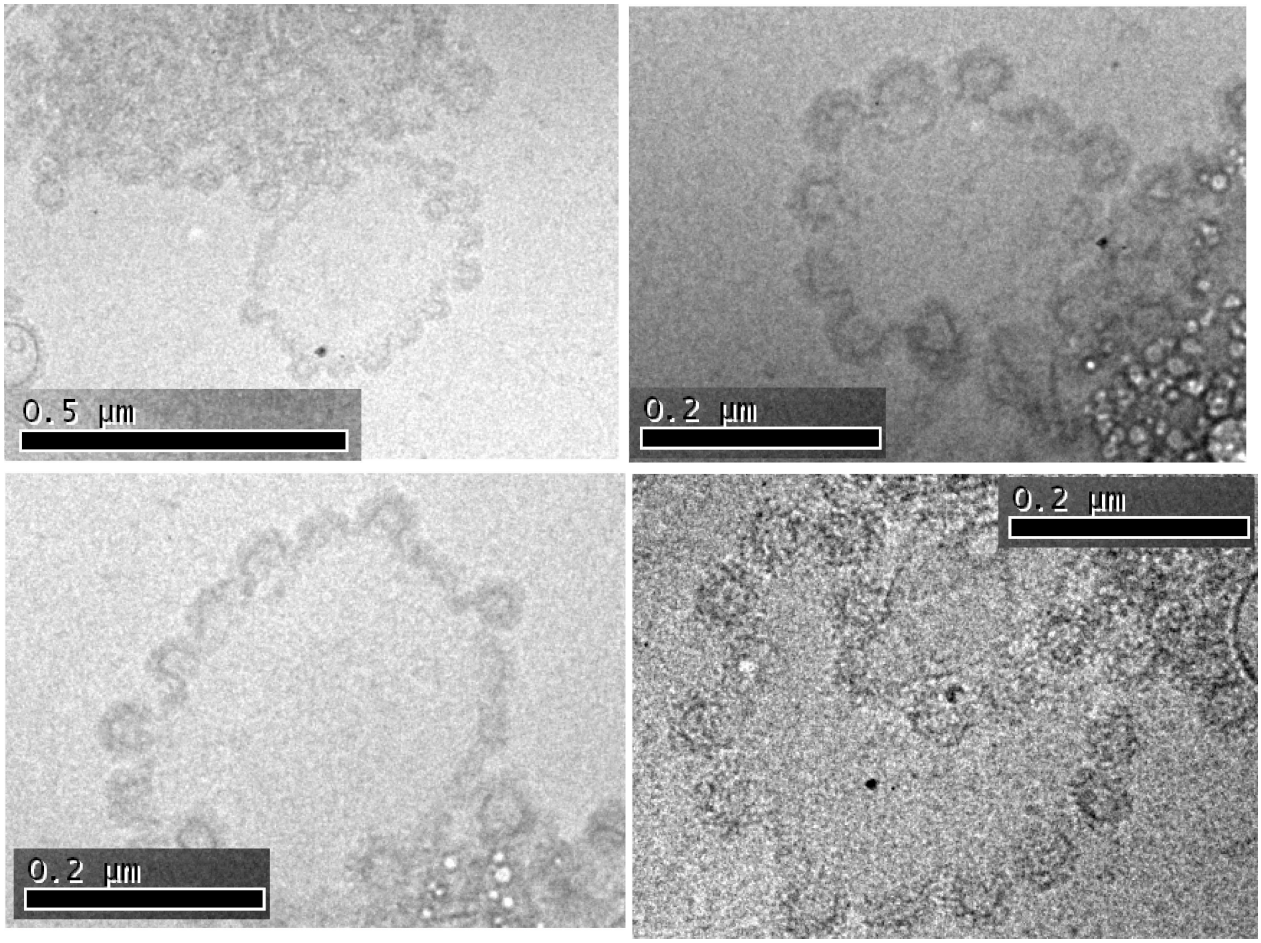

Figure 56. Cryo EM of liposomes. COPI vesicle reconstitution from liposomes with GTP, ARNO, coatomer and Arf-Y35A.

Results Part III
Coatomer Isoforms

The protein coat of COPI-vesicles consists of the heptameric coatomer complex coatomer (Serafini, *et al.*, 1991), which is recruited by four Arf1 proteins (see above), in the form of two Arf1-dimers (Beck, *et al.*, 2008). For two out of the seven coatomer subunits, γ-COP and ζ-COP, two isoforms were reported to exist (Blagitko, *et al.*, 1999; Futatsumori, *et al.*, 2000), named γ1- and γ2-COP, as well as ζ1-and ζζ2-COP. It was shown that, in a liver cytosol, three isoforms of the coatomer complex exist, defined by the subunit combinations γ1/ζ1, γ1/ζ2, and γ2/ζ1. These forms make up the total coatomer in a ratio of about 2:1:2, respectively (Wegmann, *et al.*, 2004). Recent quantifications of the coatomer isoforms in a mammalian cytosol yielded a ratio of γ1/ζ1-, γ1/ζ2-, and γ2/ζ1-COP at approximately 10:3:5 (Moelleken, *et al.*, 2007). The γ2ζ2-coatomer was found in a much smaller quantity, which was probably close to the sensitivity limit of the analytical method used. It remains unclear if γ2/ζ2-COP plays any physiologically significant role at all. In hepatic cells, the isotypic coatomer subunits γ- and ζ-COP are distributed unevenly over the Golgi, which might suggests different functions of COPI-vesicle pools that are distinct from each other in terms of coat (Moelleken, *et al.*, 2007).

To analyze the functions of the individual coatomer isoforms biochemically, recombinant coatomer complexes needed to be produced that were defined in their γ- and ζ-COP composition. To this end, Dr.med. Monika Sahlmüller set out to construct bacmid DNA encoding all seven subunits of the coatomer complex, one construct each for the four possible γ/ζ-COP permutations (Dr. med. Monika Sahlmüller, dissertation). Ovary cells from *Spodoptera frugiperda* (Sf9 cells) were transfected by electroporation with the individual bacmids to generate virus that could be used to induce expression of recombinant coatomer complexes.

Generation of the DNA-constructs, cell culture and optimizing the expression conditions was all done by Dr. Sahlmüller, assisted by Priska Eckert.

Purification of recombinant coatomer isoforms

Infection, cultivation and induction of the expression cultures were all carried out as described previously (Dr. med. Monika Sahlmüller, dissertation). To this end, 750 ml Sf9 spinner culture each was infected with a virus, encoding one of the heptameric coatomer isoforms, defined by their γ/ζ-composition, and analyzed by SDS-PAGE for expression (Figure 57).

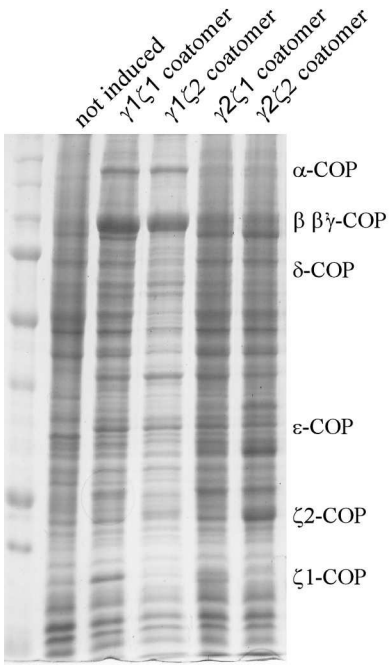

Figure 57. Expression of recombinant coatomer isoforms. Sf9 cells were infected with recombinant Baculo virus, encoding each of the heptameric coatomer isoform complexes. Expression occurred for 72 hours at 27°C. The cell pellets were frozen until further procession, an aliquot of each expression was analyzed by SDS-PAGE.

To purify the coatomer complexes from the overexpression cultures, cells were lysed by French press and subjected to ultracentrifugation. The cleared supernatant was applied to Ni^{++}IDA sepharose (Macheray & Nagel) to bind the α- and β-COP subunits that were cloned to a hexahistidine-tag, and eluted in 250 mM imidazole. A typical purification result is shown in

(Figure 58) for the three coatomer isoforms that exist in the mammalian cytosol (Wegmann, *et al.*, 2004). Purification of the γ2ζ2 coatomer complex worked equally efficient (not shown). From 750 ml cell culture, typically 20 mg of total protein was found after elution.

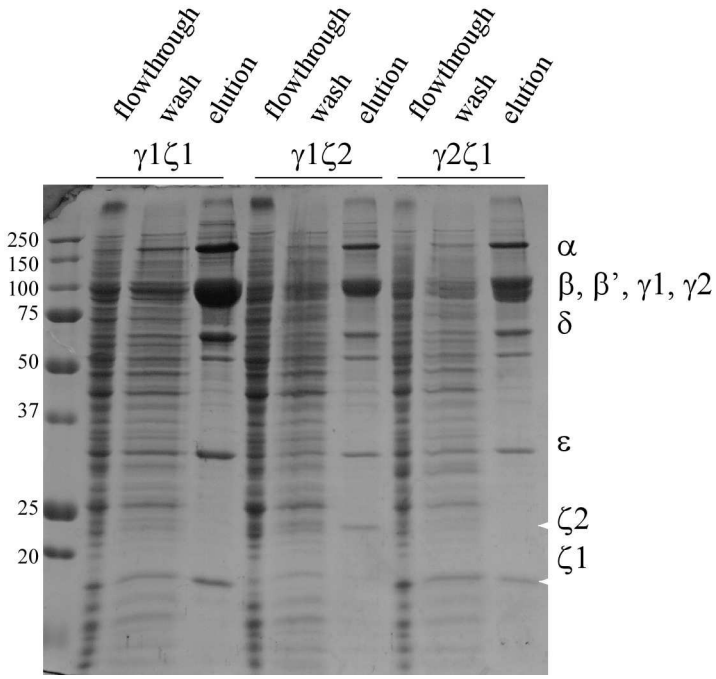

Figure 58. Purification of coatomer isotypes. Sf9 cells were infected with recombinant baculo virus, encoding each of the heptameric coatomer isoform complexes. After cell lysis and ultracentrifugation, the soluble protein extract was applied to Ni++NDI chromatography and the flowthrough, wash and eluate analyzed by SDS-PAGE.

As one could conclude from the gel in (Figure 58), this elution might reflect largely intact coatomer complexes, rather than single subunits and displayed a reasonable purity to use in biochemical assays.

Coatomer isoforms and their ability to mediate COPI-vesicle biogenesis

To analyze if the distinct four coatomer isoforms are able to form COPI-vesicles with a comparable efficiency, budding assays (see part I of this work) were performed. To this end, Golgi membranes and myrArf1-wt were incubated with either one of the purified recombinant coatomer complexes, or a mixture of the four isoforms in a ratio as described in (Moelleken, *et al.*, 2007), and analyzed by SDS-PAGE and Western blotting to estimate the yield of purified vesicles (Figure 59, left). As a control, the vesicle fractions were analyzed by electron microscopy, a representative sample image is displayed for vesicles generated in the presence of γ1/ζ1-coatomer (Figure 59, right).

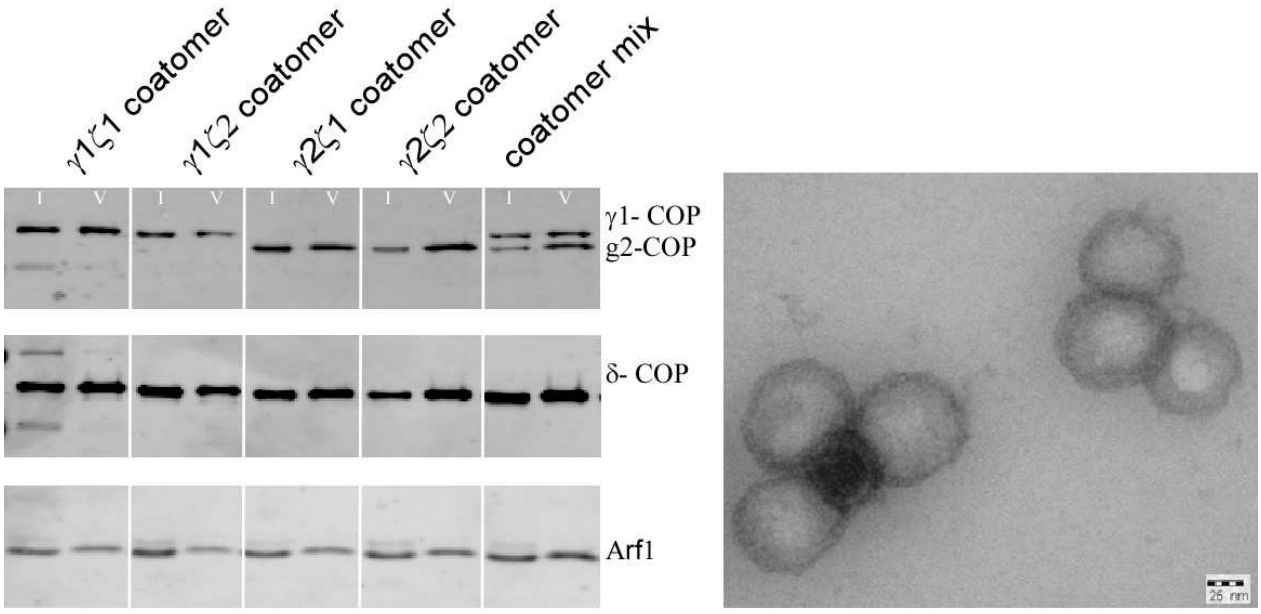

Figure 59. COPI-vesicle biogenesis with coatomer isoforms. Golgi membranes were incubated with Arf1 and recombinant coatomer isoforms that are defined by their g- and z-COP subunits, as well as a mixture of the coatomer isoforms in the ratio that was previously described for cytosol. 0.5 % of total input (I) and 50 % of isolated vesicles (V) were analyzed by SDS-PAGE and Western blotting (left). Vesicle fractions were analyzed by negative stain electron microscopy and displayed homogeneous populations of 70-80 nm structures (right).

Evaluation of the signals obtained for either γ-, δ-COP or Arf1 indicated that all four isoforms of coatomer are able to mediate the formation of COPI-vesicles with comparable efficiency.

Preferences in cargo selection of homogeneously coated COPI-vesicles

To investigate if different coatomer isoforms select distinct classes of protein cargo, COPI-vesicle budding assays were performed in the presence of either one of the four coatomer isoforms, in order to produce homogeneous pools of vesicles, that differed from each other by composition of the coat (see Figure 59). After isolation of the vesicles, the samples were probed with cargo markers and analyzed by SDS-PAGE and Western blotting (Figure 60).

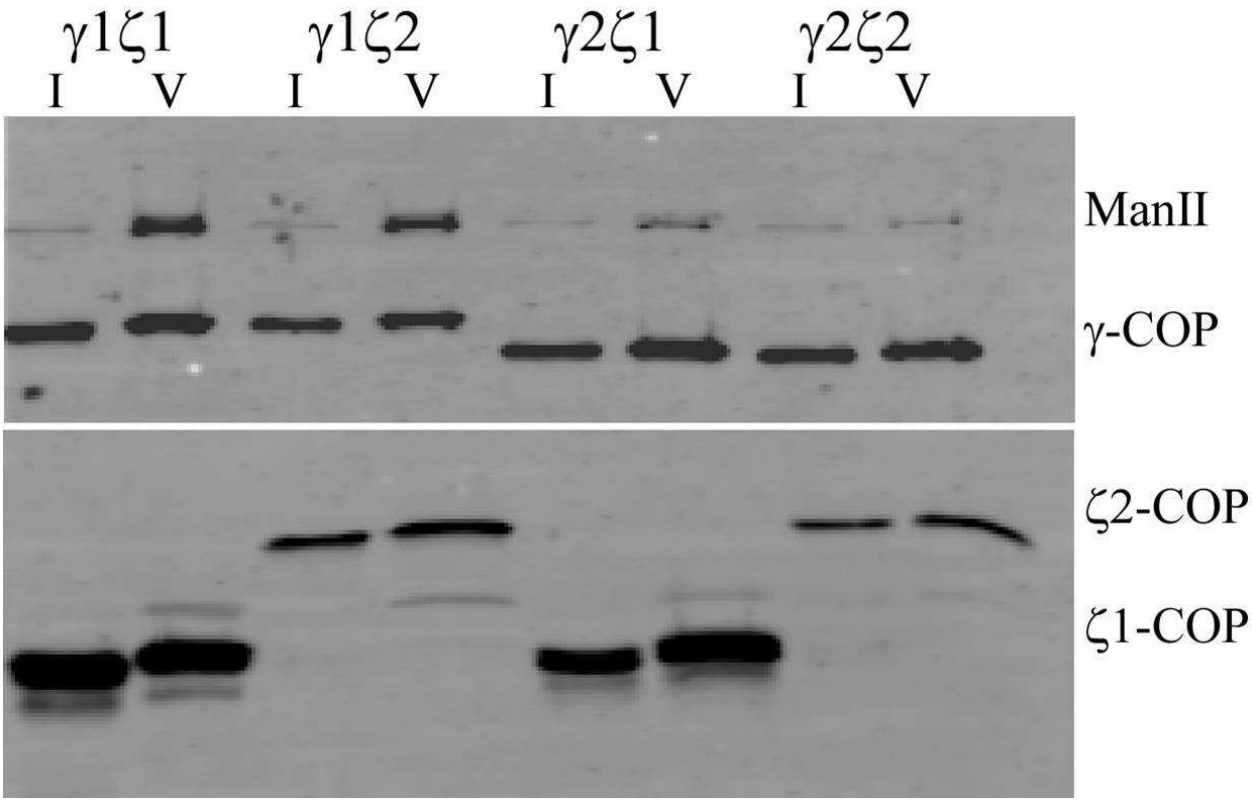

Figure 60. Coatomer isoforms and cargo uptake. Vesicle preparations in the presence of either one of the coatomer isoforms to form and isolate homogeneously coated vesicles. Analysis by SDS-PAGE and Western blotting with antibodies directed at a-mannosidase II and COP subunits.

As a preliminary result, a γ-COP specific uptake of α-mannosidase II (ManII) was observed. The experiment has been repeated with the same result twice. However, the effect could not be reproduced afterwards, so this awaits further investigation. Also, members of the p24 family are currently screened for coatomer isoform-dependent uptake into COPI vesicles.

Structural studies on coatomer

In addition to functional analysis of coatomer isoforms in COPI vesicle biogenesis and function, the protein complex is under investigation by electron microscopy studies in collaboration with Dr. John Briggs (EMBL). In order to produced pure material for structural analysis, the preparations were subjected to a sephacryl-S300 gel filtration, to select for the heptameric complex and get rid of aggregates and lower molecular mass contaminations, such as co-purified proteins and coatomer subcomplexes (Figure 61).

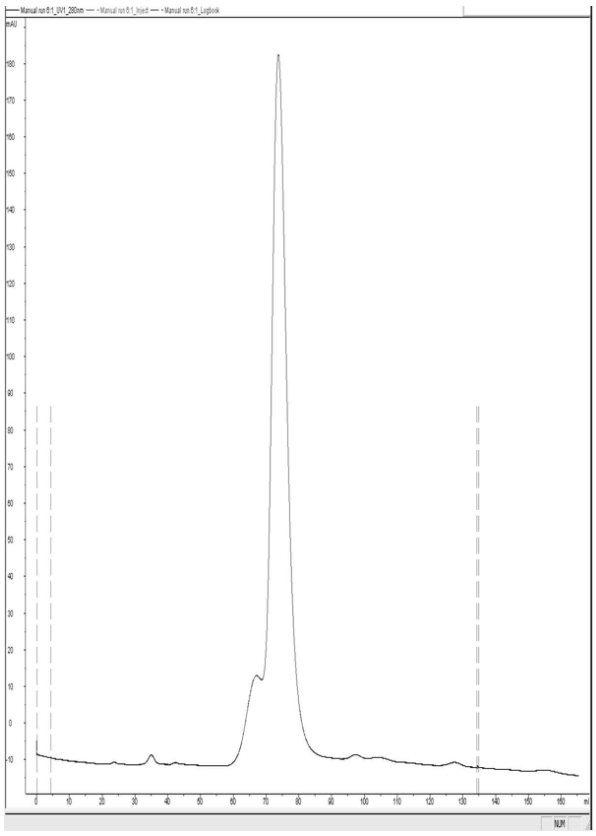

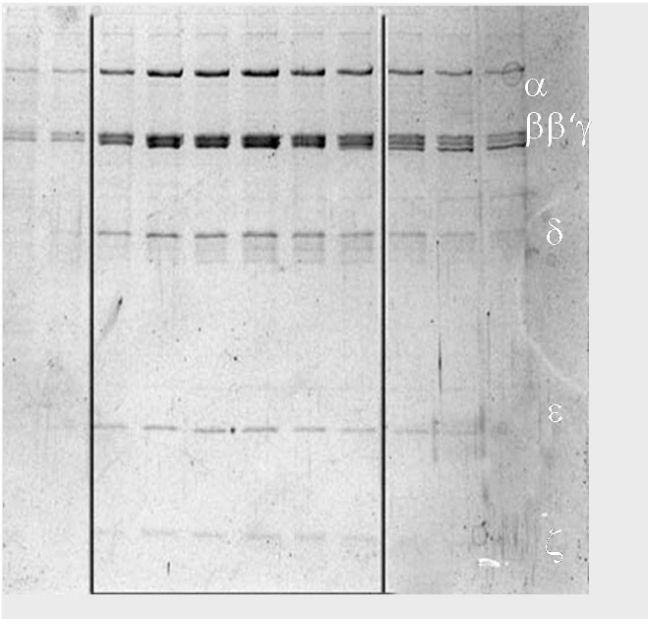

Figure 61. Purification of recombinant coatomer by gel filtration. g1/z2 coatomer was expressed and purified via Ni2+NTA affinity chromatography. Elevates were subjected to gel filtration, and the high molecular mass peak was analyzed by SDS-PAGE.

A symmetric peak corresponding to the expected mass of heptameric coatomer complex was obtained. SDS PAGE analysis and Coomassie stain of the peak fractions show a homogeneous purification, all seven subunits are visible as indicated.

In order to collect dataset of purified coatomer particles, the samples were analyzed by negative stain electron microscopy in the laboratory of Dr. John Briggs (EMBL). To this end, the samples were subjected to a glycerol/glutar aldehyde gradient by Simone Prinz, in order to gently crosslink and thereby stabilize the complex (Figure 62). This was needed as non-fixed complexes tended to dissociate during adsorption to the carbon grid (not shown). In additional experiments, this problem could also be overcome by using gel-filtered coatomer samples without any freezing steps, which allowed to omit the gradient fixation (not shown).

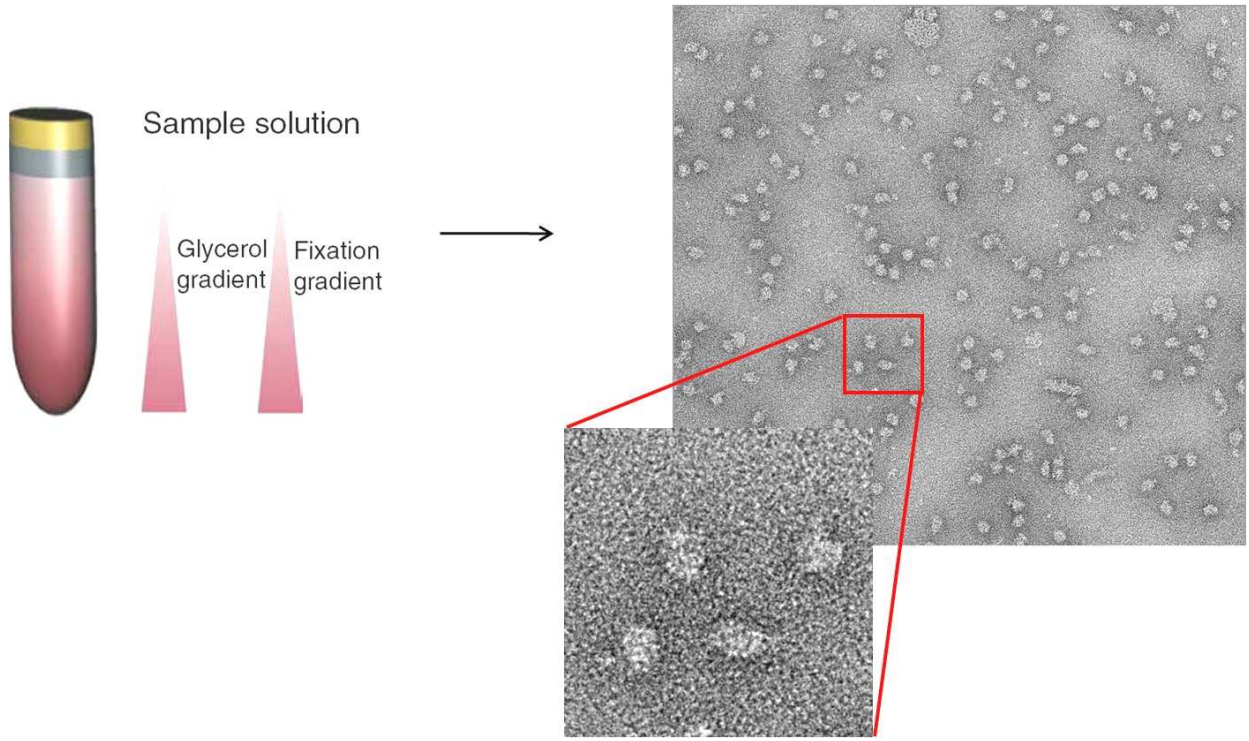

Figure 62. Gradient fixation and negative stain electron microscopy of single coatomer complexes. Samples were subjected to a glycerol and glutaraldehyde fixation gradient and analyzed by negative staining EM.

Datasets of approx. 10,000 single coatomer complexes were collected by Simone Prinz and Marco Faini (Briggs lab, EMBL), and sorted into various subclasses. A typical dataset of classified coatomer complexes is shown in (Figure 63)

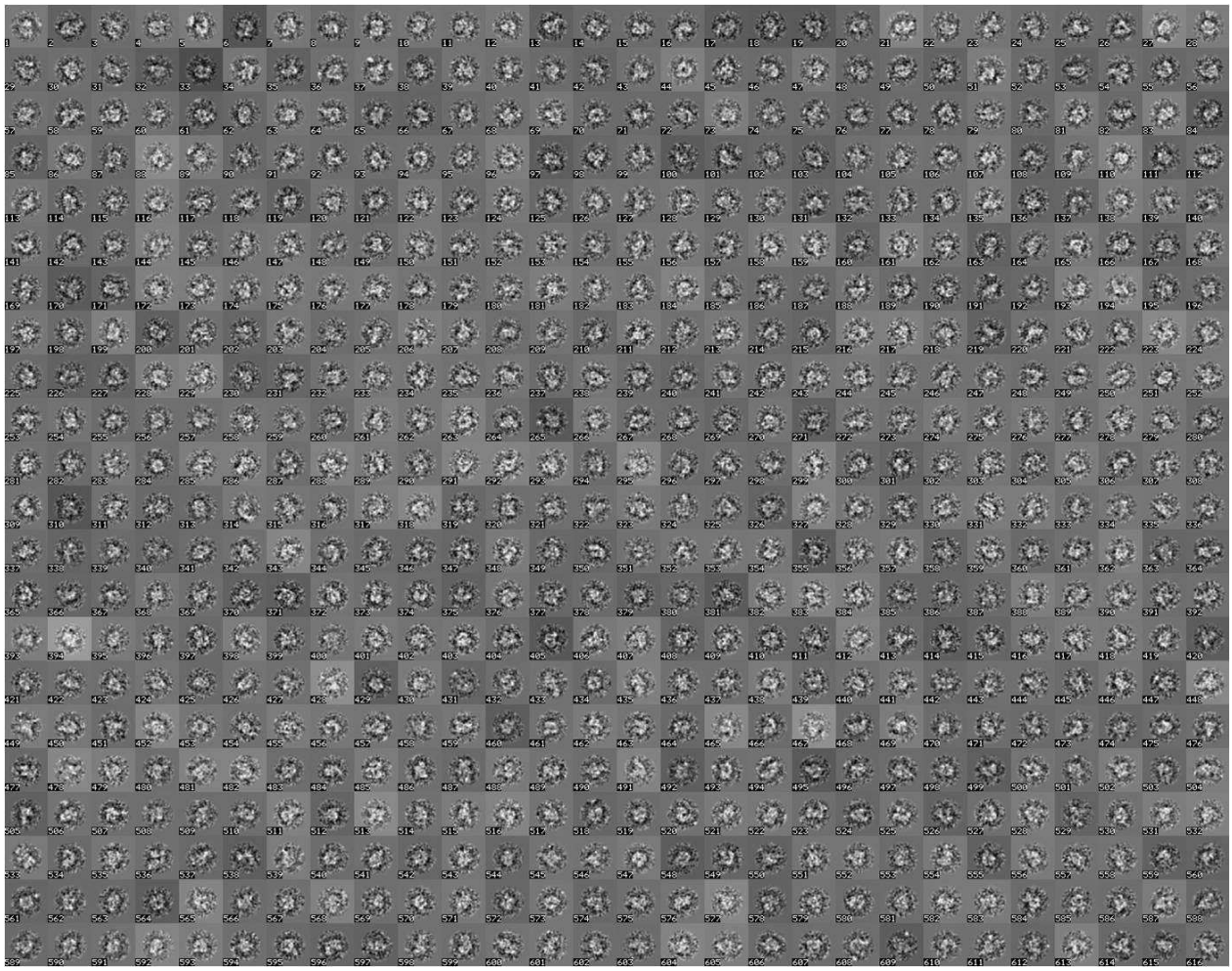

Figure 63. Dataset of coatomer complexes in negative staining EM.

Through an iterative processes of image processing, filtering and alignments into closer defined subclasses, structural information could be computed from the raw images (Figure 64).

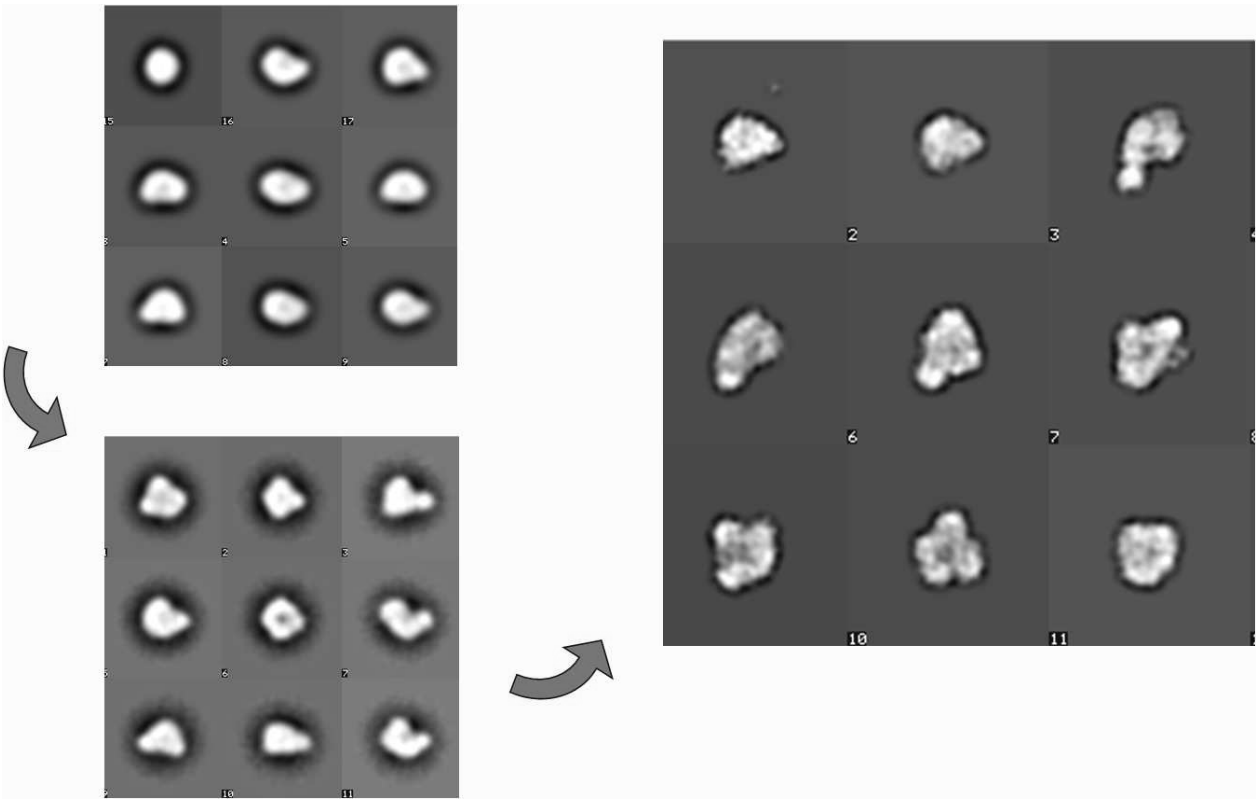

Figure 64. Image processing and classification of coatomer complexes in negative staining EM.

As can be seen in Figure 64, increasing detail could be computed from the blurred raw images but was limited due to multiple conformational heterogeneities in the samples. Stabilizing the complexes to limit heterogeneity by using known ligands, antibodies or surfaces such as lipid layers will be subject of future work.

Discussion

Part I

To study the molecular role of ArfGAP1 in COPI vesicle biogenesis and functions, a peptide antibody against human ArfGAP1 was raised, immunopurified and characterized. This antibody was successfully tested in Western blotting, immunoprecipitation and immunofluorescence.

Full length ArfGAP1 was not available at the beginning of this work. Since the protein is insoluble when expressed in bacteria, *Pichia pastoris* was chosen to express the full length protein in an eukaryotic environment. To this end, expression plasmids of full length ArfGAP1-HIS and truncation mutants were cloned, and the proteins expressed and purified. The recombinant ArfGAP1 protein was assayed for activity, and its capability to respond to membrane curvature was tested in comparison with truncation mutants that lacked a (at the time of the work unknown), lipid packing sensor motif that stimulates the GTP-activity in response to membrane curvature.

The protocol for the purification of myristoylated untagged Arf1 protein was considerably improved during the course of this work. The workload for the purification was reduced from three days to a single day, while obtaining a better yield at comparable purity.

To study the ArfGAP1 protein in a functional assay on COPI-vesicles generated in the presence of GTP, a new budding assay was developed . This assay allows to demonstrate two functions of full-length ArfGAP1 on COPI-vesicles generated from Golgi-membranes, namely cargo uptake and uncoating.

With the tools at hand, we carried out a detailed biochemical characterization of ArfGAP1 and Arf1 functions and their stoichiometry during COPI vesicle biogenesis, which aims at answering certain discrepancies found in the literature about their roles in COPI trafficking:

Arf1 has been described as a COPI coat component (Serafini, *et al.*, 1991; Donaldson, *et al.*, 1992; Sohn, *et al.*, 1996; Helms, *et al.*, 1993), and this was questioned in the literature (Yang, *et al.*, 2002; Lee, *et al.*, 2005; Yang, *et al.*, 2005). In the present study, we not only reexamined and confirmed the previously reported stoichiometry of coatomer and Arf1 on COPI-coated vesicles generated under GTP conditions, but also used the assays described in (Yang, *et al.*, 2002) to reexamine the reported lack of Arf1 in the vesicle fractions. In contrast to (Yang, *et al.*, 2002), we detect significant amounts of Arf1 in purified COPI vesicles. Furthermore, we show that Arf1 is included into COPI vesicles in a coatomer dependent manner, implying that the GTPase is incorporated into the vesicles. Apart from demonstrating that Arf1, rather than ArfGAP1, is a component of the COPI coat, the reported requirement of ArfGAP1 for COPI vesicle biogenesis (Yang, *et al.*, 2002) was more closely investigated in this study.

In a two-stage incubation system, stoichiometric amounts of ArfGAP1 had been described to be essential for the detection of COP signals in the stage II supernatant (Yang, *et al.*, 2002), and these observations were reproduced here. However, by using high salt (250 mM KCl), an even higher amount of vesicles was released into the supernatant. Thus, ArfGAP1 is not essential for the *in vitro* formation of COPI-coated vesicles. Furthermore, and in accordance with its antagonistic activity in the COPI vesicle budding assays, we provide evidence that ArfGAP1 does not represent a structural component of the COPI coat: when supernatants of stage II were subjected to ultracentrifugation, as shown in (Yang, *et al.*, 2005), ArfGAP1 was found in the pellet fraction. However, ArfGAP1 can sediment from a stage II supernatant independently of the presence of coatomer, under conditions were GTP hydrolysis is inhibited (GTPγS or

Arf1Q71L, Figure 20, and Figure 21). This indicates that ArfGAP1 associates with membranes, but not necessarily with COPI vesicle membranes, in accordance with its affinity to membranes via its ALPS domains (Bigay, *et al.*, 2003; Bigay, *et al.*, 2005).

From RNAi knock-down studies in mammalian cells it was shown that a reduction of ArfGAP1 does not lead to a significant phenotype. Only knock down of all three Gcs1 and Glo3 orthologs ArfGAP1, ArfGAP2 and ArfGAP3 together caused cell death (Frigerio, *et al.*, 2007), suggesting that the functions of ArfGAP1 can be complemented by other ArfGAPs, rendering an exclusive role of ArfGAP1 as budding component unlikely.

If indeed both ArfGAP1 and salt treatment may serve to release reconstituted COPI vesicles from the donor membranes, by which mechanism does this occur? ArfGAP1 is not needed to produce COPI vesicles in a chemically defined minimal system (Reinhard, *et al.*, 2003), nor from Golgi membranes (this thesis), which renders highly unlikely a functional role as a structural coat component. Therefore, we suggest that the reported requirement of ArfGAP1 to generate vesicles from Golgi (Yang, *et al.*, 2002) might be a result of an ArfGAP1 effect on other components of the Golgi, rather than the vesicle itself. This unknown effect of ArfGAP1 apparently can be substituted by high salt (Figure 20), suggesting a protein-protein interaction that prevents the release of the vesicles from the donor membranes. In an attempt to reconcile the opposing controversial reports on the role of ArfGAP1 activity, we conclude that either ArfGAP1 or salt are required the release vesicles from the Golgi membranes. Studies of an Arf1-specific tether, the coiled-coil protein GMAP-210, support this possibility: GMAP-210 localizes to the *cis*-Golgi (Rios, *et al.*, 1994) and its overexpression induces a dramatic accumulation of vesicles *in vivo* (Pernet-Gallay, *et al.*, 2002). Interestingly, the first 38 residues of GMAP-210 form a lipid-binding module that is remarkably sensitive to membrane curvature (Drin, *et al.*, 2007). The C-terminus contains a GRAB (GRIP-related Arf binding)

domain that interacts with Arf1 in its GTP state (Gillingham, *et al.*, 2004). This protein was shown to tether curved (vesicular) to flat membranes in an Arf1- dependent manner (Drin, *et al.*, 2008). The interactions of the GRAB domain with Arf1 could either be abrogated by ArfGAP1-mediated GTP hydrolysis (Drin, *et al.*, 2008) or, as we now suggest, by salt treatment. Such tethering mechanisms might help explain controversial findings of ArfGAP1 activity, and its requirement for the isolation of COPI vesicles as reported by (Yang, *et al.*, 2002), and will be subject to future investigations.

Part II

We have shown here that, when bound to GTP, Arf1 has a membrane tubulation activity. Upon activation, the small GTPase undergoes a conformational change, resulting in the protrusion of its N-terminally myristoylated and amphiphilic α-helix, which is generally thought to be accommodated in the donor membrane (Antonny, *et al.*, 1997). In a similar way, the amphipatic α-helix of the small GTPase Sar1p, involved in COPII vesicle formation, was reported to insert into and cause deformation of the membrane (Lee, *et al.*, 2005). Since, apart from dimerization, Arf1-Y35A behaves like wild type, we assume that in the monomeric mutant this α-helix is also inserted in membranes. It appears then that it is the insertion in a lipid leaflet of a pair of amphipatic stretches that results in the membrane tubulation activity induced by Arf1. Strikingly, synaptotagmin also induces membrane deformation by inserting a pair of C2 domains in membranes, and loses this activity if one of the two domains is removed (Martens, *et al.*, 2007). Similarly, dimerization has been proposed to regulate the membrane deformation activity of endophilin (Gallop, *et al.*, 2006) and of an EHD-ATPase (Daumke, *et al.*, 2007). Therefore, oligomerization of membrane deforming protein domains seems to regulate their effect.

In the context of vesicle formation, the interplay between Arf1 dimerization and multivalent binding to coatomer might even harbor a further mechanistic step. Indeed, as a monomeric activated Arf1 can bind to and recruit coatomer to membranes (Figure 41, Figure 44), and as multiple Arf1s are found per one coatomer in COPI vesicles (Serafini, *et al.*, 1991; Sun, *et al.*, 2007; Sohn, *et al.*, 1996; Helms, *et al.*, 1993), as well as Figure 27 from this thesis), activated Arf1 dimers could be crosslinked by the recruited coat complexes. This would result in the localized insertion of multiple pairs of amphipatic stretches, leading to a high membrane destabilization activity under a forming coat lattice, promoting the formation of a bud. Interestingly, in such a model, the final shape of the nascent bud would most probably be governed by the coat proteins, since they sit directly above the localized and concentrated membrane destabilization foci mediated by dimers of Arf1.

Together, the results in this part of the thesis suggest a mechanism of vesicle biogenesis that critically depends on bending of membranes induced by dimeric Arf1. This revisits the current paradigm for the role of Arf1 in the formation of transport vesicles, since the small GTPase was solely seen as a molecular switch that regulates the recruitment of coat proteins to membranes.

In light of recent data, our findings imply that Arf1-mediated curvature is needed for the fission step of COPI vesicle biogenesis (Figure 55 and Figure 56).

Part III

Two alternative models for intra-Golgi transport were initially proposed: cisternal progression/maturation and vesicular transport. The cisternal progression/maturation model postulates the transport of anterograde cargo *en bloc* with cisternae (Glick and Malhotra, 1998). Protein homeostasis and maintenance of cisternae with distinct compositions would be mediated by exclusively retrograde directed COPI vesicles removing resident cargo (e.g., glycosyltransferases) from the more *trans*- to the more *cis*-located cisternae, leading to the maturation of a given cisternae.

In contrast, the vesicular transport model postulates the transport of anterograde cargo between static cisternae via coordinated budding and fusion reactions of anterograde-directed COPI vesicles (Rothman and Wieland, 1996). Since the continuous loss of material at the *trans*-Golgi would be antagonized by retrograde-directed COPI vesicles, the existence of at least two distinct populations of COPI vesicles, one mediating anterograde, and one mediating retrograde transport, would be required reviewed in (Bethune, *et al.*, 2006).

In fact, a second isoform for each of the two coatomer subunits, γ- and ζ-COP, the paralogs γ2- and ζ2-COP were shown to be incorporated into coatomer complexes in a stoichiometric manner, which resulted in three major isoforms of the complex with the compositions γ1/ζ1-, γ1/ζ2-, and γ2/ζ1-COP (Wegmann, *et al.*, 2004). The localization of coatomer isoforms in NRK cells was investigated by using immunoelectron microscopy, and a striking heterogeneity within the Golgi apparatus was found (Moelleken, *et al.*, 2007): whereas γ1- and ζ2-COP seemed to be restricted to the early Golgi and a pre-Golgi compartment, the majority of γ2-COP-containing isoforms of the complex was localized to the *trans* side of the organelle. These results strongly suggested the existence of different homogeneously coated isoforms of COPI vesicles that might

serve multiple transport routes within the early secretory pathway. For this reason, a project was launched with the aim to produce recombinant heptameric isotype-specific coatomer complexes. To this end, Dr. Monika Sahlmüller cloned the sequences encoding for each of the seven isotypes into bacmid vectors, thereby generating four Baculo virus stocks, each of which encoding one of the four possible heptameric coatomer isoforms, defined by their γ/ζ-compositions. During the course of this thesis, such virus was exploited to infect insect cells and express the complexes, which could afterwards be purified via affinity chromatography, followed by gel filtration. With these defined populations of COPI coats at hand, COPI vesicle reconstitution assays were performed and the capability of vesicle generation of each coatomer isoform was assessed by using the methods described earlier in this work. While no significant differences in COPI budding efficiencies were observed for any of the four coatomer isoforms, we found striking preferences of vesicles derived from γ1-COP isoforms for the uptake of α-ManII (Figure 60). This effect with regards to differential cargo uptake needs further experiments, specifically the investigation of additional cargo proteins. In addition, we will expand the studies by using total membrane fractions, instead of Golgi enriched samples, in order to exclude that certain coatomer isoform specific Golgi- subcompartments were depleted during the preparation.

For the structural part of the ongoing coatomer isoform project, recombinant coatomer was produced to near homogeneity and analyzed by negative staining electron microscopy (Dr. John Briggs, Simone Prinz, Marco Faini, EMBL).

Materials

Chemicals

All commonly used chemicals were purchased from either Merck (Darmstadt), Sigma (Deisenhofen), Roth (Karlsruhe), Fluka (Taufkirchen), Qiagen (Hilden), Amersham-Biotech (Freiburg), BioRad (München) or Boehringer (Mannheim). The reagents were ordered directly from the company or via the chemical store of the university of Heidelberg (Theoretikum der Universität Heidelberg). Triton X-100 was purchased from Merck, Tween-20 from Sigma and NP-40 was obtained from Calbiochem. The chemical crosslinkers: EMCS and BMH were purchased from Pierce. Nucleotide ATP, ADP, GDP, GTP, GDPβS and GTPγS, myristic acid and protease inhibitor tablets were obtained from Sigma or Roche.

Peptides

The peptide with the sequence EPPKAKSPSSDSWTC to generate ArfGAP1 antisera were synthesized by Pineda Antibodyservice, Berlin. Purity was assessed by MALDI analysis and reverse phase HPLC.

The p23 protein tail peptide was synthesized and lyophilized at Center for Molecular biology of the University of Heidelberg (ZMBH). The sequence of monomer-p23 peptide was CLRRFFKAKKLIE.

Beads

For immunoprecipitation a 1:3 mixture of Protein A Sepharose and CL4B sepharose was

used (both bought from BioRad, Munich, Germany) und stored at 4°C in an aqueous 20%

EtOH solution.

Molecular weight standards for SDS – PAGE

• BMW-Marker (broad molecular weight) manufactured by BioRad (Munich, Germany)

and a marker cocktail by PEQLab (Erlangen, Germany):

Myosine 200kD	Aprotinine 6.5kD
β-Galactosidase 116kD	β-Galactosidase 116kD
Phosphorylase B 97kD	Bovine serum albumine 66kD
Bovine serum albumine 68kD	Ovalbumine 45kD
Ovalbumine 45kD	Laktat-Dehydrogenase 35kD
Carboanhydrase 30kD	RE Bsp 98I 25kD
Trypsine-Inhibitor 20kD	β-Laktoglobuline 18.4kD
Lysozyme 14.3kD	Lysozyme 14.3kD

• A prestained Marker-Cocktail with recombinant protein standards bought from BioRad

(Munich, Germany):

250kD	56kD
150kD	37kD
100kD	25kD
75kD	

Protease – Inhibitors

To inhibit proteases in the Golgi and coatomer preparation, and upon purification of recombinant proteins, protease-inhibitor-cocktail tablets ("complete, EDTA-free") manufactured by Roche Diagnostics (Mannheim, Germany) were used.

Antibodies

(a) Primary antibodies

epitope	name	species	dilution (WB)
Arf1 (CT peptide)	Arf-CT	rabbit	1:5000
p23	Henriette	rabbit	1:10 000
His_6 (Covance)	Histidin	mouse	1.1000
α-COP (CT peptide)	Nr. 1409 B	rabbit	1:2000
β-COP	B1.2	rabbit	1:2000
β´-COP	Nr. 899	rabbit	1:10 000
δ-COP	Nr. 877	rabbit	1:1000
ε-COP	Rab2	rabbit	1:1000
γ1-COP	g1.2	guinea pig	1:10 000
γ2-COP	g2.2.	guinea pig	1:10 000
γ1/γ2-COP	γR	rabbit	1:10 000
ζ1-COP	R468	rabbit	1:5000
ζ2-COP	R442	rabbit	1:5000-10 000

(b) Secondary antibodies

Two systems were used for detection in Western blotting: Horseradish peroxidase-coupled goat-anti-rabbit and goat-anti-mouse IgGs manufactured by BioRad (dilution 1:5000) for detection using films, and fluorophore-conjugated secondary antibodies (goat-anti-rabbit, and goat-anti-mouse) for detection in the LI-COR Odyssey System (LI-COR BioSciences, Lincoln, USA).

Restriction enzymes and DNA polymerases

DNA modifying enzymes were purchased by New England Biolabs (New England, USA). Pfu turbo DNA polymerase was purchased from Stratagene (La Jolla, USA).

Bacterial strains

The *E. coli* strains used for subcloning and plasmid propagation were either DH-5α (Invitrogen, Carlsbad, USA) or Nova Blue (Novagen, Bad Soden). The strains used for protein expression were $BL21_{star}$, $BL21_{star}$pLysS (Invitrogen), Origami2 (Novagen).

Growth media

Lauria-Bertani broth (LB):

In 1L of distilled water the following components were dissolved: 10 g of sodium chloride, 10 g of Bacto-Tryptone and 5 g of yeast extract. For plates, 15 g/L agar was added to the preparation. The medium was sterilized by autoclaving.

SOC medium:

In 980 ml of distilled water the following components were added: 0.5 g of sodium chloride, 20 g of Bacto-Tryptone, 5 g of yeast extract and 2.5 ml of a 1M potassium chloride solution. After sterilization by autoclaving, 10 ml of a 1M magnesium chloride sterile solution and 10 ml of a 1M glucose sterile solution were added in a sterile manner.

For the expression of Arf1, NZCYM media was purchased from Invitrogen.

Buffers

PBS:

1.47 mM KH_2PO_4

4.29 mM Na_2HPO_4

137 mM NaCl

2.68 mM KCl,

pH=7.4 for PBS-T, 0.05% (v/v) Tween 20 was added.

Pichia dialysis buffer

20 mM Tris-HCl pH 8.0

10 mM DTT

0.1 mM $ZnCl_2$

5 mM $NaCl_2$

Coatomer isoforms purification buffers

Lysis Buffer:

50mM Hepes

300mM NaCl

20mM Imidazole

1mM DTT pH7,5

Wash Buffer:

50mM Hepes

300mM NaCl

40mM Imidazol

1mM DTT pH7,5

Elution Buffer

50mM Hepes

300mM NaCl

250mM Imidazol

1mM DTT pH7,5

Gelfiltration Buffer

50mM Hepes

150mM NaCl

1mM DTT pH7,5

5x DNA loading buffer

50 mM Tris-HCl, pH 8
4 M Urea
25% (w/v) Saccharose
0.1% (w/v) Bromophenol blue
100 mM EDTA

50x TAE

242 g Tris base

57.1ml Glacial Acetic Acid

18.6 g EDTA

Endogenous coatomer purification buffers

Homogenization buffer 1

25 mM Tris-HCl, pH=7.4
500 mM KCl
250 mM saccharose
2 mM EGTA-KOH
1 mM DTT

Homogenization buffer 2

25 mM Tris-HCl, pH=7.4

2 mM EGTA-KOH

1 mM DTT

IEX1

25 mM Tris-HCL, pH=7.4

200 mM KCl

1 mM DTT, 10% (w/v) glycerol

IEX2

25 mM Tris-HCL, pH=7.4

1 M KCl

1 mM DTT

10% (w/v) glycerol

IEX3

25 mM Hepes-KOH, pH=7.4

100 mM KCl

1 mM DTT

10% (w/v) glycerol

IEX4

25 mM Hepes-KOH, pH=7.4

1 M KCl

1 mM DTT

10% (w/v) glycerol

3x SDS loading buffer

187.5 mM Tris-HCl pH 6.8

6% (w/v) SDS

15% (v/v) β-mercaptoethanol

30% (v/v) glycerol

0.0675% bromophenol blue

SDS Electrophoresis buffer

25 mM Tris-HCl, pH=8.3

250 mM glycine

0.1 % (v/v) SDS

Coomassie staining solution

400 ml ethanol

100 ml acetic acid

0.25 % (w/v) Coomassie R-250

500 ml water

Destaining solution

200 ml ethanol

50 ml acetic acid

750 ml water

Ponceau-S solution

0.8% (w/v) ponceau red S

4% (w/v) TCA

Semi-dry transfer buffers

Anode I buffer

300 mM Tris-HCl, pH=10.4

20% (v/v) methanol

Anode II buffer

30 mM Tris-HCl, pH=10.4

20% (v/v) methanol

Cathode buffer

25 mM Tris-HCl, pH =9.4

40 mM 6-aminocaproic acid

20% (v/v) methanol

SDS PAGE stock solutions

Acrylamide-solution 1

30% Acrylamide (w/v)

0.8% N,N'-Methylenbisacrylamide (w/v)

Acrylamid-solution 2

30% Acrylamide (w/v)

0.3% N,N'-Methylenbisacrylamide (w/v)

4x separation gel buffer

1.5M Tris-HCl, pH 8.8

0.4% SDS (w/v)

4x stacking gel buffer

0.5M Tris-HCl, pH 6.8

0.4% SDS (w/v)

Elektrophoresis buffer

25mM Tris

192mM Glycine

0.4% SDS (w/v)

Immunoprecipitation buffer

25 mM TRIS-HCl, pH7.4

150 mM KCl

1 mM EDTA

0.5 % NP-40

HKM buffer

50mM Hepes, pH 7.2

120mM KAcetate

1mM MgCl2

1mM DTT

Coupling buffer

100 mM Tris-HCl, pH=7.5

500 mM NaCl

1mM EDTA

Blocking buffer

100 mM sodium acetate, pH=4.5

500 mM NaCl

Methods

Agarose gel electrophoresis

DNA fragments were separated through a 1% (w/v) Agarose gel in TAE buffer. For the detection of DNA, ethidium bromide was added to a final concentration of 0.5 µg/ml. The samples were mixed with 5x DNA loading buffer and pipetted into loading wells. The gel was run at 200 V in TAE buffer. DNA bands were visualized under irradiation with UV light (260 nm).

DNA concentration determination

Samples were diluted 1:100 in mQ water and poured into a quartz cuvette. The optical density at λ = 260 nm was measured. For double stranded DNA, one absorbance unit at 260 nm corresponds to a concentration of 50 µg/ml.

Polymerase chain reactions

The following reactions were assembled:

Template DNA (30 ng/µl)	1 µl
Primer 1 (100 pmol/µl)	1 µl
Primer 2 (100 pmol/µl)	1 µl
dNTP (10 mM each)	1 µl
10 x pfu buffer	5 µl
mQ water	40 µl

pfu polymerase (2.5 u/µl) 1 µl

the polymerase chain reaction was allowed to proceed with the following parameters:

95°C	60 s	
95°C	30 s	30 cycles
60°C	45 s	
72°C	1 min/kb target gene	
4°C	10 min	

PCR products and plasmid fragments purification

DNA fragments were loaded in the wells of a 1% agarose gel and separated through electrophoresis as described above. Ethidium bromide stained bands were visualized under UV light and cut with a scalpel blade. The DNA was extracted from the gel and purified with a DNA extraction kit (Macherey-Nagel, Düren) according to manufacturer instructions.

Restriction and ligation

All restrictions enzymes were purchased from New England Biolab (Beverley, USA), they were provided with reaction buffer and BSA. DNA plasmids or PCR products were mixed with 1 µl of each restriction enzyme, 0.2 µl of a 100x BSA solution and 2 µl of the appropriate 10x buffer. The volume of the reaction was set to 20 µl with mQ water. The reaction was allowed to proceed for one hour at 37°C.

Ligations were either performed with T4 DNA ligase (Fermentas, Vilnius, Lithuania) or with the following kits: Alligator ligation kit (Genaxxon, Biberach) or DNA ligation kit (Takara, Shiga, Japan) according to manufacturer instructions.

Transformation

50 µl of DH-5α *E. coli* competent cells (Invitrogen, Carlsbad, USA) were mixed with 1 to 3 µl of ligation reaction. Cells were then incubated for 10 to 30 min on ice and were heat shocked at 37°C for 20 s. They were then incubated back on ice for 2 min and 300 µl SOC medium were added. The cells were then incubated for 1 h at 37°C with agitation and spread on LB agar plates containing the appropriate antibiotic.

Site directed mutagenesis

Point mutations were introduced using the Quick change site directed mutagenesis kit (Stratagene). Primers for the (+) and (-) DNA strand of the gene to be mutated were ordered from Biomers.net, Ulm. They encoded the mutant codon flanked by 15 to 18 bases annealing to the sequence upstream and downstream the targeted mutation. The following reaction was assembled:

Template DNA (10 ng/µl)	1 µl
Primer 1 (100 ng/µl)	1.25 µl
Primer 2 (100 ng/µl)	1.25 µl
dNTP (10 mM each)	1 µl
10 x pfu buffer	5 µl
mQ water	39.5 µl
pfu polymerase (2.5 u/µl)	1 µl

Polymerase chain reaction was allowed to proceed with the following parameters:

95°C	60 s	
95°C	30 s	16 cycles
55°C	45 s	
72°C	1 min/kb target gene	

4°C 10 min

After polymerase chain reaction, the restriction enzyme DpnI (New England Biolab) was added to the incubation to units (1 µl) and was allowed to digest the methylated template DNA for 1 h at 37°C. The mutated DNA, which is not methylated, is not altered by DpnI. After DpnI treatment, 10 µl of NovaBlue Giga single cells (Novagen) were transformed with 1 µl of the DpnI treated sample: DNA and cells were incubated together for 5 min on ice before heat shock at 42°C for 30 s, the cells were then incubated back on ice for two minutes and 100 µl of SOC medium was added. The cells were then incubated at 37°C with agitation for 1 h and the whole incubation was then plated on an LB agar plate with the appropriate antibiotic selection.

Protein expression

(a) Transformation

5 µl of $BL21_{STAR}$ (Invitrogen) *E. coli* competent cells were mixed with 0.5 µl of plasmid stock solution and incubated on ice for 5 min. The cells were then heat shocked at 42°C for 30 s and incubated back on ice for 2 min. 80 µl of SOC medium were then added and the cells were incubated for 1 h at 37°C with agitation. The cells were then spread on LB agar plates containing appropriate antibiotic.

(b) Expression

One colony of *E. coli* was picked from an LB agar plate and used to inoculate 3 ml of LB medium containing the appropriate antibiotic. The pre-culture was incubated overnight at 37°C with agitation. On the next day, 2 L of LB medium containing antibiotic were inoculated with

the pre-culture and grown at 37°C, 180 rpm until OD_{600} reaches about 0.6. IPTG was then added to 1 mM and the incubation resumed at 37°C for another 3 h.

(c) Cell lysis

After protein expression the cells were recovered by centrifugation (4000 x g, 10 min) and the pellet resuspended in the appropriate lysis buffer (see below). The suspension was then flash frozen in liquid nitrogen and stored at -80°C until further processing.

Resuspended cell pellets were thawed in a water bath and disrupted by multiple passages through a high pressure cell homogenizer (EmulsiFlex C-5, Avestin, Mannheim). The lysate was then centrifuged at 30000 x g, 4°C for 10 min. The supernatant was recentrifuged at 100000 x g, 4°C for 1 h. The second supernatant was the starting material for the purification.

Protein purification

(a) Immobilized Metal Affinity Chromatography (IMAC)

The lysis buffer for this purification was 50 mM Na_2HPO_4, pH=8, 500 mM NaCl, 10 mM imidazole, 1% Triton X-100. 0.5 ml of Ni-NTA beads (HisTrap HP, Amersham biosciences, Freiburg) were pre-equilibrated with lysis buffer. They were then mixed with the cell lysate and incubated for 30 min at 4°C. The beads were recovered by centrifugation (1000 x g, 3 min) and washed three times with 40 ml of washing buffer (50 mM Na_2HPO_4, pH=8, 500 mM NaCl, 50 mM imidazole). The beads were then mixed with 1 ml of elution buffer (50 mM Na_2HPO_4, pH=8, 500 mM NaCl, 250 mM imidazole) and poured in a 5 ml disposable column with a frit (Bio-Rad, Munich) to recover the eluted material. Three 1 ml elution fractions were collected.

(b) Glutathione sepharose chromatography

The lysis buffer for this purification was PBS containing 1 mM DTT. 1 ml of glutathione beads (glutathione sepharose high performance, Amersham biosciences, Freiburg) was pre-equilibrated in PBS and then incubated with the cell lysate for 1 h at room temperature. The beads were then recovered by centrifugation (1000 x g , 30 min) and washed three times with 40 ml of PBS containing 1mM DTT. The beads were then incubated with 1 ml of elution buffer (20 mM Tris, pH=8, 150 mM NaCl, 20 mM glutathione, 1 mM DTT) for 10 min at room temperature and poured in a 5 ml disposable column with a frit (Bio-Rad, Munich) to recover the eluted material. Three 1 ml elution fractions were collected.

(c) Gel filtration

The column of choice was equilibrated with 150 ml of buffer A (50 mM Hepes, pH = 7.4, 300 mM NaCl, 90 mM KCl, 10 % glycerol). The column was calibrated with a mixture of protein standards of known molecular weight (Bio-Rad, Munich). The protein samples were loaded in a volume, appropriate for the column used (1% of the column bed volume max.). As the protein sample obtained after IMAC was typically 1.5 ml, three consecutive runs were performed and fractions were collected in the same collection tubes. Aliquots from each fraction were analyzed by non-reducing SDS-PAGE. The peak eluting at the elution time predicted for the size of the dimer (estimated from the calibration) was pooled and, after protein concentration determination, snap frozen in liquid nitrogen and stored at -80°C.

Peptide coupling to thiopropyl-sepharose beads

150 mg of dry thiopropyl-sepharose beads (Amersham biosciences, Freiburg) were dissolved in 10 ml of coupled buffer and allowed to swell for 20 min at room temperature. The excess of buffer was then removed and the beads were then mixed with 0.75 µmol of peptide (the first residue of all peptides to be coupled was a cystein) in a total of 500 µl of coupling buffer. Beads

and peptide were then incubated overnight at room temperature with end-over-end agitation. As the peptide gets coupled to the activated thiopropyl group of the beads, a thiopyridon, absorbing light at λ=343 nm, is released. After coupling, the beads were recovered by centrifugation (1000 x g, 3 min) and the absorbance of the resulting supernatant was measured at λ=343 nm. The extinction coefficient of the thiopyridon being known (ε=8080 M^{-1}), its concentration could be determined and it was assumed that the amount of peptide coupled to the beads was the same as the amount of thiopyridon released. The beads were then washed five times with 10 ml of blocking buffer. To quench the remaining activated thiopropyl groups, the beads were then incubated with 10 ml of blocking buffer containing 200 µmol of β-mercaptoethanol for 15 min at room temperature. The beads were washed five times with 10 ml of coupling buffer and then finally resuspended in 5 ml of coupling buffer containing 0.02% sodium azide to generate a 1:10 slurry that was store at 4°C.

SDS PAGE

SDS-treated proteins were analyzed using a modified, discontinuous gel system (Laemmli, 1970). Both in the stacking and in the separation gel the voltage was kept constant (120V in the stacking gel, 180V in the separation gel).

Separation gels

If not stated otherwise, a custom-built gel system allowing a long separation gel (15cm) and simultaneous loading of 22 samples, or the Protean III gel system by BioRad were used. Homogenous separation gels contained 6%, 7.5%, 10% and 12%.

Gel:	7.5%	10%	12%
Acrylamide-solution	2 2.5ml	3.33 ml	4.0 ml

4x separation gel buffer	2.75ml	2.5 ml	2.5 ml
H20	5.5ml	4.16 ml	3.5ml
TEMED	10 µl	10 µl	10 µl
APS (10%)	40µl	40µl	40µl

The gel cartridge contain a separation gel volume of appr. 10ml (15x7x0.1cm). The gel solutions were added either directly or via a gradient mixer, and covered with isopropanol. The comb was already inserted during separation gel polymerization.

Stacking gels

After one hour polymerization at room temperature, the isopropanol was removed and washed with H2O. Residual H2O was removed using filter paper, and ca. 5ml of stacking gel solution with the composition described below were applied on top of the separation gel already in the cartridge. To from pockets, combs with 15 and 22 teeth were used. After 1h of polymerization at room temperature, the gels were packed in wet paper towels, sealed in plastic wrapping and stored at 4°C.

Acrylamide-solution 1	0.6 ml	**TEMED**	6 µl
4x separation gel buffer	1.25 ml	**APS (10%)**	30 µl
H20	3.1 ml		

Sample preparation for SDS – PAGE

The protein solution were diluted with 4x sample buffer in a ratio of 3:4, and heated either to 70° for 10 minutes, or to 95°C for 5 minutes, as stated in the protocol. After a short

centrifugation, the samples were injected into the gel pockets. Bromphenolblau was added to the sample buffer to obtain a blue-colored sample buffer, to facilitate loading of the samples.

Coomassie-Staining

The gels were incubated in Coomassie staining solution for 1h at room temperature, which led to a complete staining of the gel. Using destaining solution, the gels were subsequently washed to give the appropriate staining levels.

Western blot analysis

Transfer of proteins separated by SDS-PAGE onto PVDF-membranes

Proteins were transferred from SDS-PAGE onto PVDF-membranes (Immobilon-P, Millipore, Eschborn) using a "semi-dry" procedure in Trans-Blot SD cells manufactured by BioRad (Munich, Germany). Per gel, 7 filter papers (Whatman 3mm) and a membrane were cut in the size of the gel to be blotted. Two papers each were soaked in Anode buffers 1 and 2, and deposited on the anode board (anode 1 soaked paper on bottom). After application of the PVDF-membrane, the gel was deposited on top, and subsequently covered with the 3 remaining paper slips soaked in cathode buffer. After careful removal of air bubbles using a round object, the cathode plate was set on top. Proteins were then transferred onto the membrane at 24V (constant voltage) for 90 minutes.

Ponceau-Staining of proteins on PVDF-membranes

This method was used for staining of proteins separated by SDS-PAGE and transferred onto PVDF-membranes. The blots were incubated for 5 minutes in Ponceau-staining solution, and subsequently washed with water until the desired destaining levels were reached.

Immunochemical detection of proteins on PVDF-membranes

Membranes with transferred proteins were either incubated 1h at room temperature or over night at 4°C in PBS-T containing 5% (w/v) milk powder. Subsequently, membranes were washed 2x10 min in PBS-T. The blots were then incubated with the corresponding primary antibodies in PBS-T containing 1% BSA for 30 minutes at room temperature. The blots were washed 3x10 min with PBS-T, and subsequently incubated with secondary antibody in PBS-T containing 3% milk powder for 30 minutes at room temperature. The blot was then developed using either one of the two following systems:

1. The ECL system by the company Amersham Pharmacia Biotech (Freiburg, Germany) for detection of peroxidase coupled secondary antibodies. Here, the protocol of the manufacturer was used. For detection of the chemoluminescence, CEA RP New films (Strangnas, Sweden) were used. 2. The LI-COR Odissey system manufactured by LI-COR Biosciences (Lincoln, USA). For detection, the protocol of the manufacturer was followed.

Bradford assay

Protein concentrations were determined using staining solutions bought from BioRad (Munich, Germany). An appropriate volume of protein solution (about 10 – 20 µg) was diluted to a final volume of 800µl in mp water (triplicate measurements with different dilutions), with an 8-point calibration curve in a range of 2.5 – 20µg BSA (0, 2.5, 5, 10, 15, 20 and 255g/ml final concentration, in 800 µl final volume). Then, 2005l of Bradford reagent were added to all samples and incubated at room temperature for 10 minutes. 2005l of each sample were transferred into a microtiterplate and the optical density at 620nm measured in the microplate reader.

Tri-Chloro-acetic acid (TCA) – precipitation

Desoxycholate (2% stock solution) were added to the protein sample to a final concentration of 0.2% and incubated at room temperature for 15 minutes. The sample was the adjusted to a final concentration of 10% TCA by addition of cold 50% TCA solution (stored in ice-water), and incubated on ice for 30 minutes. The sample containing the precipitated proteins was then centrifuged (Heraeus-Biofuge, 13000 g, 4°C, 15min), and the supernatant discarded. The precipitate was washed with cold aceton (stored at -20°C) and centrifuged again (see above). After removing the supernatant, the precipitate was dried at room temperature for 5 minutes, and the precipitates proteins resuspended in an appropriate volume of 1x SDS sample buffer.

Immunoprecipitation (IP)

To bind ca. 30µg of protein, 20µl antibody solution and 120µl Protein A sepharose beads were used. The samples were agitated in an overhead shaker at room temperature, or overnight, washed with IP buffer and subjected to SDS PAGE.

Synthesis of p23 lipopeptide

The commercially available phosphatidylethanolamin (PE) derivative 1,2-dioleoylsn-glycero-3-phosphoethanolamine-n-[4-(malaeimidophenyl)butyramide] (MPB-PE) was purchased from Avanti polar lipids.. Prior to use, the cystine containing peptides were analyzed for their potential oxidation of the cysteine thiol group that reacts to the MPB-PE lipid. According to the manufacturer recommendations (Pierce), Ellman reagent was used for this purpose and typically 70% of the peptides were found having a functional reduced thiol group. MPB-PE (500nmol) was added to a glass vial and solvent was removed under a gentle stream of Argon. Depending

on the degree of oxidation of p23 peptide (typically 30%), a suitable amount of p23 peptide dissolved in dimethylformamide (DMF) was added to the lipid film (10% excess of peptide over MPB-PE) and the mixture was kept at least 4hr on a rotating wheel. Free maleimido groups were quenched by addition of 1μmol of β-mercaptoethanol. The mixture was dried under Argon and the sample was resuspended in 1ml 30% acetonitrile (AN) / 0.1% trifluoroacetic acid (TFA). Sep-Pak C18 cartridges were used to purify the lipopeptide. The Cartridge was washed with 1 x bed volume (1ml) of 100% AN/0.1% TFA and equilibrated with 30ml of 30%AN /0.1% TFA before loading of the sample. The cartridge was then submitted to a step gradient that consisted of 2ml of 30% AN / 0.1%TFA, 2ml of 40% AN / 0.1%TFA, 2ml of 60% AN / 0.1%TFA, 2ml of 80% AN / 0.1%TFA, 4ml of 90% AN / 0.1%TFA and 2ml of 100% AN / 0.1%TFA. The p23 lipopeptide was eluted at 80% and 90% AN / 0.1% TFA. Each fraction was lyophilized and dissolved in 200μL 30% AN / 0.1%TFA, and 10μL was analyzed by thin layer chromatography (standard silica gel 60 plates, 20 x 20cm) (Merck). A mixture of butanol, pyridine, acetic acid (glacial) and water (9.7:7.5:1.5:6, v:v:v:v) was used as the solvent. Silica plates were developed for 3hr, then dried and placed in a chamber containing solider iodine to stain lipids and lipopeptides. Peptides were also stained due to their hydrophobic amino acids (two phenylalanine residues). After quantification of the phosphate content, aliquots of 15nmol mono-lipopeptides were dried and stored under Argon at -80ºC.

Isolation of coatomer from rabbit liver

To achieve a higher yield and purity of the coatomer complex, the original protocol (Pavel, *et al.*, 1998) was slightly modified.

Isolation of rabbit liver cytosol

For one preparation, 3 livers (ca. 160g) from freshly killed rabbits (starved for 12h to reduce glycogen in the livers) were used. The livers were transferred into ice/water right after extraction, cut into thin slices (>1cm) and placed into homogenization buffer (200ml). Homogenization of the tissue was performed in a Warring blender with pulses of 2x 30s and a pause for cooling (2min) on ice. The homogenate was centrifuged at 15000xg at 4°C for 1h (Heraeus-Suprafuge 22, Rotor: HFA 12.500). The supernatant was filtered through 4 layers of mull and centrifuged at 100000 x g, 4°C (Ultracentrifuge, Rotor: TFT 50.38). The supernatant ("rabbit liver cytosol") was filtered through 4 layers of mull again.

Ammoniumsulfate precipitation of rabbit liver cytosol

Rabbit liver cytosol was diluted 1:2 with cold homogenization buffer 2 and transferred into a glass beaker. Slowly, freshly pulverized Ammoniumsulfate was added to a final concentration of 35% under constant stirring on ice, and after completed addition stirred for another 45 minutes. The precipitate was centrifuged for 30 minutes at 10.000 x g, 4°C (Heraeus- Suprafuge 22, Rotor: HFA 12.500), and the supernatant was discarded. The precipitate was resuspended in 100ml of resuspension buffer, homogenized in a douncer and dialyzed 2x 1h and 1x overnight against 5l IEX-1 (Ion-Exchange chromatography buffer 1) each. Insoluble proteins were precipitated by a centrifugation at 100000 x g (Ultracentrifuge, Rotor: TFT 50.38) for 30 minutes at 4°C. This centrifugation was repeated until the supernatant was a clear solution. This fraction was then filtered through a membrane with a pore size of 0,45µm ("ammoniumsulfate precipitate, ASP").

DEAE anion exchange chromatography of ASP

A 300ml DEAD-FF column (Amersham Pharmacia Biotech, Freiburg, Germany) was equilibrated with 1l of IEX-1. Subsequently, the ammoniumsulfate precipitate was applied to the

column at a flow rate of 10ml/min and washed with IEX-1 until baseline absorption was reached again. Bound protein was then eluted with mixture of 50% IEX-1 and 50% IEX-2 at a flow rate of 10ml/min. The whole protein peak was collected and the conductivity set to the value of IEX-1 ("DEAE-Pool").

SourceQ anionic exchange chromatography of the DEAE pool

A SourceQ column with a bed volume of 15ml (Amersham Pharmacia Biotech, Freiburg, Germany) was equilibrated with 50ml of IEX-1 (flow rate 2ml/min), and the DEAE-pool applied to the column over night (max. flow rate 1mg/ml). Subsequently, the column was washed with IEX-1 until baseline absorption was reached again. Bound protein was eluted in a linear gradient from IEX-1 to IEX-2 over 200ml. The eluate was collected in fractions of 3ml, and 5µl of each fraction submitted to SDS PAGE and Coomassie staining and Western blotting. The fractions containing coatomer were pooled and adjusted with conductivity buffer to the conductivity of IEX-1 ("SourceQ-Pool").

Concentration of the SourceQ-Pools

A SourceQ column with a bed volume of 1ml (Amersham Pharmacia Biotech, Freiburg, Germany) was equilibrated with 5ml IEX-1 (flow rate 250µl/min). The SourceQ pool was loaded onto the column with the same flow rate, and the column re-equilibrated to IEX-3. Coatomer was eluted in a linear gradient of IEX-3 to IEX-4 (0%-60% IEX-4) in a volume of 6.5ml. Coatomer was collected in fractions of 300µl and checked in Coomassie stained gels and by Western blotting against coatomer subunits. According to purity, different fractions were pooled. Protein concentration was adjusted to 5mg/ml, aliquoted into 10µl aliquots, snap-frozen in liquid nitrogen and stored at -80°C.

Isolation of rat liver Golgi

For one preparation, 11 male Wistar rats were killed and left to bleed out briefly. The livers were instantly upon excision transferred into precooled homogenization buffer and cut into small pieces (<1cm). After weighing, 3 parts (v/w) of homogenization buffer per liver mass were added. The liver were then homogenized using an Ultrathorax for 30s at highest possible speed. The homogenate was transferred into 50ml Falcon tubes and centrifuged for 10min at 2200rpm at 4°C. The supernatant was filtered through 4 layers of mull to obtain Perinuclear supernatant (PNS). This supernatant was applied onto 20ml of a 1.25M Sucrose/Tris solution (ca. 16ml of PNS in SW-28 tube, appr. 10 tubes). The samples were centrifuged for 1:30h at 25000rpm at 4°C. The interphase (IPH) was harvested with a plastic pipette (appr. 35ml). The sucrose concentration of this fraction was adjusted to 1.255M by adding 2M sucrose. The IPH was then applied to a second gradient in SW-28 tubes, as described below (pour from bottom):

+ 10ml 0.5M Sucrose (top)

+ 10ml 1.0M Sucrose

+ 10ml 1.1M Sucrose

+ 6ml IPH (bottom)

The samples were then centrifuged for 2:30h at 25000rpm (4°C). The interphase between 0.5M and 1.0M sucrose was harvested, containing the Golgi (recognizable by white flakes on white layer). The purified Golgi membranes were then snap-frozen in liquid nitrogen and stored at -80°C.

Recombinant Coatomer isoforms purification

3Pellets (0,75 liter expressions culture) where thawed in a 37°C water bath and protease inhibitor cocktails (Roche) were added. Cells were broken using a Cell Disrupter (AG Sinning) in 5 Passages. The lysate was cleared by centrifugation at 100,000g for 30 min in a 52.3 Ti and the supernatant was bound to 2x 0,75g Ni-IDA Beads in 35ml fractions. Incubation for 2h 30min at 4°C. Bound material was washed 2x with 35ml Wash-Buffer for 5 min at 4°C. The samples were eluted with Elution buffer in 0.5 ml fractions and analyzed by SDS PAGE. Coatomer containing fractions were pooled and desalted by PD10 desalting columns (GE Healthcare) and stored at -80°C.

Purification of ArfGAP1 from *Pichia pastoris*

The pellet of two liters expression culture was resuspended in 15ml pichia lysis buffer and mixed with 20g acid-washed glass beads. Lysis by vortexing 8x for 30 sec at 4°C. The lysate was cleared by centrifugation at 100.00g for 1 hour and incubated with 1ml Ni^{++}-NTA sepharose for 1 hour at 4°C, rotating. The beads were then placed in a column and washed extensively at a flow of 1 mg/ml with Pichia binding buffer. The protein was eluted with a linear gradient of 10 to 250 mM immidazole in 2 column volumes, the eluate fractionated and analyzed by SDS-PAGE. Fractions containing ArfGAP1 were pooled and dialyzed against pichia dialysis buffer. The purification yielded 1.2 mg full length ArfGAP1, at a concentration of 0.2 mg/ml.

Purification of myrArf1-wt from *E.coli*

In this work, the original purification protocol for the expression and isolation of full length, untagged and myristoylated Arf1 (Franco, *et al.*, 1995) was modified, which allowed a faster and more reliable purification procedure. Please refer to Results Part I.

Purification of Arf1-Y35A from *E.coli*

Arf1-Y35A was, after cell lysis and ultracentrifugation, subjected to a 35% ammonium sulfate precipitation, centrifuged, and the supernatant bound to a phenylsepharose HP column (Pharmacia Biotech) was developed with a descending gradient from 35% to 0% ammonium sulfate in 20 mM Tris-HCl buffer pH 8.0, 1 mM $MgCl_2$, at RT. Eluted fractions were analyzed by immunoblotting with anti-Arf1 antibody, pooled and concentrated in spin column filters with a 10 kDa cutoff (Milipore), and subsequently purified by gel filtration on a superdex-75. Fractions of interest were pooled and concentrated.

Preparation of liposomes

All phospholipids and cholesterol were purchased from Avanti Polar Lipids except for phosphatidic acid, which was from Sigma. Lipids were derived from natural sources (Nickel and Wieland, 2001).

Golgi-like liposomes were prepared according to (Reinhard, *et al.*, 2003), containing 1 mol% phosphatidylinositol-4,5-bisphosphate ($PI(4,5)P_2$) and 2 mol% p23 lipopeptide, which was synthesized according to (Bremser, *et al.*, 1999). Size selection was performed by extrusion through 100 nm polycarbonate filter membranes (Avestin).

Golgi binding assay

Binding of Arf1 and coatomer to HeLa and rat liver Golgi membranes was performed as described (Zhao, *et al.*, 1997). Briefly, following a 3 min incubation at 37°C of 10 µg HeLa Golgi membranes with 0.6 µg of either Arf1-wt or Arf1-Y35A in the presence of 50 µM nucleotide (GDPβS or GTPγS) in assay buffer (25 mM HEPES-KOH pH 7.2, 2.5 mM magnesium acetate, 20 mM KCl, ovalbumin (1mg/ml), 1 mM DTT and 200 mM sucrose), 2 µg rabbit liver coatomer was added to an end volume of 50 µl. After additional 15 min incubation, Golgi membranes were pelleted by loading the sample onto a 300 µl cushion of 15 % sucrose (wt/vol), followed by a 30 min centrifugation at 14,000 rpm (4°C). Pellets were resuspended in SDS sample buffer and after separation by SDS-PAGE, analyzed by Western blotting with antibodies against Arf1 and COP-subunits.

Chemical crosslinking

For analysis of Arf1 dimers, the Golgi binding assay was performed as described above. Following binding, pelleted membranes were resuspended in PBS (e.g. 12.5 µg membranes in 20 µl), and 0.5 mM crosslinker, either EMCS or BMH (Pierce) was added from a 10 mM solution in DMSO. The reaction mixture was incubated for 1 h at RT, and then SDS sample buffer was added. Samples were analyzed by SDS-PAGE and Western blotting with an antibody against Arf1 and by mass spectrometry.

Dimerization assay with protein-free liposomes

To analyze dimerization of Arf1-wt and Arf1-Y35A on liposomes, Arf1 proteins were incubated with liposomes containing 2 mol% p23 lipopeptide and 1 mol% $PI(4,5)P_2$ (200 nmol total lipids)

with 33 µg (0.1 µM) coatomer, 10 µg (1 µM) Arf1, 2µg (0.1 µM) ARNO and 100 µM GTPγS or GDPβS at 37°C for 40 min in 500 µl PBS. Thereafter, the sucrose concentration was adjusted to 52 % (wt/wt) by the addition of 65 % (wt/wt) sucrose in PBS. The sample was transferred to a SW60 tube, and overlaid with 750 µl 42% (wt/wt) sucrose in PBS and 750 µl 10% (wt/wt) sucrose in PBS. Centrifugation was performed at 44,000 rpm for 2.5 h (4°C). Typically, liposomes are visible as an opalescent band at the interface between 42% and 10% sucrose. The liposome fractions were collected and membrane bound Arf1 was analyzed by Western blotting with an antibody against Arf1. Incubation with crosslinker was as described for Golgi membranes. Alternatively, Golgi-like liposomes without lipopeptide were incubated with Arf1-wt and nucleotide exchange was performed by addition of EDTA, GTPγS and thereafter $MgCl_2$, as described (Franco, *et al.*, 1996), followed by chemical crosslinking.

Nucleotide exchange activity on Golgi membranes of Arf1-wt and Arf1-Y35A

Arf1 proteins were incubated with Golgi-enriched membranes, radiolabeled GTP and the Arf-GEF ARNO. Protein-bound and free nucleotide was separated by gel filtration, and the fractions collected were analyzed in a scintillation counter.

20 µg Golgi-enriched membranes from rat liver were extruded through 200 nm pore size polycarbonate filter membranes (Avestin) and incubated with 0.2 µM Arf1, 20 µM GTP, 0.2 µM [8-3H]-GTP (0.1µCi) and 1 nM ARNO with assay buffer (25 mM HEPES-KOH pH 7.4, 150 mM KCl) in a final volume of 50 µl. After incubation for 5 minutes at 25°C, the reactions were subjected to gel filtration on Sephadex G-50.

Recruitment to Golgi membranes of coatomer and adaptin-1 by Arf1-wt and Arf1-Y35A

Golgi-enriched membranes were incubated with Arf1-wt, Arf1-Y35A, GDPβS (D) or GTPγS (T), and Arf1-depleted cytosol. Golgi-bound material was analyzed by Western blotting with antibodies against Arf1, adaptin-1 and the coatomer subunit δ-COP.

Binding of Arf1 and coatomer to HeLa and rat liver Golgi membranes was performed as described (Zhao, *et al.*, 1997). Following a 3 min incubation at 37°C of 10 µg HeLa Golgi membranes with 0.6 µg of either Arf1-wt or Arf1-Y35A in the presence of 50 µM nucleotide (GDPβS or GTPγS) in assay buffer (25 mM HEPES-KOH pH 7.2, 2.5 mM magnesium acetate, 20 mM KCl, ovalbumin (1 mg/ml), 1 mM DTT and 200 mM sucrose), 2 µg rabbit liver coatomer was added to an end volume of 50 µl. After additional 15 min incubation, Golgi membranes were pelleted by loading the sample onto a 300 µl cushion of 15 % sucrose (wt/vol), followed by a 30 min centrifugation at 14,000 rpm (4°C). Pellets were resuspended in SDS sample buffer and after separation by SDS-PAGE analyzed by Western blotting.

Arf1 nucleotide exchange measurements by trpytophane fluorescence according to (Bigay*, et al.*, 2003)

Tryptophan fluorescence was measured at 340nm (bandwidth 20 nm) upon excitation at 297.5nm (bandwidth 3 nm) in a Jasco fluorimeter equipped with stirring and injection facilities. All experiments were performed at 371C. The cylindrical quartz cuvette initially contained extruded liposomes (0.2mM) in HKM buffer (50mM Hepes pH 7.2, 120mM KAc, 1mM MgCl2, 1mM DTT). Arf1-GDP (0.5 mM) was added and activated by the sequential addition of 40 mM

GTP and 2mM EDTA (giving 1 mM $[Mg^{2+}]_{free}$). After 10 min, 2mM MgCl2 (giving 1mM $[Mg^{2+}]_{free}$) was added. GTP hydrolysis was initiated by the addition of Gcs1p, ArfGAP1 or the indicated constructs. For simplicity, the fluorescence level of Arf1-GDP was arbitrary set at zero and the fluorescence level after the GTP loading step was set at 100%. Therefore, the fluorescence scale shown in the figures directly reflects the fraction of Arf1 that undergoes GTP hydrolysis.

Monitoring Arf1-mediated coat recruitment and release in real time by static light scattering according to (Bigay and Antonny, 2005)

Light scattering of Golgi-like liposomes containing 1 mol% $PI(4,5)P_2$ and 2 mol% p23 lipopeptide was monitored in 25 mM HEPES-KOH pH 7.4, 2.5 mM potassium acetate by using a Jasco FP-6500 spectral photometer over time. 1µM Arf1-wt or 2µM Arf1-Y35A was added as indicated (after 100 sec), followed by 100 µM GTP (after 200 sec). Nucleotide exchange was started by the addition of 0.1 µM ARNO (after 300 sec), and after a further 200 seconds, coatomer was added at a concentration of 160 nM. The signal observed after addition of coatomer is composed of light scattering of soluble coatomer plus light scattering of recruited coatomer, as shown by the response in the absence of Arf1. Interestingly, whereas a signal is seen for Arf1-wt after addition of ARNO, nucleotide exchange of Arf1-Y35A seems to be stimulated by coatomer. From these experiments we conclude that on liposomes, the activity of Arf1-Y35A to recruit coatomer is about 20% of Arf1-wt. In order to further challenge the nucleotide specificity of the binding observed, recombinant ArfGAP1 (0.2 µM) was added (after 750 sec). Both, the signals with Arf1-wt and Arf1-Y35A were reversed with similar kinetics and

efficiency, indicating that in both cases the proteins were bound via Arf1-GTP and released by GTP hydrolysis.

Flotation experiments according to (Bigay*, et al.*, 2003)

Proteins (0.5–1 mM) and liposomes (0.5–1mM) were incubated in HKM buffer at room temperature for 5 min in a total volume of 150 ml. The suspension was adjusted to 30% sucrose by adding and mixing 100 ml of a 75% w/v sucrose solution in HKM buffer. The resulting high-sucrose suspension was overlaid with 200 ml HKM containing 25% w/v sucrose and 50 ml HKM containing no sucrose. The sample was centrifuged at 55 000 r.p.m. (240 000 g) in a Beckman swing rotor (TLS 55) for 1 h. The bottom (250 ml), middle (150 ml) and top (50 ml) fractions were manually collected from the bottom using a Hamilton syringe and analyzed by SDS–PAGE

Arf1-wt and mutant localization to the Golgi

Immunofluorescence of Vero cells transfected with Arf1-wt YFP (upper panel) and Arf1-Y35A YFP (lower panel). The localization was analyzed by immunofluorescence with an antibody directed against Giantin.

Vero cells (ATCC CCL-81) were routinely cultured in DMEM supplemented with 10% FCS, 100 units penicillin/ml, 100 µg streptomycin/µl, 2 mM L-glutamine, at 5% CO2 at 37 C. For electroporation, cells of one confluent 10 cm dish were trypsinized, washed three times with PBS and transferred into 300 µl internal medium (10 mM K_2HPO_4, 100 mM potassium glutamate, 2 mM EGTA, 5 mM $MgCl_2$, 0.15 mM $CaCl_2$, 25 mM HEPES-KOH pH 7.4 and 0.2 mM ATP). 15 µg of the respective plasmids were added to this suspension, and one pulse of 600 V and 50 µF was applied. Electroporated cells were kept at RT for 10 min, plated on coverslips

in full DMEM medium and subsequently incubated at 37°C for 24 hours. The ARF1-wt-YFP plasmid was received as a kind gift by Rainer Duden (Majoul, *et al.*, 2001), Royal Holloway University, London. The ARF1-Y35A-YFP plasmid was generated by site directed mutagenesis.

Cells were washed with PBS, fixed in 3% paraformaldehyde for 20 min and subsequently permeabilized in 0.5% Triton X-100 for 5 min. After blocking with 5 % BSA in PBS for 15 min, the samples were incubated with anti-Giantin antibody diluted 1:500 in PBS containing 5% BSA for 30 min. After washing twice with PBS for 10 min, the samples were incubated with Alexa-546-labeled anti rabbit secondary antibody for another 30 min, washed twice with PBS for 10 min, and subsequently mounted in Mowiol 4-88 (Calbiochem, San Diego, USA). All steps were carried out at RT.

Images were taken with an inverted laser scanning confocal microscope (LSM 510, Carl Zeiss, Jena, Germany), using a 63x objective lens, 4x zoom and a pinhole size equivalent to one Airy disk diameter.

Complementation assays in yeast

The yeast strain NYY539 (arf1Δ, arf2Δ, pURA3-Arf1) was kindly provided by A. Nakano (Takeuchi, *et al.*, 2002). pRS315-Arf1-wt and pRS315-arf1-Y35A were generated using standard procedures and transformed into NYY539. The cells were incubated at 23,30 and 37°C for various times and transformants were spotted on SDC+FOA.

GAL1-overexpression of Arf1-Y35A in yeast

Therf1Δarf2Δ (pURA3 ARF1) strain was transformed with plasmids that encode ARF1-wt and Y35A allele, under control of the GAL1 promotor. The transformants were then plated on SGC+FOA to remove pURA3 ARF1 plasmid.

Formation of COPI vesicles in vitro

COPI vesicle budding assays with rat liver Golgi membranes and Arf1 (Arf1-wt or Arf1-Y35A,) were performed as described (Serafini, *et al.*, 1991). For the rapid generation of COP vesicles in the presence of GTP the method was modified:

200 µg rat liver Golgi membranes (pretreated with 500 mM KCl), 10 µg myristoylated Arf1 protein, and 25 µg coatomer was incubated for 10 minutes at 37°C in a total volume of 250 µl in assay buffer (25 mM HEPES-KOH pH 7.4, 2.5 mM magnesium acetate, 50 mM KCl, 1.2 mM GTP, 300 mM sucrose and 0.25 mM DTT) and 1% of the input was taken for Western blot analysis. The sample was subjected to 250 mM KCl in order to dissociate tethered COPI vesicles from the donor Golgi membranes, which were pelleted by a 10 min centrifugation at 14,000 rpm at 4°C. The supernatant, containing COPI vesicles, was laid on top of two sucrose cushions in a Beckman SW55-mini tube of 37.5% (50 µl) and 45% (5 µl) sucrose. After centrifugation for 50 minutes at 100,000g, the vesicles were collected at the 45/37.5% sucrose interphase and the collected material was analyzed by Western blotting, negative staining electron microscopy and by electrospray ionization tandem mass spectrometry to assess the lipid content.

Complementation assays in yeast

The yeast strain NYY539 (arf1Δ, arf2Δ, pURA3-Arf1) was kindly provided by A. Nakano (Takeuchi, *et al.*, 2002). pRS315-Arf1-wt and pRS315-arf1-Y35A were generated using standard procedures and transformed into NYY539. The cells were incubated at 23,30 and 37°C for various times and transformants were spotted on SDC+FOA.

Arf1 induced tubulation of membrane sheets

A system similar to that described in (Roux, *et al.*, 2006) was used. A chamber of approx. 30 µl was built between two microscope slides with two layers of parafilm as a spacer. Golgi-like lipids, containing 1 mol% PI(4,5)P_2, and 2 mol% p23 lipopeptide (Bremser, *et al.*, 1999), were spotted on the glass surface and the solvent (CH_3Cl) was evaporated. The lipids were hydrated in the presence of nucleotide with 20 µl assay buffer (25 mM HEPES-KOH pH 7.4, 150 mM KCl, 1 mM DTT, 1 mM GTP or GDP). Then, protein samples were sequentially added at the concentrations indicated in the legend of Fig.1, and membrane morphology was observed in a phase contrast light microscope. Real time recordings are appended to supporting information.

References

1. Jamieson JD & Palade GE (1966) Role of the Golgi complex in the intracellular transport of secretory proteins. (Translated from eng) *Proceedings of the National Academy of Sciences of the United States of America* 55(2):424-431 (in eng).

2. Barlowe C*, et al.* (1994) COPII: a membrane coat formed by Sec proteins that drive vesicle budding from the endoplasmic reticulum. *Cell* 77(6):895-907.

3. Hauri HP, Kappeler F, Andersson H, & Appenzeller C (2000) ERGIC-53 and traffic in the secretory pathway. *Journal of cell science* 113 (Pt 4):587-596.

4. Martinez-Menarguez JA, Geuze HJ, Slot JW, & Klumperman J (1999) Vesicular tubular clusters between the ER and Golgi mediate concentration of soluble secretory proteins by exclusion from COPI-coated vesicles. *Cell* 98(1):81-90.

5. Rodriguez-Boulan E & Musch A (2005) Protein sorting in the Golgi complex: shifting paradigms. *Biochimica et biophysica acta* 1744(3):455-464.

6. Paleotti O*, et al.* (2005) The small G-protein Arf6GTP recruits the AP-2 adaptor complex to membranes. *The Journal of biological chemistry* 280(22):21661-21666.

7. Owen DJ, Collins BM, & Evans PR (2004) Adaptors for clathrin coats: structure and function. *Annual review of cell and developmental biology* 20:153-191.

8. Glick BS & Malhotra V (1998) The curious status of the Golgi apparatus. *Cell* 95(7):883-889.

9. Rothman JE & Wieland FT (1996) Protein sorting by transport vesicles. *Science (New York, N.Y* 272(5259):227-234.

10. Chardin P*, et al.* (1996) A human exchange factor for ARF contains Sec7- and pleckstrin-homology domains. *Nature* 384(6608):481-484.

11. Franco M, Chardin P, Chabre M, & Paris S (1996) Myristoylation-facilitated binding of the G protein ARF1GDP to membrane phospholipids is required for its activation by a soluble nucleotide exchange factor. *The Journal of biological chemistry* 271(3):1573-1578.

12. Antonny B, Beraud-Dufour S, Chardin P, & Chabre M (1997) N-terminal hydrophobic residues of the G-protein ADP-ribosylation factor-1 insert into membrane phospholipids upon GDP to GTP exchange. *Biochemistry* 36(15):4675-4684.

13. Klarlund JK, Tsiaras W, Holik JJ, Chawla A, & Czech MP (2000) Distinct polyphosphoinositide binding selectivities for pleckstrin homology domains of GRP1-like proteins based on diglycine versus triglycine motifs. *The Journal of biological chemistry* 275(42):32816-32821.

14. De Matteis MA, Di Campli A, & Godi A (2005) The role of the phosphoinositides at the Golgi complex. *Biochimica et biophysica acta* 1744(3):396-405.

15. Zhao X, Lasell TK, & Melancon P (2002) Localization of large ADP-ribosylation factor-guanine nucleotide exchange factors to different Golgi compartments: evidence for distinct functions in protein traffic. (Translated from eng) *Molecular biology of the cell* 13(1):119-133 (in eng).

16. Niu TK, Pfeifer AC, Lippincott-Schwartz J, & Jackson CL (2005) Dynamics of GBF1, a Brefeldin A-sensitive Arf1 exchange factor at the Golgi. *Molecular biology of the cell* 16(3):1213-1222.

17. Hara-Kuge S*, et al.* (1994) En bloc incorporation of coatomer subunits during the assembly of COP-coated vesicles. (Translated from eng) *The Journal of cell biology* 124(6):883-892 (in eng).

18. Zhao L*, et al.* (1997) Direct and GTP-dependent interaction of ADP ribosylation factor 1 with coatomer subunit beta. *Proceedings of the National Academy of Sciences of the United States of America* 94(9):4418-4423.

19. Zhao L, Helms JB, Brunner J, & Wieland FT (1999) GTP-dependent binding of ADP-ribosylation factor to coatomer in close proximity to the binding site for dilysine retrieval motifs and p23. *The Journal of biological chemistry* 274(20):14198-14203.

20. Harter C*, et al.* (1996) Nonclathrin coat protein gamma, a subunit of coatomer, binds to the cytoplasmic dilysine motif of membrane proteins of the early secretory pathway. *Proceedings of the National Academy of Sciences of the United States of America* 93(5):1902-1906.

21. Cosson P & Letourneur F (1994) Coatomer interaction with di-lysine endoplasmic reticulum retention motifs. *Science (New York, N.Y* 263(5153):1629-1631.

22. Reinhard C*, et al.* (1999) Receptor-induced polymerization of coatomer. *Proceedings of the National Academy of Sciences of the United States of America* 96(4):1224-1228.

23. Langer JD*, et al.* (2008) A conformational change in the alpha-subunit of coatomer induced by ligand binding to gamma-COP revealed by single-pair FRET. (Translated from eng) *Traffic (Copenhagen, Denmark)* 9(4):597-607 (in eng).

24. Frigerio G, Grimsey N, Dale M, Majoul I, & Duden R (2007) Two human ARFGAPs associated with COP-I-coated vesicles. (Translated from eng) *Traffic (Copenhagen, Denmark)* 8(11):1644-1655 (in eng).

25. Cukierman E, Huber I, Rotman M, & Cassel D (1995) The ARF1 GTPase-activating protein: zinc finger motif and Golgi complex localization. *Science (New York, N.Y* 270(5244):1999-2002.

26. Reinhard C, Schweikert M, Wieland FT, & Nickel W (2003) Functional reconstitution of COPI coat assembly and disassembly using chemically defined components. *Proceedings of the National Academy of Sciences of the United States of America* 100(14):8253-8257.

27. Tanigawa G*, et al.* (1993) Hydrolysis of bound GTP by ARF protein triggers uncoating of Golgi-derived COP-coated vesicles. *The Journal of cell biology* 123(6 Pt 1):1365-1371.

28. Nickel W*, et al.* (1998) Uptake by COPI-coated vesicles of both anterograde and retrograde cargo is inhibited by GTPgammaS in vitro. *Journal of cell science* 111 (Pt 20):3081-3090.

29. Malsam J, Gommel D, Wieland FT, & Nickel W (1999) A role for ADP ribosylation factor in the control of cargo uptake during COPI-coated vesicle biogenesis. *FEBS letters* 462(3):267-272.

30. Pepperkok R, Whitney JA, Gomez M, & Kreis TE (2000) COPI vesicles accumulating in the presence of a GTP restricted arf1 mutant are depleted of anterograde and retrograde cargo. *Journal of cell science* 113 (Pt 1):135-144.

31. Lanoix J*, et al.* (2001) Sorting of Golgi resident proteins into different subpopulations of COPI vesicles: a role for ArfGAP1. *The Journal of cell biology* 155(7):1199-1212.

32. Serafini T*, et al.* (1991) ADP-ribosylation factor is a subunit of the coat of Golgi-derived COP-coated vesicles: a novel role for a GTP-binding protein. *Cell* 67(2):239-253.

33. Ostermann J*, et al.* (1993) Stepwise assembly of functionally active transport vesicles. *Cell* 75(5):1015-1025.

34. Serafini T*, et al.* (1991) A coat subunit of Golgi-derived non-clathrin-coated vesicles with homology to the clathrin-coated vesicle coat protein beta-adaptin. *Nature* 349(6306):215-220.

35. Yang JS*, et al.* (2002) ARFGAP1 promotes the formation of COPI vesicles, suggesting function as a component of the coat. *The Journal of cell biology* 159(1):69-78.

36. Vetter IR & Wittinghofer A (2001) The guanine nucleotide-binding switch in three dimensions. *Science (New York, N.Y* 294(5545):1299-1304.

37. D'Souza-Schorey C & Chavrier P (2006) ARF proteins: roles in membrane traffic and beyond. *Nat Rev Mol Cell Biol* 7(5):347-358.

38. Boehm M, Aguilar RC, & Bonifacino JS (2001) Functional and physical interactions of the adaptor protein complex AP-4 with ADP-ribosylation factors (ARFs). *The EMBO journal* 20(22):6265-6276.

39. Austin C, Boehm M, & Tooze SA (2002) Site-specific cross-linking reveals a differential direct interaction of class 1, 2, and 3 ADP-ribosylation factors with adaptor protein complexes 1 and 3. *Biochemistry* 41(14):4669-4677.

40. Donaldson JG, Cassel D, Kahn RA, & Klausner RD (1992) ADP-ribosylation factor, a small GTP-binding protein, is required for binding of the coatomer protein beta-COP to Golgi membranes. *Proceedings of the National Academy of Sciences of the United States of America* 89(14):6408-6412.

41. Ooi CE, Dell'Angelica EC, & Bonifacino JS (1998) ADP-Ribosylation factor 1 (ARF1) regulates recruitment of the AP-3 adaptor complex to membranes. *The Journal of cell biology* 142(2):391-402.

42. Stamnes MA & Rothman JE (1993) The binding of AP-1 clathrin adaptor particles to Golgi membranes requires ADP-ribosylation factor, a small GTP-binding protein. *Cell* 73(5):999-1005.

43. Zhu Y, Traub LM, & Kornfeld S (1998) ADP-ribosylation factor 1 transiently activates high-affinity adaptor protein complex AP-1 binding sites on Golgi membranes. *Molecular biology of the cell* 9(6):1323-1337.

44. Waters MG, Serafini T, & Rothman JE (1991) 'Coatomer': a cytosolic protein complex containing subunits of non-clathrin-coated Golgi transport vesicles. *Nature* 349(6306):248-251.

45. Sun Z*, et al.* (2007) Multiple and stepwise interactions between coatomer and ADP-ribosylation factor-1 (Arf1)-GTP. *Traffic (Copenhagen, Denmark)* 8(5):582-593.

46. Sohn K*, et al.* (1996) A major transmembrane protein of Golgi-derived COPI-coated vesicles involved in coatomer binding. *The Journal of cell biology* 135(5):1239-1248.

47. Helms JB, Palmer DJ, & Rothman JE (1993) Two distinct populations of ARF bound to Golgi membranes. *The Journal of cell biology* 121(4):751-760.

48. Robinson MS (2004) Adaptable adaptors for coated vesicles. *Trends Cell Biol* 14(4):167-174.

49. Bonfanti L*, et al.* (1998) Procollagen traverses the Golgi stack without leaving the lumen of cisternae: evidence for cisternal maturation. *Cell* 95(7):993-1003.

50. Blagitko N, Schulz U, Schinzel AA, Ropers HH, & Kalscheuer VM (1999) gamma2-COP, a novel imprinted gene on chromosome 7q32, defines a new imprinting cluster in the human genome. *Hum Mol Genet* 8(13):2387-2396.

51. Futatsumori M, Kasai K, Takatsu H, Shin HW, & Nakayama K (2000) Identification and characterization of novel isoforms of COP I subunits. *J Biochem (Tokyo)* 128(5):793-801.

52. Wegmann D, Hess P, Baier C, Wieland FT, & Reinhard C (2004) Novel isotypic gamma/zeta subunits reveal three coatomer complexes in mammals. *Mol Cell Biol* 24(3):1070-1080.

53. Moelleken J*, et al.* (2007) Differential localization of coatomer complex isoforms within the Golgi apparatus. (Translated from eng) *Proceedings of the National Academy of Sciences of the United States of America* 104(11):4425-4430 (in eng).

54. Liu W, Duden R, Phair RD, & Lippincott-Schwartz J (2005) ArfGAP1 dynamics and its role in COPI coat assembly on Golgi membranes of living cells. *J. Cell Biol.* 168(7):1053-1063.

55. Franco M, Chardin P, Chabre M, & Paris S (1995) Myristoylation of ADP-ribosylation factor 1 facilitates nucleotide exchange at physiological Mg2+ levels. (Translated from eng) *The Journal of biological chemistry* 270(3):1337-1341 (in eng).

56. Antonny B, Huber I, Paris S, Chabre M, & Cassel D (1997) Activation of ADP-ribosylation factor 1 GTPase-activating protein by phosphatidylcholine-derived diacylglycerols. (Translated from eng) *The Journal of biological chemistry* 272(49):30848-30851 (in eng).

57. Mayer LD, Hope MJ, & Cullis PR (1986) Vesicles of variable sizes produced by a rapid extrusion procedure. (Translated from eng) *Biochimica et biophysica acta* 858(1):161-168 (in eng).

58. Bigay J, Gounon P, Robineau S, & Antonny B (2003) Lipid packing sensed by ArfGAP1 couples COPI coat disassembly to membrane bilayer curvature. *Nature* 426(6966):563-566.

59. Bigay J, Casella JF, Drin G, Mesmin B, & Antonny B (2005) ArfGAP1 responds to membrane curvature through the folding of a lipid packing sensor motif. *The EMBO journal* 24(13):2244-2253.

60. Bremser M*, et al.* (1999) Coupling of coat assembly and vesicle budding to packaging of putative cargo receptors. *Cell* 96(4):495-506.

61. Malsam J, Satoh A, Pelletier L, & Warren G (2005) Golgin tethers define subpopulations of COPI vesicles. *Science (New York, N.Y* 307(5712):1095-1098.

62. Pavel J, Harter C, & Wieland FT (1998) Reversible dissociation of coatomer: functional characterization of a beta/delta-coat protein subcomplex. *Proceedings of the National Academy of Sciences of the United States of America* 95(5):2140-2145.

63. Tabas I & Kornfeld S (1979) Purification and characterization of a rat liver Golgi alpha-mannosidase capable of processing asparagine-linked oligosaccharides. (Translated from eng) *The Journal of biological chemistry* 254(22):11655-11663 (in eng).

64. Lee SY, Yang JS, Hong W, Premont RT, & Hsu VW (2005) ARFGAP1 plays a central role in coupling COPI cargo sorting with vesicle formation. *The Journal of cell biology* 168(2):281-290.

65. Serafini T & Rothman JE (1992) Purification of Golgi cisternae-derived non-clathrin-coated vesicles. *Methods in enzymology* 219:286-299.

66. Pfeffer SR (1999) Transport-vesicle targeting: tethers before SNAREs. (Translated from eng) *Nature cell biology* 1(1):E17-22 (in eng).

67. Barr F (2000) Joining tethers and SNAREs. (Translated from Eng) *Trends in biochemical sciences* 25(10):486 (in Eng).

68. Whyte JR & Munro S (2002) Vesicle tethering complexes in membrane traffic. (Translated from eng) *Journal of cell science* 115(Pt 13):2627-2637 (in eng).

69. Gillingham AK & Munro S (2003) Long coiled-coil proteins and membrane traffic. (Translated from eng) *Biochimica et biophysica acta* 1641(2-3):71-85 (in eng).

70. Shorter J & Warren G (2002) Golgi architecture and inheritance. (Translated from eng) *Annual review of cell and developmental biology* 18:379-420 (in eng).

71. Orci L*, et al.* (2000) Anterograde flow of cargo across the golgi stack potentially mediated via bidirectional "percolating" COPI vesicles. *Proceedings of the National Academy of Sciences of the United States of America* 97(19):10400-10405.

72. Orci L, Perrelet A, & Rothman JE (1998) Vesicles on strings: morphological evidence for processive transport within the Golgi stack. (Translated from eng) *Proceedings of the National Academy of Sciences of the United States of America* 95(5):2279-2283 (in eng).

73. Yang JS*, et al.* (2005) A role for BARS at the fission step of COPI vesicle formation from Golgi membrane. (Translated from eng) *The EMBO journal* 24(23):4133-4143 (in eng).

74. Beck R*, et al.* (2008) Membrane curvature induced by Arf1-GTP is essential for vesicle formation. (Translated from eng) *Proceedings of the National Academy of Sciences of the United States of America* 105(33):11731-11736 (in eng).

75. Lee MC*, et al.* (2005) Sar1p N-Terminal Helix Initiates Membrane Curvature and Completes the Fission of a COPII Vesicle. *Cell* 122(4):605-617.

76. Roux A, Uyhazi K, Frost A, & De Camilli P (2006) GTP-dependent twisting of dynamin implicates constriction and tension in membrane fission. *Nature* 441(7092):528-531.

77. Bigay J & Antonny B (2005) Real-time assays for the assembly-disassembly cycle of COP coats on liposomes of defined size. (Translated from eng) *Methods in enzymology* 404:95-107 (in eng).

78. Chen H*, et al.* (1998) Epsin is an EH-domain-binding protein implicated in clathrin-mediated endocytosis. (Translated from eng) *Nature* 394(6695):793-797 (in eng).

79. Ford MG*, et al.* (2002) Curvature of clathrin-coated pits driven by epsin. *Nature* 419(6905):361-366.

80. Frost A*, et al.* (2008) Structural basis of membrane invagination by F-BAR domains. (Translated from eng) *Cell* 132(5):807-817 (in eng).

81. Martens S, Kozlov MM, & McMahon HT (2007) How synaptotagmin promotes membrane fusion. *Science (New York, N.Y* 316(5828):1205-1208.

82. Peter BJ*, et al.* (2004) BAR domains as sensors of membrane curvature: the amphiphysin BAR structure. *Science (New York, N.Y* 303(5657):495-499.

83. Shiba T*, et al.* (2003) Molecular mechanism of membrane recruitment of GGA by ARF in lysosomal protein transport. (Translated from eng) *Nature structural biology* 10(5):386-393 (in eng).

84. Amor JC, Harrison DH, Kahn RA, & Ringe D (1994) Structure of the human ADP-ribosylation factor 1 complexed with GDP. (Translated from eng) *Nature* 372(6507):704-708 (in eng).

85. Gommel DU*, et al.* (2001) Recruitment to Golgi membranes of ADP-ribosylation factor 1 is mediated by the cytoplasmic domain of p23. *The EMBO journal* 20(23):6751-6760.

86. Hosobuchi M, Kreis T, & Schekman R (1992) SEC21 is a gene required for ER to Golgi protein transport that encodes a subunit of a yeast coatomer. *Nature* 360(6404):603-605.

87. Kahn RA, Kern FG, Clark J, Gelmann EP, & Rulka C (1991) Human ADP-ribosylation factors. A functionally conserved family of GTP-binding proteins. *The Journal of biological chemistry* 266(4):2606-2614.

88. Stearns T, Kahn RA, Botstein D, & Hoyt MA (1990) ADP ribosylation factor is an essential protein in Saccharomyces cerevisiae and is encoded by two genes. *Mol Cell Biol* 10(12):6690-6699.

89. Takeuchi M, Ueda T, Yahara N, & Nakano A (2002) Arf1 GTPase plays roles in the protein traffic between the endoplasmic reticulum and the Golgi apparatus in tobacco and Arabidopsis cultured cells. *Plant J* 31(4):499-515.

90. Waters MG, Griff IC, & Rothman JE (1991) Proteins involved in vesicular transport and membrane fusion. *Curr Opin Cell Biol* 3(4):615-620.

91. Rios RM*, et al.* (1994) A peripheral protein associated with the cis-Golgi network redistributes in the intermediate compartment upon brefeldin A treatment. (Translated from eng) *The Journal of cell biology* 125(5):997-1013 (in eng).

92. Pernet-Gallay K*, et al.* (2002) The overexpression of GMAP-210 blocks anterograde and retrograde transport between the ER and the Golgi apparatus. (Translated from eng) *Traffic (Copenhagen, Denmark)* 3(11):822-832 (in eng).

93. Drin G*, et al.* (2007) A general amphipathic alpha-helical motif for sensing membrane curvature. (Translated from eng) *Nature structural & molecular biology* 14(2):138-146 (in eng).

94. Gillingham AK, Tong AH, Boone C, & Munro S (2004) The GTPase Arf1p and the ER to Golgi cargo receptor Erv14p cooperate to recruit the golgin Rud3p to the cis-Golgi. (Translated from eng) *The Journal of cell biology* 167(2):281-292 (in eng).

95. Drin G, Morello V, Casella JF, Gounon P, & Antonny B (2008) Asymmetric tethering of flat and curved lipid membranes by a golgin. (Translated from eng) *Science (New York, N.Y* 320(5876):670-673 (in eng).

96. Gallop JL*, et al.* (2006) Mechanism of endophilin N-BAR domain-mediated membrane curvature. (Translated from eng) *The EMBO journal* 25(12):2898-2910 (in eng).

97. Daumke O*, et al.* (2007) Architectural and mechanistic insights into an EHD ATPase involved in membrane remodelling. (Translated from Eng) *Nature* 449(7164):923-927 (in Eng).

98. Bethune J, Wieland F, & Moelleken J (2006) COPI-mediated transport. (Translated from eng) *The Journal of membrane biology* 211(2):65-79 (in eng).

99. Laemmli UK (1970) Cleavage of structural proteins during the assembly of the head of bacteriophage T4. (Translated from eng) *Nature* 227(5259):680-685 (in eng).

100. Nickel W & Wieland FT (2001) Receptor-dependent formation of COPI-coated vesicles from chemically defined donor liposomes. (Translated from eng) *Methods in enzymology* 329:388-404 (in eng).

101. Majoul I, Straub M, Hell SW, Duden R, & Soling HD (2001) KDEL-cargo regulates interactions between proteins involved in COPI vesicle traffic: measurements in living cells using FRET. *Dev Cell* 1(1):139-153.

Acknowledgements

At the end of this thesis I would like to thank Prof. Dr. Felix Wieland for this very rewarding experience at the BZH. Both Prof. Dr. Felix Wieland and PD Dr. Britta Brügger have been fantastic and amicable mentors, I owe both of them everything I know about this profession.

Also, I would like to thank all members of this group that I had the honor to work with. I met you as colleagues and now I regard many of you as friends.

Special thanks go out to Carolin Weimer for the fruitful collaboration on the ArfGAP projects, Frank Adolph for his contributions to the Arf1 project, as well as Ingrid Meissner and Priska Eckert for their contributions to the coatomer isotype project. I could not have done this work alone.

Prof. Dr. Volker Haucke and Dr. John Briggs (with his co-workers Simone Prinz and Marco Faini) have been fantastic collaboration partners, I would like to thank them as well.

For funding, I thank Prof. Dr. Felix Wieland, and the Graduiertenkolleg 1188.

This work, like the rest of my education, would not have been possible without the financial and emotional support from my parents.

Last but not least, I thank Katharina for her understanding, and love.